AALBORG UNIVERSITY
STUDENT REPORT

Bachelor project

Attitude control system for AAUSAT4

Authors:
Brian Gasberg Thomsen
Jens Nielsen
Mikael Juhl Kristensen
Nikolaj Holm

Supervisor:
Christoffer Eg Sloth

May 27, 2014

AALBORG UNIVERSITY
STUDENT REPORT

Department of Electronic Systems
Fredrik Bajers Vej 7
9220 Aalborg Ø
Telephone: 96 35 86 90
http://es.aau.dk

Title: Attitude Control System for AAUSAT4

Theme: Control Engineering

Project period: 3/2 - 28/5 2014

Project group: 624

Group members:

Brian Gasberg Thomsen
Jens Nielsen
Mikael Juhl Kristensen
Nikolaj Holm

Supervisor:

Christoffer Eg Sloth

Copies: 6

Pages: 105

Appendices: 4

Finished 28th of May 2014

Abstract:

In this study an attitude control system is designed for a cubesat. The analysis is based on the AAUSAT4 and the orbit of that. Models are made, for the satellite and the disturbances influencing it, and then linearized. The models are adjusted based on test results to make an optimal fit. Based on root locus controllers are designed both for the satellite in space and for a test stand on Earth. In time of writing AAUSAT4 has not been launched into space. Because of this the controller for the satellite in space has only been simulated. The test stand is based on a satellite mass dummy, and VICON motion tracking setup used as attitude determination. The controller is converted into discrete time and implemented, the output is sent wireless to the satellite dummy in order not to get the disturbances physical wires would have applied to the test. Finally the controller for the test station is tested against scaled requirements to see if it fulfils the requirements for the actual satellite.

Foreword

This project has been carried out by group 624 with supervision of Christoffer Eg Sloth, as a Bachelor of science project in the Control engineering specialization of the Bsc. in Electronics engineering and IT. The study is a part of the AAUSAT project which is a project with the purpose of educating students by creating satellites. The study is made in the period from the 3rd of February to the 28th of May 2014.

We would like to thank our supervisor Christoffer Eg Sloth, Jesper Abildgaard Larsen for helping out with satellite specific issues, Daniel Uhrenholt for help with the test setup, and Anders La-Cour Harbo for introducing us to the VICON system.

Brian Gasberg Thomsen

Jens Nielsen

Mikael Juhl Kristensen

Nikolaj Holm

Reading guide

A short description of the relevant notations can be found in the following.

References

References to equations are written in parenthesis for example: (2.13). As for all other references it is stated what kind of reference it is e.g. Figure C.4.

General notation

Matrices :	$\underline{\mathbf{A}}$
Vector :	$\bar{\boldsymbol{v}}$
Identity matrix :	$\underline{\mathbf{1}}$
Inertia matrix :	$\underline{\mathbf{I}}$

Reference frames

There are some different reference frames used. Each reference frame has its own letter assigned to it. These are:

Earth centred initial reference frame:	i
Earth centred earth fixed reference frame:	f
Orbit reference frame:	o
Satellite reference frame:	s
Satellite control reference frame:	c

Constants or variables defined in a certain reference frame are notated ${}^{\mathrm{i}}X$ for Earth centred initial reference frame and so on. As for rotation matrices and quaternions the reference frame that is rotated from is lowered and the reference frame rotated to is raised e.g. ${}^{\mathrm{s}}_{\mathrm{i}}\underline{\mathbf{R}}$.

CD

In addition to the report a CD attached which includes:

- The report
- Video of the acceptance test
- MATLAB and Arduino code used in the project
- Simulation environments for Simulink used in the project
- Data from the Helmholtz coil
- Documentation of AAUSAT

Abbreviations will be explained when they are first used in the report.

Abbreviations

Abbreviations

AAU	Aalborg University
ACS	Attitude Control System
ADCS	Attitude Determination and Control System
ADS	Attitude Determination System
CDD	Cubesat Design Description
CoM	Centre of Mass
ECEF	Earth Centred Earth Fixed reference frame
ECI	Earth Centred Initial reference frame
GM	Gain Margin
NORAD	North American Aerospace Defense Command
ORF	Orbit Reference Frame
PM	Phase Margin
PWM	Pulse Width Modulation
SBRF	Satellite Body Reference frame
SCRF	Satellite Controller Reference frame
SSD	System Specification Document
TLE	Two-Line Element

Table of Contents

Chapter 1

Introduction

This project deals with the attitude control on AAUSAT4. In this chapter there will be a general description of AAUSAT4, why it is made, how it is structured and what hardware that is available for the Attitude Determination and Control System (ADCS).

1.1 AAU cubesats

The AAUSAT mission is primarily to educate students. This is done by designing, building and maintaining Cubesats [Nielsen and Larsen, 2013] in low earth orbits (160 km -2000 km). A Cubesat is a satellite that meets a set of specifications set by California Polytechnic State University and Stanford University in 1999 [California Polytechnic State University, 2009]. The most significant specification is the dimensions and the weight. A Cubesat unit must have the dimensions $10 \times 10 \times 11.35$ cm and may not weigh above 1.33 kg. This means that the satellite must be very compact. The Cubesat will need a photo voltaic system to generate power, and an antenna for communication with Earth. So far the AAUSAT program has sent three Cubesats into space. These have brought different payloads, such as a camera and an Automatic Identification systems for ships. The Cubesats also carried a variety of custom experimental software and hardware developed at Aalborg University (AAU). The two first Cubesats have entered a state where they cannot be of any use. The third and latest Cubesat is fully functioning.

1.2 AAUSAT4

AAUSAT4 is based on a modular distributed design principle which means that each subsystem is fully functional independently of other subsystems in the satellite. The satellite includes the following elements in which the Automatic Identification System is the payload and the rest is considered the platform.

- Electronic Power System (EPS)
- Communication System
- Log System
- Attitude detemination and control system (ADCS)
- Flight Planner
- Automatic Identification System

In addition to these there is a ground station to allow communication with the satellite. That consists of the following elements.

- Mission Control Center (MCC)
- Mission Control Server (MCS)
- Radio
- Antenna

That makes the following structure:

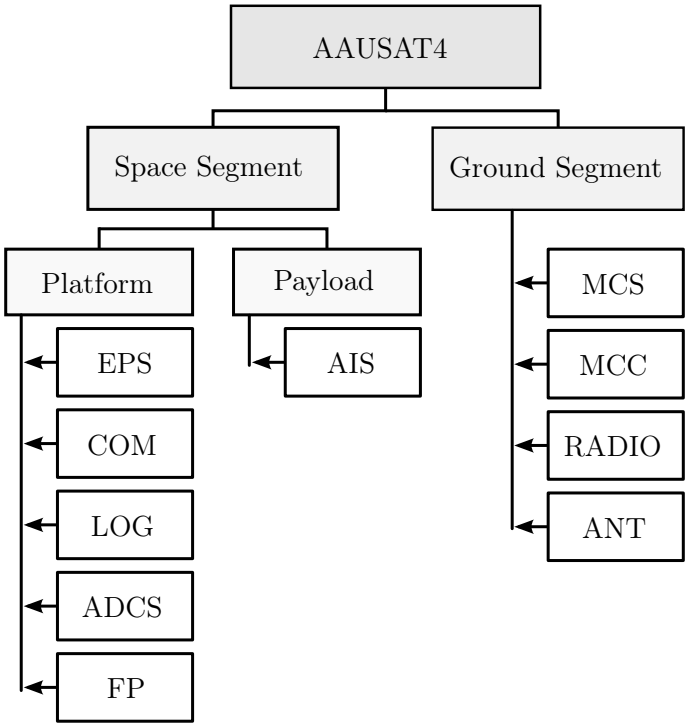

Figure 1.1: Shows the overall system block diagram of the AAUSAT4

The main focus of this project is the ADCS, which will be described in the next section. (Cubesat Design Description (CDD) [Mølgaard et al., 2013])

1.3 Attitude determination and control system

When a Cubesat is launched it may start to tumble (rotate randomly about one or several axes). This is not good for communication and the general use of the satellite. To stop this, and point the satellite in a correct direction an ADCS can be used.

For redundancy ADCS is divided into two parts on AAUSAT4. A simple detumbling section (ADCS1) and a more advanced attitude control system (ADCS2). The ADCS1 is a backup system, only for detumbling. ADCS2 is for precision control and pointing of the satellite but is also able to keep the satellite detumbled. ADCS2 can be divided further into attitude determination and attitude control. The attitude determination samples at a frequency on 1Hz.

As for detumbling the more advanced ADCS2 should at least be able to detumble the satellite as well as ADCS1. The performance of the existing ADCS1 is described in AAUSAT4 System Specification Document (SSD). The ADCS1 is able to detumble the satellite down to 2 revolutions per orbit from 10 degrees/s within 3 orbits and from 720 degrees/s within 3 weeks.

1.3.1 Actuator speed

The ADCS2 has to fulfill the attitude control requirements stated in the SSD [Mølgaard et al., 2014]. These states that the system must be able to return from a detumbled state to a certain attitude and that the system has to be able to maintain a certain attitude within 10 degrees precision with a 95% confidence interval. Furthermore the system must be able to point at the centre of the Earth, this means that the satellite must rotate a full rotation about its Centre of Mass (CoM) during an orbit to maintain pointing at the target. From this statement it is possible find to minimum actuation velocity required in order to point at nadir (centre of Earth).

$$\omega = \frac{v}{r \cdot 2\pi} \cdot 2\pi \tag{1.1}$$

where:

ω	angular velocity of the satellite	[rad/s]
v	orbital velocity vector	[m/s]
r	distance from the centre of Earth to the satellite	[m]

(1.2)

For the satellite to sustain a stable Low Earth Orbit (LEO), around 200 km to 600 km altitude for the AAUSAT4, the satellite has to keep a velocity at ∼7.8 km/s. The altitude of 200 km is the minimum operational altitude of the attitude controller and 600 km is the maximum altitude. The required angular velocity of the satellite can be calculated from equation 1.1

$$\begin{aligned} \omega_{600\,km} &= \frac{7800}{(6371+600)\cdot 10^3 \cdot 2\pi} \cdot 2\pi = 1.1 \cdot 10^{-3}\ \frac{\text{rad}}{\text{s}} \\ \omega_{200\,km} &= \frac{7800}{(6371+200)\cdot 10^3 \cdot 2\pi} \cdot 2\pi = 1.2 \cdot 10^{-3}\ \frac{\text{rad}}{\text{s}} \end{aligned} \tag{1.3}$$

It is seen from the calculations in 1.3 that the required angular velocity for the satellite about its CoM is maximum 0.0012 rad/s to keep pointing to the nadir. It is also seen that the actuation speed is approximately compared to the angular velocity at 600 km. This means that the satellite attitude controller will be designed with the actuation speed requirements for 200 km altitude.

The ADCS uses a variety of sensors, including magnetometers, gyroscopes and sun sensors to determine the attitude, and then corrects it by using magnetorquers as actuators. ADCS1 is the fall back system for detumbling. Detumbling is the action of lowering the tumbling to a level where it is not a problem, but is not actively pointing in a direction. This is done by using a simple algorithm, that responds to change in the magnetic field. ADCS2 is a system meant for obtaining a specific attitude for the satellite. The software part of the ADCS2 has not been implemented on any of the AAUSATs yet, but the hardware in space and in the next satellites are ready for it. The basic principle is:

1. Measure with sun-sensors and magnetic field sensors

2. Based on sensors determine attitude
3. A Controller calculates the needed reaction
4. The reaction is executed with the magnetorquers

In order to execute these steps, some hardware is needed. The hardware for this system will be described in the next section.

1.4 Accessible hardware

In the following a short description of the accessible hardware is presented. Figure 1.2 show a blockdiagram of the hardware available on AAUSAT4: (CDD [Mølgaard et al., 2013])

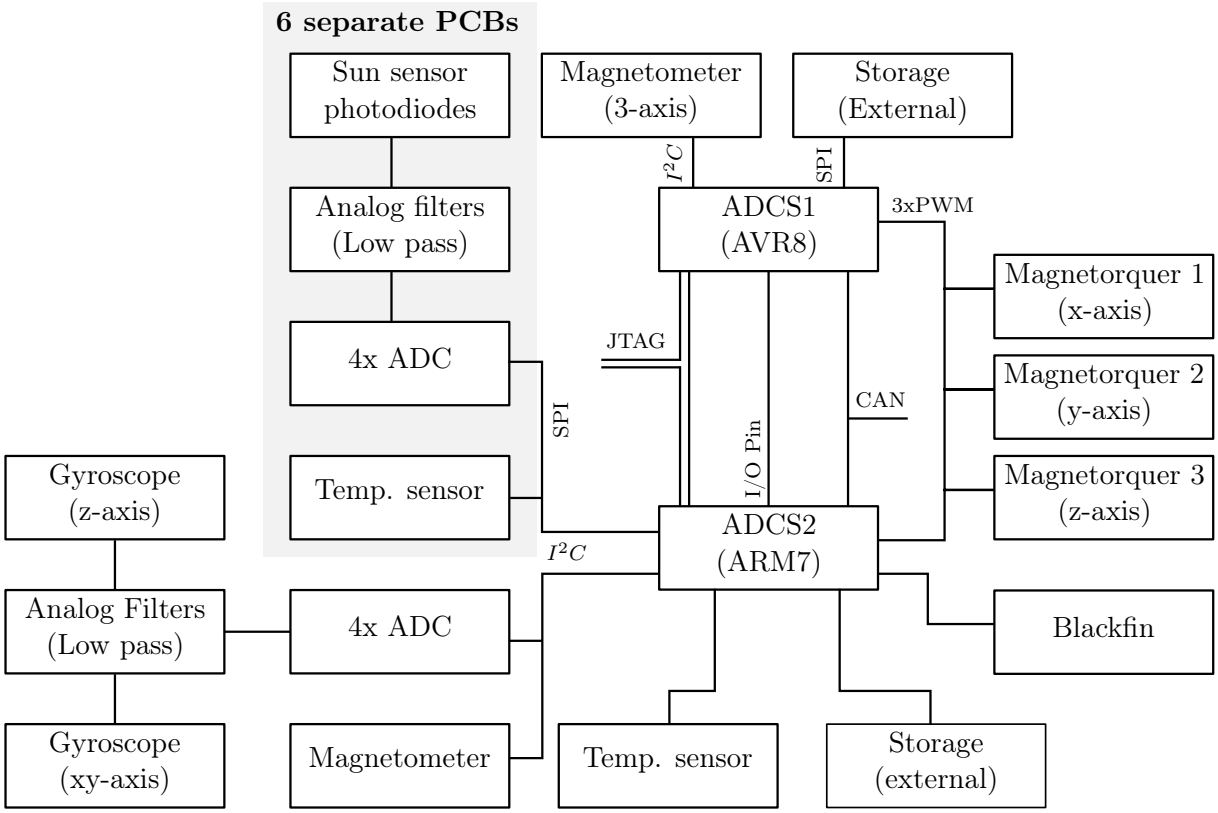

Figure 1.2: Diagram of hardware relevant to ADCS

1.4.1 Magnetorquer

The magnetorquers are constructed as coils with 275 windings of AWG36 [Micronmeters] insulated copper wire. They are almost squares with the dimensions 0.075 m times 0.075 m. The magnetorquer can generate from 0.5 to 1.1 μNm at 700 km altitude [Mølgaard et al., 2013]. The three coils are mounted orthogonal to each other.

1.4.2 Magnetometer

The magnetometer on the AAUSAT4 that is used for ADCS2 is a Freescale Xtrinsic MAG3110FS [Xtrinsic]. It measures the magnetic field with 80 Hz, with a 0.1 μT sensitivity.

1.4.3 Gyroscope

The satellite is fitted with two, two-axis gyroscopes, of the LPY403A [ST.com, 2009] type. This will allow measurements of the satellites rotation even without a magnetic field. The chosen sensor can measure up to 120 degrees per second, and sample at 140 Hz.

1.4.4 Sun sensor

Sun sensors are implemented on all six sides of the satellite. The suns sensors are designed and produced in-house at AAUSAT.

1.4.5 ADCS2 processor

TheADCS2 has its own dedicated processor. It is an ARM7 processor, which has 32 bits and runs at 600MHz.

1.4.6 Blackfin

The software on the ARM processor cannot be changed. Therefore the satellites Analog Devices Blackfin BF537 [Devices], which is part of the Automatic Identification System circuit, is used, since it can receive and execute new code in its Linux environment. The BF537 runs at 600 MHz.

1.4.7 Solar cells

The energy source on the satellite is solar cells. There are 12 units of TJ Solar Cell 3G28C model from Azurspace [Azurspace, 2012], two on each side, of the satellite. These are expected to deliver a total of 1500 mW. Since all the subsystems needs to run using only this energy source the ADCS2 is only allowed to use 80 mW average. (CDD, [Mølgaard et al., 2013])

1.5 Robustness

Based on experience from previous AAU cubesat missions robustness is considered essential when building a satellite. Systems are more prone to bit errors and flips in space, due to the high level of radiation in space. For obvious reasons hardware cannot be changed if it fails during the mission, and software might also be difficult or even impossible to change after launch, depending on the infrastructure of the satellite.

This challenge can be dealt with in several ways. Building the satellite in such a way that it does not have a single point that can lead to an overall failure of the system, is a good way to prevent total failure. Another way is making critical parts redundant so that in case of failure it will fall back to a backup system. In attitude control, this will be done by having the simple ADCS1 that is only capable of detumbling and a more advanced ADCS2 that is able to do actual attitude control and is able to fall back to ADCS1 in case of failure (CDD [Mølgaard et al., 2013]).

1.6 Project limitations

Since AAUSAT4 is largely based on the AAUSAT3 it is considered fully functional with regard to the mission. That said there is only implemented detumbling (ADCS1) and not the ADCS2. The determination part though, is already made by another student group

[Hemme et al., 2013] which means that the control part needs to be made. This study will focus on designing this part.

In order to design the control system, a model of the satellite needs to be made and verified. Based on that the Attitude Control System (ACS) can be designed, and tested both in simulations and on AAUSAT3 and AAUSAT4. Testing on the AAUSAT4 though, can only be performed after the project is done due to the launch date which in the time of writing is scheduled to ultimo 2014. The controller is instead tested in a test stand.

Based on this chapter requirements will be listed in chapter 3.

1.7 Problem description

Based on this chapter the main problem for this project is now found and can be formulated as follows:

How can an Attitude Control System be designed to control the AAUSAT4 in low Earth orbit. How can the controller be verified following the requirements of a CUBESAT, in the environment of the Earth's surface

These main tasks can be divided into a series of steps:

- Make a model of the satellite in space
- Verify the model through tests
- List the requirements given by the problem analysis
- Design a controller that meets the requirements
- Test the controller in a simulation environment
- Test the controller in a practical test setup

1.8 Summary

AAUSAT is a project with the main purpose of educating students. So far 3 student made Cubesats have been sent into space which has given valuable experience for future satellites including the ongoing AAUSAT4. Two of the main experiences are that each subsystem must be independent from the others both in tests and in implementation, and that each system should be redundant if possible. Based on that; AAUSAT3 and AAUSAT4 is carrying two ADCSs. A simple detumbling system ADCS1 and a more advanced ADCS2 that also makes attitude control and is able to fall back to ADCS1. Since an Attitude Determination System (ADS) is already made this project focuses on making an ACS.

Chapter 2

Modeling of the Satellite

Attitude determination and control of a satellite in orbit around the Earth, requires knowledge of how it behaves in the environment of vacuum and weightlessness. A model of the orbit and the satellite's equation of motion must be derived in order to describe its behaviour in space.

To give an overview a block diagram of the system is made. This includes both the ACS, the ADS and the satellite with disturbances.

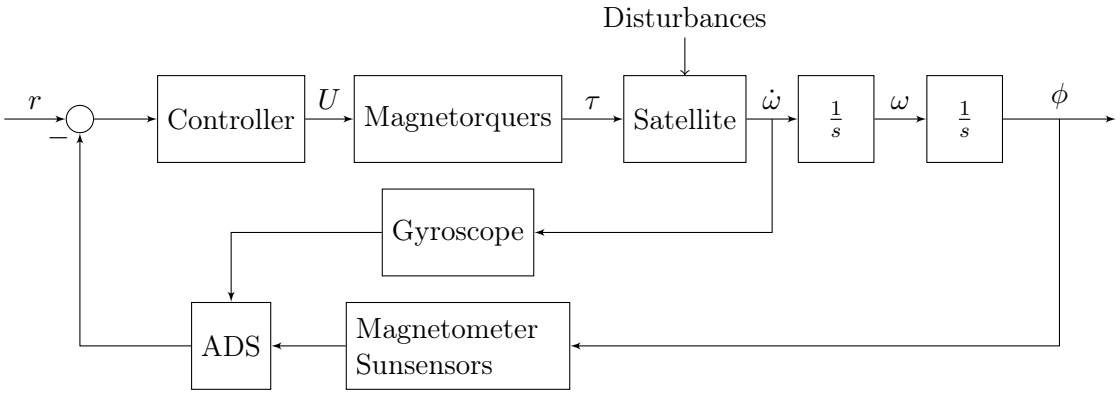

Figure 2.1: Block diagram for the ADCS.

This chapter will start by defining the reference frames in section 2.1. Then in section 2.2 a description of the Keplerian orbit elements which is an approximation used to describe a satellite's orbit around the Earth. Section 2.3 then describes how rotations are defined. In order to do so quaternions will be introduced in section 2.3.1. Section 2.5 will then describe the kinematics and dynamic equations of motion of the satellite.

The output from the ADS shown in Figure 2.1 needs to be defined since it will not be designed in this project but is a part of the model. This will be done in section 2.6, then models for the magnetorquers and the disturbances are derived. This will be done in section 2.7 and 2.9. Based on these, the controller can then be designed so it fulfills the previous mentioned requirements that are also listed in chapter 3.

2.1 Reference frames

To ease the understanding of how an object is orientated in space, relative to other objects, a set of reference frames are defined for the Earth and satellite. These coordinate systems

are a tool to describe the satellite's attitude relative to the Earth. When the reference frames are defined, a rotation of the satellite relative to the Earth can be derived.

2.1.1 Earth centred initial reference frame (ECI)

For orbits around the Earth it is common to define an Earth Centred Initial reference frame (ECI) with origin at the CoM as shown in Figure 2.2. The direction of the coordinate system is fixed relative to the solar system. The ${}^{\mathrm{i}}z$-axis is defined as the rotational axis of the Earth with positive direction through the geographic north pole. The ${}^{\mathrm{i}}x$-${}^{\mathrm{i}}y$ plane lies in the equatorial plane which is perpendicular to the Earth's axis of rotation.

The ${}^{\mathrm{i}}x$-axis is defined by looking at the Earth's orbit around the sun. The Earth's equatorial plan is inclined to the elliptic plane of the Earth's orbit around the sun by 23.5°[Wertz, 1995]. These two planes intersects along a line which coincides with the ${}^{\mathrm{i}}x$-axis (${}^{\mathrm{i}}x_{\Upsilon}$) of the inertial coordinate system, two times a year. This line is also called the vernal equinox vector. This alignment happens the first day of the astronomical spring and autumn (Around March 20$^{\mathrm{th}}$ and September 23$^{\mathrm{rd}}$).

The third axis y completes the orthogonal right-handed Cartesian coordinate system and is thereby perpendicular to the ${}^{\mathrm{i}}x$-${}^{\mathrm{i}}z$ plane.

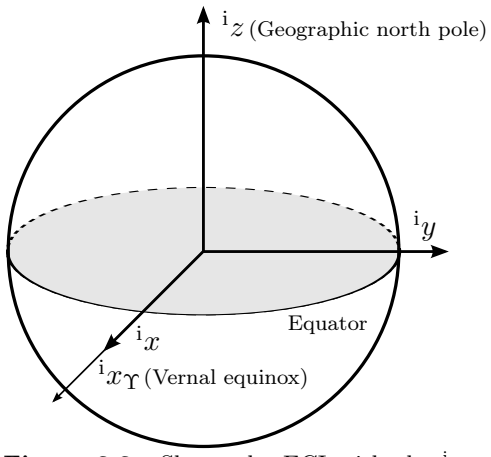

Figure 2.2: Shows the ECI with the ${}^{\mathrm{i}}x$ pointing at the vernal equinox.

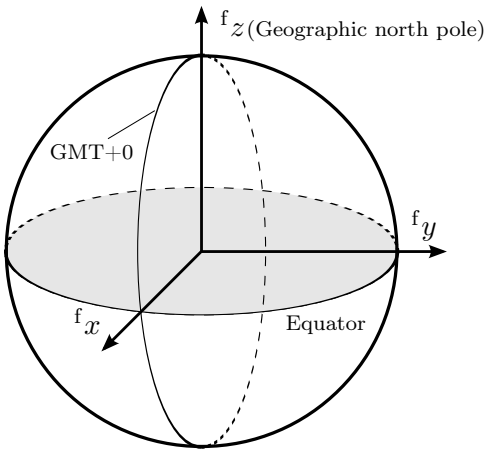

Figure 2.3: Shows the Earth Centred Earth Fixed reference frame (ECEF).

2.1.2 Earth centred earth fixed reference frame (ECEF)

It is convenient to define a reference frame that is fixed relative to the surface of the Earth. This can benefit the mapping of the Earth's magnetic field vectors and positioning of potential ground stations. The ECEF is shown in Figure 2.3 and is centred at CoM, where the ${}^{\mathrm{f}}z$-axis is the Earth's rotational axis and the ${}^{\mathrm{f}}x$-axis pointing out to where the Greenwich meridian crosses the equator (0°longitude, 0°latitude). The ${}^{\mathrm{f}}y$-axis is then the cross product of ${}^{\mathrm{f}}x$ and ${}^{\mathrm{f}}z$ creating a right handed Cartesian coordinate system.

2.1.3 Orbit reference frame (ORF)

The Orbit Reference Frame (ORF) origin is positioned at the satellites CoM where the z_0-axis is allways pointing at the centre of the Earth (Nadir) as shown in Figure 2.4. The x_0-axis is perpendicular to the z_0-axis and is parallel to the orbit plane. If the orbit is circular the x_0-axis corresponds to the velocity vector of the satellite. The y_0-axis is the

right-handed cross product of the z_0 and x_0-axis hence creating a right handed Cartesian system.

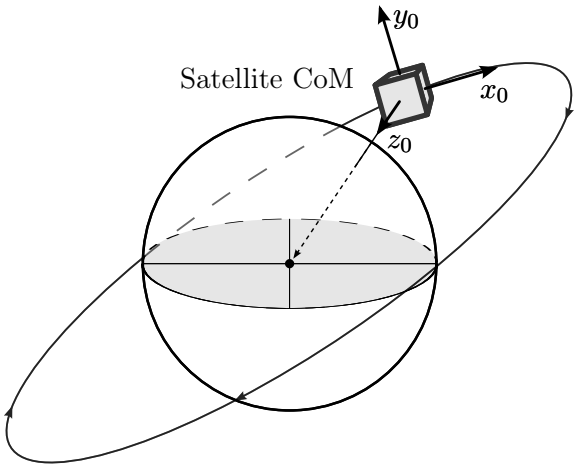

Figure 2.4: Shows the ORF of the satellite in orbit around the Earth. The reference frame origin is defined to be in the CoM of the satellite and the orientation of the z_0-axis is in nadir.

2.1.4 Satellite reference frames (SRF)

The satellite is divided into two different reference frames, the Satellite Body Reference frame (SBRF) and the Satellite Controller Reference frame (SCRF) as illustrated in Figure 2.5 and Figure 2.6. This separation of reference frames makes it possible to define the orientation of the satellite's ADCS attitude relative to the previous defined ORF from the known SBRF. Also the SCRF can be used to describe which direction the controller is actuating.

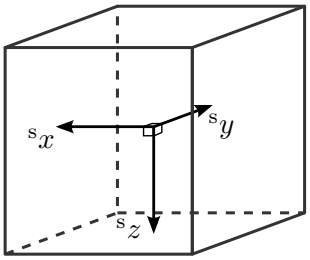

Figure 2.5: Shows the SBRF which defines the geometric orientation of the satellite with origin in the geometric centre. This is used to determine the attitude of the satellites ADCS in relation to the ORF.

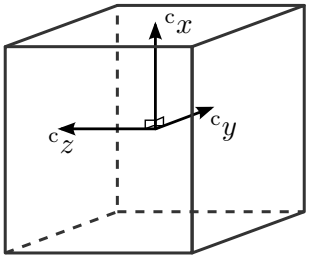

Figure 2.6: Shows the SCRF used to describe the mechanics of the satellite and has origin in the CoM.

Satellite body reference frame (SBRF)

The SBRF is a fixed reference frame used to describe the orientation of the satellite's structure including the orientation of sensors and actuators. The SBRF's centre is placed in the geometric centre of the satellite where the ^{s}z-axis points through the opposite direction of the antenna side panel. The ^{s}x-axis is then parallel to the structure of the satellite and points along the direction of the batteries. The ^{s}y-axis is then given as the right-handed cross product of the ^{s}z- and ^{s}x-axis.

Satellite control reference frame (SCRF)

The SCRF is used to describe the mechanics of the satellite in relation to the actuation of the magnetorquers. The reference frame has it's origin in the CoM of the satellite and is shown in Figure 2.6. The ${}^{\mathrm{c}}z$-axis is pointing in the major-axis of the satellite where the largest moment of inertia is, and the ${}^{\mathrm{c}}x$-axis is pointing towards the minor-axis where the moment of inertia in smallest. These can be derived from the satellite's inertia matrix and is defined as the largest and smallest eigenvalues of the matrix. The ${}^{\mathrm{c}}y$-axis is then the right-handed cross product of ${}^{\mathrm{c}}z$ and ${}^{\mathrm{c}}x$ creating a right-handed Cartesian system.

2.2 Orbit description

A satellite in orbit around the Earth can be considered as a two body problem, where they both are influenced by their mutual gravitational attraction. This can be described by the observations made in Kepler's three empirical laws of planetary motion, or by using Newton's more general laws of motion and law of gravity [Sidi, 1997]. Kepler's laws of motion describe an ideal orbit, but they do not correspond with the real world behavior. Perturbing forces and physical anomalies will cause the satellite orbit to have a different shape. The possibilities in finding an approximation on how a satellite will orbit the Earth can benefit the disturbance model. The following subsections will elaborate on how to approximate the orbit of a satellite.

2.2.1 Keplerian orbit

A Keplerian orbit can be used to describe an orbit of an object around the Earth showed in Figure 2.7. The elements of the Keplerian orbit are used to describe the size, shape and orientation of the orbit and may be given as the Keplerian elements. These elements are also known as the orbit parameters [Sidi, 1997] and are described as:

- a_{s}, the semi major axis
- e_{o}, the orbit eccentricity
- i_{e}, the inclination to the equatorial plane
- Ω_{a}, the Right Ascension of the Ascending Node
- ω, the argument of perigee
- M_{a}, the mean anomaly

Where a_{s} is the distance from the Perigee (the point closest to the Earth) to the centre of the ellipsoid. The eccentricity e_{o} is the relation between the distance from the focus point F (Earth's centre of mass) to the centre of the ellipsoid c_{F} (see Figure 2.7) and a_{s}. The eccentricity is given as:

$$e_{\mathrm{o}} = \frac{c_{\mathrm{F}}}{a_{\mathrm{s}}} \tag{2.1}$$

The parameters i_{e}, Ω_{a}, ω and M_{a} will be described in the following sections. The eccentricity basically describes the shape of the orbit. If $e_{\mathrm{o}} = 0$ the orbit is a *Circular Orbit* with the radius of a_{s}. For an *Elliptic Orbit* the eccentricity value is within $0 < e_{\mathrm{o}} < 1$. If $e_{\mathrm{o}} > 1$ the orbit is hyperbolic which means that the total energy of the satellite is $E_{\mathrm{total}} > 0$. This means that the kinetic energy of the satellite is larger than the potential

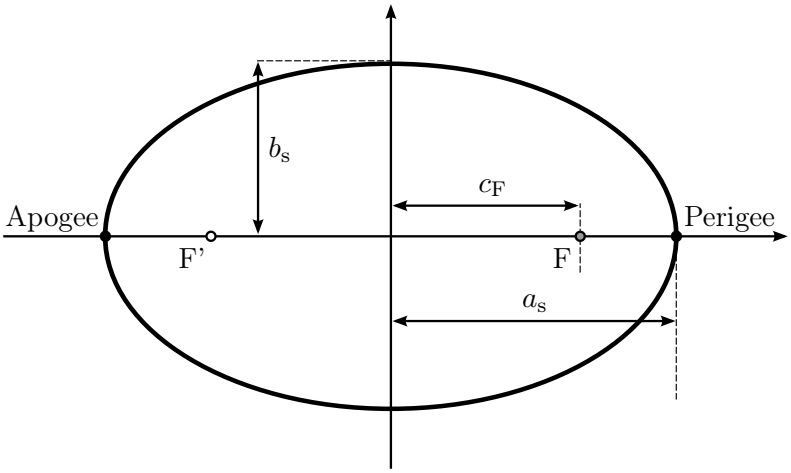

Figure 2.7: Geometric definition of the Keplerian elliptic orbit, where F is the primary focus point and F' is the secondary focus point. a_s is the semi major axis and b_s is the semi minor axis along with c_F describing the distance from the main focus point F to the centre of the orbit [Sidi, 1997].

energy, which makes it possible for the satellite to escape the gravitational attraction of the Earth.

In the previous section 2.1 the inertial Earth reference frame was defined. This initial coordinate system makes it possible to describe an orientation of an orbit relative to the Earth. Recall the orbit parameters. These are pictured in Figure 2.8 where the inclination i_e is the angle between the orbit plane and the equatorial plane of the Earth. The Right Ascension of the Ascending Node Ω_a is the angle between the vernal equinox x_Υ and the ascending node. The argument of perigee ω is the angle between the perigee vector and the node line.

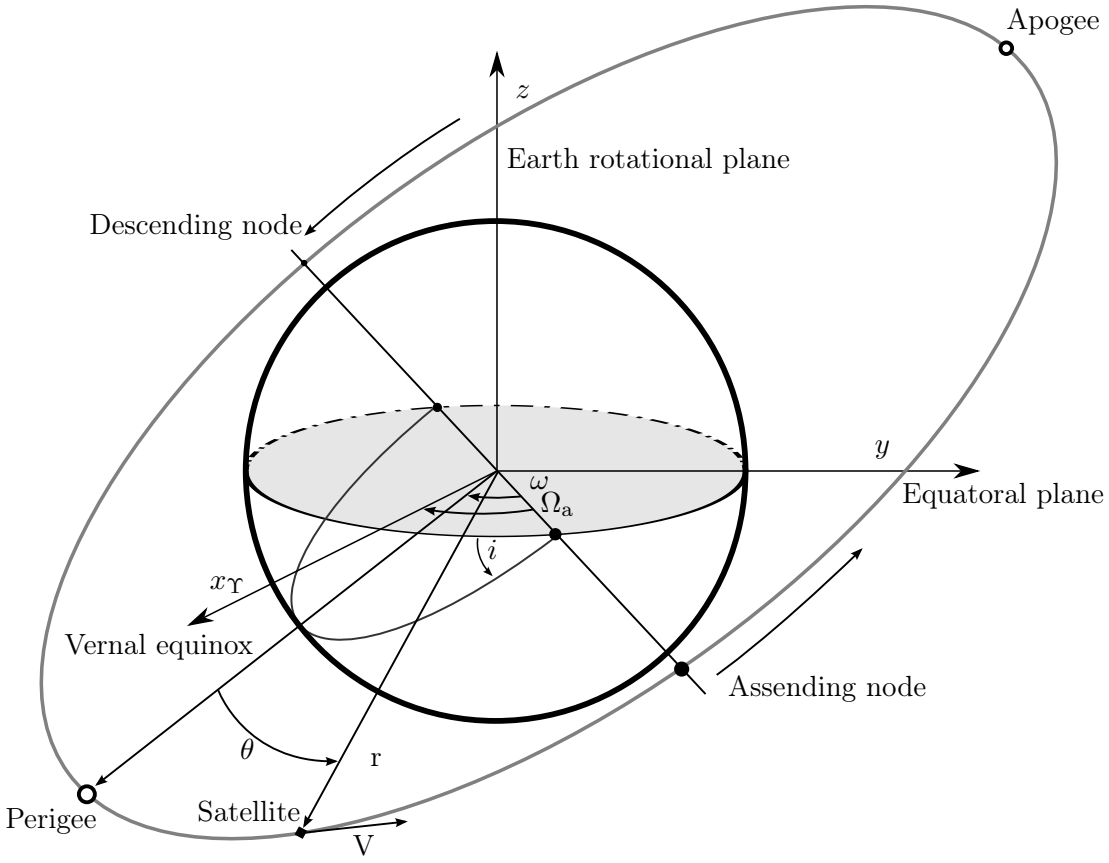

Figure 2.8: Shows a satellite's orbit around the Earth, where the orbit parameters describes orientation of the orbital plane in relation to the Earth's inertial reference frame. i_e is the orbits inclination relative to the equatorial plane. Ω_a is the Right Ascension of the Ascending Node, describing the angle between the vernal equinox and the point where the orbital plane coincide with the equatorial plane. ω is the argument of perigee and described the angle between the vernal equinox axis x_Υ and the Ascending node [Sidi, 1997].

M_a is the *mean anomaly* which describes the angle the satellite has moved since last perigee passage, viewed form the centre of the Earth. The *mean anomaly*, M_a is only a good approximation assuming the orbit is circular [Wertz, 1995]. The mean anomaly is calculated as follows:

$$M_a = 360^\circ \cdot \frac{\Delta t}{P_t} \tag{2.2}$$

where:

Δt	is the time since last perigee passage	[s]
P_t	is the orbital period	[s]

(2.3)

To calculate the *true anomaly*, v_a, of a Keplerian orbit, M_a must first be evaluated and the eccentricity anomaly, E_a, is introduced and illustrated in Figure 2.9. The eccentricity anomaly E_a is the angle between the object in orbit and the perigee viewed from the centre of the orbit. Equation 2.4 describes the relation between M_a and E_a.

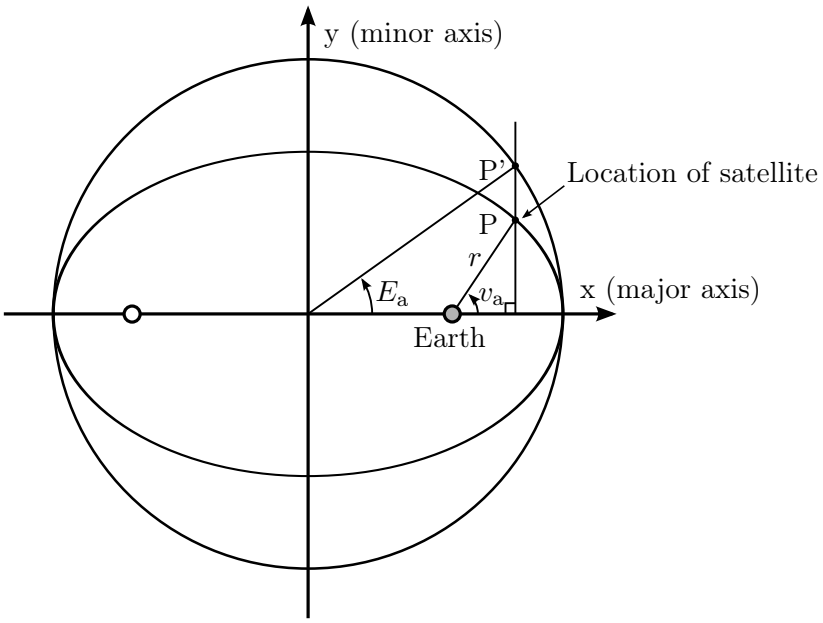

Figure 2.9: Definition of true anomaly, v_a, which is the angle between the perigee and the current position of the satellite on a Keplerian orbit viewed form the focus point. The eccentricity anomaly, E_a is the angle between the perigee and the current position of the satellite on a circular orbit viewed from the centre of the orbit. The outer circle is an orbit with $e_o = 0$ [Wertz, 1995].

$$M_a(t) = 360^\circ \cdot \frac{\Delta t}{P_t} = E_a(t) - e_o \cdot \sin E_a(t) \tag{2.4}$$

The *true anomaly*, v_a, is then related to E_a.

$$\tan \frac{v_a(t)}{2} = \left(\frac{1+e_o}{1-e_o}\right)^{1/2} \tan \frac{E(t)}{2} \tag{2.5}$$

The use of Keplerian orbits are accurate enough to describe general mission characteristics, such as altitude and orbit period. The attitude determination requires more parameters and makes the orbit description irrelevant for the ACS, however when it comes to analyzing the disturbances acting on the satellite, the orbit description can be used in describing these disturbance models. This knowledge will insure versatility in the satellite attitude controller.

2.3 Parametrization of the attitude

As an extension of the reference frames, the next topic to discuss is the rotation of these reference frames relative to each other. In a three dimensional space every attitude and movement can be described by rotations. These rotations are described relative to a reference frame thus making it possible to define rotations for each of the defined reference frames to convert coordinates between reference frames. During a rotation it is important that the rotation preserves orthogonality of the frame being rotated. A brief description of the applicable parametrization of attitude is presented in the following. Afterwards the chosen parametrization is described further.

Rotation matrix

A rotation matrix is a general method of describing some orientation relative to a reference frame. The rotation matrix is a real orthonormal matrix with a determinant of one [Wertz, 1995]. Being real and orthonormal means that a rotation can be reversed by multiplying by its inverse. A rotation matrix consists of a set of three orthonormal vectors which forms a basis in a reference frame. A rotation matrix consists of a set of 9 parameters making it "expensive" to store [Bak, 1999].

Euler angles

In space, every attitude can be represented by three consecutive rotations, about the three axes of the particular reference frame. This means that every attitude can be obtained by e.g. a 3-2-3 sequence of rotations where three and two are respectively the z-axis and the y-axis. These sequences are not commutative. The direction cosine matrices for x, y and z-axis rotations can be seen on (2.6) [Wertz, 1995].

$$\begin{aligned}\underline{\mathbf{R}}_1(\Phi) &= \begin{bmatrix}1 & 0 & 0\\ 0 & \cos(\Phi) & \sin(\Phi)\\ 0 & -\sin(\Phi) & \cos(\Phi)\end{bmatrix} \quad \underline{\mathbf{R}}_2(\Phi) = \begin{bmatrix}\cos(\Phi) & 0 & -\sin(\Phi)\\ 0 & 1 & 0\\ \sin(\Phi) & 0 & \cos(\Phi)\end{bmatrix}\\ \underline{\mathbf{R}}_3(\Phi) &= \begin{bmatrix}\cos(\Phi) & \sin(\Phi) & 0\\ -\sin(\Phi) & \cos(\Phi) & 0\\ 0 & 0 & 1\end{bmatrix}\end{aligned} \tag{2.6}$$

These rotation matrices can be represented in general by [Wertz, 1995]:

$$\begin{aligned}\underline{\mathbf{R}} &= \begin{bmatrix}\cos(\Phi)+u_1^2(1-\cos(\Phi)) & u_1u_2(1-\cos(\Phi))+u_3\sin(\Phi) & u_1u_3(1-\cos(\Phi))-u_2\sin(\Phi)\\ u_1u_2(1-\cos(\Phi))-u_3\sin(\Phi) & \cos(\Phi)+u_2^2(1-\cos(\Phi)) & u_2u_3(1-\cos(\Phi))+u_1\sin(\Phi)\\ u_1u_3(1-\cos(\Phi))+u_2\sin(\Phi) & u_2u_3(1-\cos(\Phi))-u_1\sin(\Phi) & \cos(\Phi)+u_3^2(1-\cos(\Phi))\end{bmatrix}\\ &= \cos(\Phi)\underline{\mathbf{1}}_{3\times3} + (1-\cos(\Phi))\bar{\boldsymbol{u}}\bar{\boldsymbol{u}}^{\mathrm{T}} - \sin(\Phi)\underline{\mathbf{U}}\end{aligned} \tag{2.7}$$

$\bar{\boldsymbol{u}} = \begin{bmatrix}u_1\\ u_2\\ u_3\end{bmatrix}$ is a unit vector, and the rotation matrix $\underline{\mathbf{R}}$ describes a rotation about it for Φ degrees. Then $\underline{\mathbf{U}}$:

$$\underline{\mathbf{U}} = \begin{bmatrix}0 & -u_3 & u_2\\ u_3 & 0 & -u_1\\ -u_2 & u_1 & 0\end{bmatrix} \tag{2.8}$$

The angles that are being used are called Euler angles. This sequential way of doing attitude representation suffers from singularities for some rotations. This is called a gimbal lock where two rotation axes can align and then two different rotations results in the same movement.

Quaternions

Because of quaternion's linear kinematic equations and because they have no singularities they are widely used as attitude representations [Wertz, 1995]. Two rotations can easily be combined by using multiplication, they have set of parameters consisting of only four values.

In Table 2.1 the described rotation methods are summed up [Bak, 1999].

Representation	Par.	Characteristics	Applications
Rotation matrix	9	- Inherently nonsingular - Intuitive representation - Difficult to maintain orthogonality - Expensive to store - Six redundant parameters	Analytical studies and transformation of vectors.
Euler angles	3	- Minimal set - Clear physical interpretation - Trigonometric functions in rotation matrix - No simple composition rule - Singular for certain rotations - Trigonometric functions in kinematic relation	Theoretical physics, spinning spacecraft and attitude maneuvers. Used in analytical studies.
Quaternions	4	- Easy orthogonality of rotation matrix - Bilinear composition rule - Not singular at any rotation - Linear kinematic equation - No clear physical interpretation - One redundant parameter - Simple kinematic relation	Widely used in simulations and data processing. Preferred attitude representation for attitude control systems.

Table 2.1: Different methods for describing algebraic rotations [Bak, 1999]

Due to the easy orthogonality, no singularities and the simple kinematic equations; quaternions will be the chosen for attitude representation.

2.3.1 Quaternions

In the following section, quaternions will be described. Quaternions provide a convenient method for describing algebraic rotations in a three dimensional space; just as complex numbers do in a plane [Kuipers, 2002]. Firstly the basics of quaternions will be described.

The quaternion $\mathbf{q}$ is written as:

$$\mathbf{q} \equiv q_0 + \bar{\boldsymbol{i}} q_1 + \bar{\boldsymbol{j}} q_2 + \bar{\boldsymbol{k}} q_3 \tag{2.9}$$

Where $\bar{\boldsymbol{i}}, \bar{\boldsymbol{j}}$ and $\bar{\boldsymbol{k}}$ are vectors forming a orthonormal basis in $\mathbb{R}^3$. The quaternion can also be written as a vector part and a real part:

$$\mathbf{q} = q_0 + \bar{\boldsymbol{q}} = \begin{bmatrix} q_0 \\ \bar{\boldsymbol{q}} \end{bmatrix} \tag{2.10}$$

Where the vector $\bar{\boldsymbol{q}}$ is a vector in $\mathbb{R}^3$. Furthermore $\bar{\boldsymbol{i}}$, $\bar{\boldsymbol{j}}$ and $\bar{\boldsymbol{k}}$ are hyper complex numbers which satisfies the following[Kuipers, 2002]:

$$\begin{aligned} \bar{\boldsymbol{i}}^2 = \bar{\boldsymbol{j}}^2 = \bar{\boldsymbol{k}}^2 = \bar{\boldsymbol{i}}\bar{\boldsymbol{j}}\bar{\boldsymbol{k}} = -1 \\ \bar{\boldsymbol{i}}\bar{\boldsymbol{j}} = \bar{\boldsymbol{k}} = -\bar{\boldsymbol{j}}\bar{\boldsymbol{i}} \\ \bar{\boldsymbol{j}}\bar{\boldsymbol{k}} = \bar{\boldsymbol{i}} = -\bar{\boldsymbol{k}}\bar{\boldsymbol{j}} \\ \bar{\boldsymbol{k}}\bar{\boldsymbol{i}} = \bar{\boldsymbol{j}} = -\bar{\boldsymbol{i}}\bar{\boldsymbol{k}} \end{aligned} \tag{2.11}$$

By (2.11) it can be seen that quaternion multiplication is not commutative. Multiplication of two quaternions can be done by [Kuipers, 2002]:

$$\begin{aligned}
\mathbf{q} &= q_0 + \bar{\boldsymbol{i}} q_1 + \bar{\boldsymbol{j}} q_2 + \bar{\boldsymbol{k}} q_3 \\
\mathbf{p} &= p_0 + \bar{\boldsymbol{i}} p_1 + \bar{\boldsymbol{j}} p_2 + \bar{\boldsymbol{k}} p_3 \\
\mathbf{q} \otimes \mathbf{p} &= \left(q_0 + \bar{\boldsymbol{i}} q_1 + \bar{\boldsymbol{j}} q_2 + \bar{\boldsymbol{k}} q_3\right)\left(p_0 + \bar{\boldsymbol{i}} p_1 + \bar{\boldsymbol{j}} p_2 + \bar{\boldsymbol{k}} p_3\right) \\
&= \left(q_0 p_0 - q_1 p_1 - q_2 p_2 - q_3 p_3\right) \\
&\quad + \bar{\boldsymbol{i}}\left(q_1 p_0 + q_2 p_3 - q_3 p_2 + q_0 p_1\right) \\
&\quad + \bar{\boldsymbol{j}}\left(-q_1 p_3 + q_2 p_0 + q_3 p_1 + q_0 p_2\right) \\
&\quad + \bar{\boldsymbol{k}}\left(q_1 p_2 - q_2 p_1 + q_3 p_0 + q_0 p_3\right) \\
&= q_0 \cdot p_0 - \bar{\boldsymbol{q}} \bullet \bar{\boldsymbol{p}} + q_0 \cdot \bar{\boldsymbol{p}} + p_0 \cdot \bar{\boldsymbol{q}} + \bar{\boldsymbol{q}} \times \bar{\boldsymbol{p}}
\end{aligned} \tag{2.12}$$

This can be written as a multiplication between a matrix and a vector such that:

$$\mathbf{q} \otimes \mathbf{p} = \begin{bmatrix} q_0 & -q_1 & -q_2 & -q_3 \\ q_1 & q_0 & -q_3 & q_2 \\ q_2 & q_3 & q_0 & -q_1 \\ q_3 & -q_2 & q_1 & q_0 \end{bmatrix} \begin{bmatrix} p_0 \\ p_1 \\ p_2 \\ p_3 \end{bmatrix} \tag{2.13}$$

If a quaternion is:

$$\mathbf{q} = q_0 + \bar{\boldsymbol{q}} = q_0 + \bar{\boldsymbol{i}} q_1 + \bar{\boldsymbol{j}} q_2 + \bar{\boldsymbol{k}} q_3 \tag{2.14}$$

then the complex conjugated $\mathbf{q}^*$ is [Kuipers, 2002]:

$$\mathbf{q}^* = q_0 - \bar{\boldsymbol{q}} = q_0 - \bar{\boldsymbol{i}} q_1 - \bar{\boldsymbol{j}} q_2 - \bar{\boldsymbol{k}} q_3 \tag{2.15}$$

The norm $|\mathbf{q}|$ of a quaternion is [Kuipers, 2002]:

$$|\mathbf{q}| = \sqrt{\mathbf{q}^* \otimes \mathbf{q}} = \sqrt{(q_0 - \bar{\boldsymbol{q}}) \otimes (q_0 + \bar{\boldsymbol{q}})} \tag{2.16}$$

The inverse $\mathbf{q}^{-1}$ of a quaternion is:

$$\mathbf{q}^{-1} = \frac{\mathbf{q}^*}{|\mathbf{q}|^2} \tag{2.17}$$

Quaternions and rotations

In the complex plane any complex number $z = a + bi$ maps to a unique point in $\mathbb{R}^2$. This point can be rotated around origin by multiplication by a complex number with norm 1. This can be done in $\mathbb{R}^3$ by using unit quaternions. A unit quaternion can be constructed as [Kuipers, 2002]:

$$|\mathbf{q}| = 1 \;\Rightarrow\; \mathbf{q} = q_0 + \bar{\boldsymbol{q}} = \cos\left(\frac{\Phi}{2}\right) + \bar{\boldsymbol{u}} \sin\left(\frac{\Phi}{2}\right) \tag{2.18}$$

Where $\bar{\boldsymbol{u}}$ is a *pure* quaternion with $|\bar{\boldsymbol{u}}| = 1$ and Φ is the degrees for rotation. A *pure* quaternion is a quaternion with a zero real part. A rotation of a vector can be done by:

$$\bar{\boldsymbol{n}} = \mathbf{q} \otimes \bar{\boldsymbol{v}} \otimes \mathbf{q}^* \tag{2.19}$$

Where the vector $\bar{\boldsymbol{v}}$ is rotated around $\bar{\boldsymbol{u}}$, Φ degrees this is depicted on Figure 2.10.

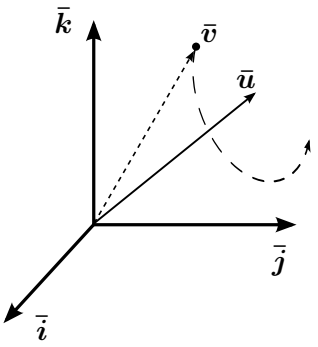

Figure 2.10: A quaternion rotation around $\bar{u}$.

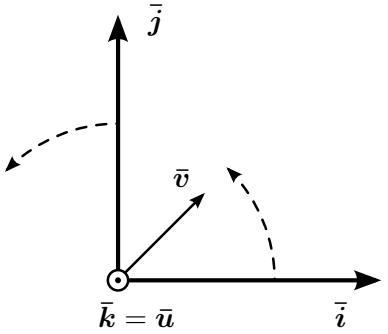

Figure 2.11: Frame rotation around $\bar{k}$.

If instead the vector $\bar{v}$ is considered fixed and $\bar{u}$ is chosen as $\bar{i}$, $\bar{j}$ or $\bar{k}$; recall that $\bar{u}$ is a part of $\mathbf{q}$. Then the reference frame is rotated around this element, the rotation is then constructed as:

$$\bar{w} = \mathbf{q}^* \otimes \bar{v} \otimes \mathbf{q} \tag{2.20}$$

An example of frame rotation around $\mathbf{k}$ is depicted in Figure 2.11. If for example a frame needs two successive rotations this can be done by:

$$\begin{aligned} \bar{w} &= \mathbf{q}^* \otimes \bar{v} \otimes \mathbf{q} \\ \mathbf{p}^* \otimes \bar{w} \otimes \mathbf{p} &= \mathbf{p}^* \otimes (\mathbf{q}^* \otimes \bar{v} \otimes \mathbf{q}) \otimes \mathbf{p} = (\mathbf{q} \otimes \mathbf{p})^* \otimes \bar{v} \otimes (\mathbf{q} \otimes \mathbf{p}) \end{aligned} \tag{2.21}$$

This means that multiple successive rotations, here two, can be done by multiplying the quaternions to create a combined quaternion to be used for a rotation. Notice the sequence of rotations in equation (2.21) the frame is first rotated by $\mathbf{q}$ then by $\mathbf{p}$.

2.3.2 Constructing a quaternion rotation operator

In equation (2.20) a rotation of a reference frame about a basis vector is constructed. Suppose that this where to be implemented in an embedded system this would be computationally heavy because of the many calculations. If instead this could be distilled into a single matrix, this would be preferable opposed to the current, due to the fact that a rotation will then be done by only one matrix multiplication. In the following the reasoning behind and the procedure is discussed. The rotation operator is denoted by:

$$L_q(\bar{v}) = \mathbf{q}^* \otimes \bar{v} \otimes \mathbf{q} \tag{2.22}$$

This amounts to the following computation [Kuipers, 2002]:

$$L_q(\bar{v}) = \left(2q_0^2 - 1\right)\bar{v} + 2\bar{q}\left(\bar{v}\bar{q}^T\right) + 2q_0\left(\bar{v} \times \bar{q}\right) \tag{2.23}$$

This can be presented in matrix form by observing the different parts of (2.23) as matrices [Kuipers, 2002].

The first part of (2.23) can be written as:

$$\left(2q_0^2 - 1\right)\bar{v} = \begin{bmatrix} \left(2q_0^2 - 1\right) & 0 & 0 \\ 0 & \left(2q_0^2 - 1\right) & 0 \\ 0 & 0 & \left(2q_0^2 - 1\right) \end{bmatrix} \begin{bmatrix} v_1 \\ v_2 \\ v_3 \end{bmatrix} \tag{2.24}$$

The second part:

$$2\bar{q}\left(\bar{v}\bar{q}^T\right) = \begin{bmatrix} 2q_1^2 & 2q_1q_2 & 2q_1q_3 \\ 2q_1q_2 & 2q_2^2 & 2q_2q_3 \\ 2q_1q_3 & 2q_2q_3 & 2q_3^2 \end{bmatrix} \begin{bmatrix} v_1 \\ v_2 \\ v_3 \end{bmatrix} \tag{2.25}$$

Third part:

$$2q_0\left(\bar{\boldsymbol{v}}\times\bar{\boldsymbol{q}}\right)=\begin{bmatrix}0 & 2q_0q_3 & -2q_0q_2\\ -2q_0q_3 & 0 & 2q_0q_1\\ 2q_0q_2 & -2q_0q_1 & 0\end{bmatrix}\begin{bmatrix}v_1\\ v_2\\ v_3\end{bmatrix} \tag{2.26}$$

This can now be collected into one matrix as:

$$\bar{\boldsymbol{w}}=L_q(\bar{\boldsymbol{v}})=\underline{\mathbf{R}}\bar{\boldsymbol{v}}=\begin{bmatrix}2q_0^2-1+2q_1^2 & 2q_1q_2+2q_0q_3 & 2q_1q_3-2q_0q_2\\ 2q_1q_2-2q_0q_3 & 2q_0^2-1+2q_2^2 & 2q_2q_3+2q_0q_1\\ 2q_1q_3+2q_0q_2 & 2q_2q_3-2q_0q_1 & 2q_0^2-1+2q_3^2\end{bmatrix}\begin{bmatrix}v_1\\ v_2\\ v_3\end{bmatrix} \tag{2.27}$$

A method for constructing a rotation operator is now constructed. If an operator needs to be constructed of multiple rotations, a $\mathbf{q}$ needs to be made by using the method of (2.21) and then the same steps shown from (2.23) to (2.27) on that new $\mathbf{q}$.

2.4 Reference frame translations

Now that a Quaternion rotation operator is defined, the next step is to find the specific rotation operators to convert between the reference frames defined in section 2.1. It might be convenient to express some orientations and vectors in one reference frame for a particular calculation and another frame for another calculation. This could for example be calculations for the control algorithms which will be performed in SCRF but the pointing of the satellite will be performed by the SBRF. When an attitude estimation is received from ADS it is represented in ECI, this renders it necessary for a rotation between these two frames. The necessary rotations are identified and derived in the following.

2.4.1 Rotation between ECI and ORF

In section 2.1.3 the ORF is described; it states that the ORF's z_0 axis always points in nadir and the x_0 axis is parallel to the satellites velocity vector. With these two statements, it is possible to derive the relation between ECI and the ORF. First off, the nadir vector can be obtained from the Two-Line Element (TLE), see Appendix A, simply by taking the directionality vector given in ECI, normalize it and reverse it.

$${}^{\mathrm{o}}\bar{\boldsymbol{z}}_0=\frac{1}{\sqrt{{}^{\mathrm{i}}x_0^2+{}^{\mathrm{i}}y_0^2+{}^{\mathrm{i}}z_0^2}}\begin{bmatrix}-{}^{\mathrm{i}}x_0\\ -{}^{\mathrm{i}}y_0\\ -{}^{\mathrm{i}}z_0\end{bmatrix} \tag{2.28}$$

The x_0 axis is the normalized velocity vector.

$${}^{\mathrm{o}}\bar{\boldsymbol{x}}_0=\frac{1}{\sqrt{{}^{\mathrm{i}}x_0^2+{}^{\mathrm{i}}y_0^2+{}^{\mathrm{i}}z_0^2}}\begin{bmatrix}{}^{\mathrm{i}}\dot{x}_0\\ {}^{\mathrm{i}}\dot{y}_0\\ {}^{\mathrm{i}}\dot{z}_0\end{bmatrix} \tag{2.29}$$

And the right handed cross product as the y_0 axis.

$${}^{\mathrm{o}}\bar{\boldsymbol{y}}_0={}^{\mathrm{o}}\bar{\boldsymbol{z}}_0\times{}^{\mathrm{o}}\bar{\boldsymbol{x}}_0 \tag{2.30}$$

This amount to the rotation matrix between ORF and ECI:

$${}^{\mathrm{o}}_{\mathrm{i}}\underline{\mathbf{R}}=\begin{bmatrix}{}^{\mathrm{o}}\bar{\boldsymbol{x}}_0 & {}^{\mathrm{o}}\bar{\boldsymbol{y}}_0 & {}^{\mathrm{o}}\bar{\boldsymbol{z}}_0\end{bmatrix} \tag{2.31}$$

This matrix can be converted to a quaternion by observing the matrix $\underline{\mathbf{R}}$ from equation (2.27):

$$\underline{\mathbf{R}}=\begin{bmatrix}2q_0^2-1+2q_1^2 & 2q_1q_2+2q_0q_3 & 2q_1q_3-2q_0q_2\\ 2q_1q_2-2q_0q_3 & 2q_0^2-1+2q_2^2 & 2q_2q_3+2q_0q_1\\ 2q_1q_3+2q_0q_2 & 2q_2q_3-2q_0q_1 & 2q_0^2-1+2q_3^2\end{bmatrix} \tag{2.32}$$

From this matrix it can be seen that [Kuipers, 2002] (recall that the norm of the quaternion is 1):

$$\begin{aligned} 4q_0^2 - 1 &= r_{11} + r_{22} + r_{33} \\ 4q_0q_1 &= r_{23} - r_{32} \\ 4q_0q_2 &= r_{31} - r_{13} \\ 4q_0q_3 &= r_{12} - r_{21} \end{aligned} \tag{2.33}$$

Hence the quaternion can be written as:

$$\begin{aligned} {}^{\mathrm{o}}_{\mathrm{i}}q_0 &= \frac{1}{2}\sqrt{r_{11} + r_{22} + r_{33} + 1} \\ {}^{\mathrm{o}}_{\mathrm{i}}q_1 &= \frac{(r_{23} - r_{32})}{4q_0} \\ {}^{\mathrm{o}}_{\mathrm{i}}q_2 &= \frac{(r_{31} - r_{13})}{4q_0} \\ {}^{\mathrm{o}}_{\mathrm{i}}q_3 &= \frac{(r_{12} - r_{21})}{4q_0} \end{aligned} \tag{2.34}$$

2.4.2 Rotation between ECI and ECEF

In section 2.1.1 and section 2.1.2 ECEF and ECI are described. It states that these two reference frames share the same z axis and have xy plane in the equatorial plane. The ECI is rotating about the z axis and the ECEF is fixed. Furthermore the x and y axises of the two frames coincides two times per day.

With these statements it is possible to derive the relation between them. A direction cosine matrix designed to rotate about the z axis looks as follows:

$${}^{\mathrm{f}}_{\mathrm{i}}\underline{\mathbf{R}} = \begin{bmatrix} \cos(\theta) & -\sin(\theta) & 0 \\ \sin(\theta) & \cos(\theta) & 0 \\ 0 & 0 & 1 \end{bmatrix} \tag{2.35}$$

The fact that the x and y axises coincides once a day can be used to obtain the angle between ECI and ECEF. One day is defined to be 86164.09055 s - a sidereal day. A side real day is defined as one complete rotation of the Earth relative to the stars [Wertz, 1995].

This means that the angle θ as a function of time is:

$$\theta = \frac{2\pi t}{86164.09055} \tag{2.36}$$

Where

$$t \qquad \text{is the time since last alignment} \qquad [s]$$

The direction cosine matrix ${}^{\mathrm{f}}_{\mathrm{i}}\underline{\mathbf{R}}$ can be written as a quaternion as [Kuipers, 2002]:

$$\begin{aligned} {}^{\mathrm{f}}_{\mathrm{i}}q_0 &= \frac{1}{2}\sqrt{r_{11} + r_{22} + r_{33} + 1} = \sqrt{\frac{1 + \cos(\theta)}{2}} \\ {}^{\mathrm{f}}_{\mathrm{i}}q_1 &= \frac{(r_{23} - r_{32})}{4q_0} = 0 \\ {}^{\mathrm{f}}_{\mathrm{i}}q_2 &= \frac{(r_{31} - r_{13})}{4q_0} = 0 \\ {}^{\mathrm{f}}_{\mathrm{i}}q_3 &= \frac{(r_{12} - r_{21})}{4q_0} = \frac{-\sqrt{2}\sin(\theta)}{2\sqrt{1 + \cos(\theta)}} \end{aligned} \tag{2.37}$$

2.4.3 Rotation between ECI and SBRF

The rotation between ECI and SBRF is the satellites attitude in ECI. This means that the attitude determination system is the one calculating this rotation, and is outside the scope of this project. The attitude determination system returns a quaternion which describes the rotation.

2.4.4 Rotation between SBRF and SCRF

In section 2.1.4 and in section 2.1.4 the SBRF and SCRF are defined. SBRF is defined as having origin in CoM with ${}^{\mathrm{s}}z$ axis pointing opposite the antenna side panel, ${}^{\mathrm{s}}x$ axis pointing along the direction of the batteries and ${}^{\mathrm{s}}y$ axis as a right handed crossproduct of the two. The SCRF is defined as the principal axes of the inertia matrix in SBRF.

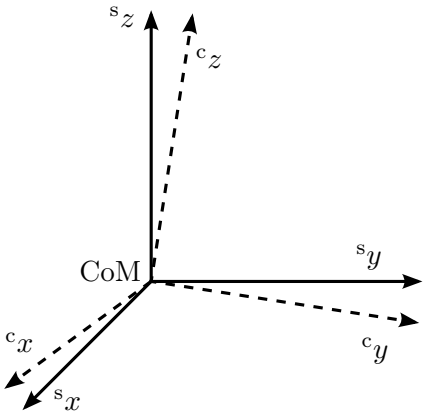

Figure 2.12: Example SCRF and SBRF their relative orientation.

The inertia matrix in SBRF is a real symmetric matrix, this allows for an Eigenvalue decomposition of the matrix. The Eigenvalue decomposition results in two matrices, one diagonal matrix containing the eigenvalues and one consisting of the eigenvectors. The resulting diagonal matrix will form an orthonormal basis with eigenvalues describing the principal moments of inertia [Sylvester, 1852]. An example:

$$\underline{\mathbf{A}} = \underline{\mathbf{R}}\,\underline{\mathbf{\Lambda}}\,\underline{\mathbf{R}}^{-1} \tag{2.38}$$

This calculation is done in section 2.8.2. The matrix that diagonalize the inertia matrix is the rotation matrix $\underline{\mathbf{R}}$; which rotates a vector in SBRF to a vector in SCRF. It can be seen below:

$${}^{\mathrm{c}}_{\mathrm{s}}\underline{\mathbf{R}} = \begin{bmatrix} 0.1608 & -0.7488 & -0.6430 \\ 0.5374 & 0.6129 & -0.5793 \\ 0.8278 & -0.2524 & 0.5010 \end{bmatrix} \tag{2.39}$$

The quaternion describing this particular rotation can be calculated as:

$$\begin{aligned} {}^{\mathrm{c}}_{\mathrm{s}}q_0 &= \frac{1}{2}\sqrt{r_{11}+r_{22}+r_{33}+1} = \frac{1}{2}\sqrt{0.1608+0.6129+0.5010+1} = 0.7541 \\ {}^{\mathrm{c}}_{\mathrm{s}}q_1 &= \frac{(r_{23}-r_{32})}{4q_0} = \frac{(-0.5793+0.2524)}{4\cdot 0.7541} = -0.1084 \\ {}^{\mathrm{c}}_{\mathrm{s}}q_2 &= \frac{(r_{31}-r_{13})}{4q_0} = \frac{(0.8278+0.6430)}{4\cdot 0.7541} = 0.4876 \\ {}^{\mathrm{c}}_{\mathrm{s}}q_3 &= \frac{(r_{12}-r_{21})}{4q_0} = \frac{(-0.7488-0.5374)}{4\cdot 0.7541} = -0.4264 \end{aligned} \tag{2.40}$$

2.5 Equations of motion

In this section the relations between both the angular velocity and orientation and between the the angular acceleration and angular velocity will be derived. The following section is based on the following sources: [Wertz, 1995], [Vinter and Jensen, 2010] and [Bak, 1999].

2.5.1 Kinematic equation

Let $\mathbf{q}(t)$ be the quaternion that describes the orientation from one reference frame to another at the time t. $\mathbf{q}(t + \Delta t)$ is then the orientation at the time $t + \Delta t$. This can be split into the rotation $\mathbf{q}(t)$ and the additional rotation $\mathbf{q}'(\Delta t)$ which is the rotation at time $t + \Delta t$ compared to the time t. As shown in (2.21) two consecutive rotations can be described as the quaternion multiplication of the two giving.

$$\mathbf{q}(t + \Delta t) = \mathbf{q}(t) \otimes \mathbf{q}'(\Delta t) \tag{2.41}$$

As stated in (2.18) a quaternion can be divided into a real part and a pure quaternion. When dividing $\mathbf{q}'(\Delta t)$ the following four parts are obtained:

$$\begin{aligned} q'_0(\Delta t) &= \cos\left(\frac{\Delta\Phi}{2}\right) \\ q'_1(\Delta t) &= u_1 \sin\left(\frac{\Delta\Phi}{2}\right) \\ q'_2(\Delta t) &= u_2 \sin\left(\frac{\Delta\Phi}{2}\right) \\ q'_3(\Delta t) &= u_3 \sin\left(\frac{\Delta\Phi}{2}\right) \end{aligned} \tag{2.42}$$

Where Φ is the rotation, $\Delta\Phi$ the rotation from time t to time $t + \Delta t$ and $\bar{\boldsymbol{u}}$ the pure quaternion from (2.18). Letting $\Delta\Phi$ be an infinitesimal small angle which can be approximated as:

$$\begin{aligned} \cos\left(\frac{\Delta\Phi}{2}\right) &\approx 1 \\ \sin\left(\frac{\Delta\Phi}{2}\right) &\approx \frac{1}{2}\omega\Delta t \end{aligned} \tag{2.43}$$

Where ω is the angular velocity [rad/s]. As described in (2.13) a quaternion multiplication can be described as a matrix multiplied by a quaternion. By using this and inserting (2.43) in (2.41) the following is obtained:

$$\mathbf{q}(t + \Delta t) \approx \left(\underline{\mathbf{1}}_{4\times4} + \frac{1}{2}\omega\Delta t \begin{bmatrix} 0 & -u_1 & -u_2 & -u_3 \\ u_1 & 0 & -u_3 & u_2 \\ u_2 & u_3 & 0 & -u_1 \\ u_3 & -u_2 & u_1 & 0 \end{bmatrix} \right) \mathbf{q}(t) \tag{2.44}$$

Where $\underline{\mathbf{1}}_{4\times4}$ is a 4 by 4 identity matrix and $\underline{\mathbf{u}}$ is a skew symmetric matrix obtained as described in (2.13). This can be rewritten as:

$$\frac{\mathbf{q}(t + \Delta t) - \mathbf{q}(t)}{\Delta t} = \frac{1}{2}\underline{\boldsymbol{\Omega}}(t)_{4\times4} \cdot \mathbf{q}(t) \tag{2.45}$$

Where:

$$\underline{\boldsymbol{\Omega}}(t)_{4\times4} = \begin{bmatrix} 0 & -\omega_1(t) & -\omega_2(t) & -\omega_3(t) \\ \omega_1(t) & 0 & -\omega_3(t) & \omega_2(t) \\ \omega_2(t) & \omega_3(t) & 0 & -\omega_1(t) \\ \omega_3(t) & -\omega_2(t) & \omega_1(t) & 0 \end{bmatrix}, \bar{\boldsymbol{\omega}} = \omega\bar{\boldsymbol{u}} \tag{2.46}$$

By letting Δt go towards 0 the derivative of $\mathbf{q}(t)$ can be found, resulting in the kinematic equation of the satellite:

$$\dot{\mathbf{q}}(t) = \lim_{\Delta t\to 0} \frac{\mathbf{q}(t+\Delta t) - \mathbf{q}(t)}{\Delta t} = \frac{1}{2}\underline{\boldsymbol{\Omega}}(t)_{4\times4} \cdot \mathbf{q}(t) \tag{2.47}$$

Notice that a change in the rotation quaternion corresponds to a change in orientation of the satellite.

Likewise is the quaternion rotation operator split up as in (2.41).

$$\underline{\mathbf{R}}(t+\Delta t) = \underline{\mathbf{R}}(t) \cdot \underline{\mathbf{R}}'(\Delta t) \tag{2.48}$$

A general direction cosine matrix is given as described in (2.7) by:

$$\underline{\mathbf{R}} = \cos(\Phi)\underline{\mathbf{1}}_{3\times3} + (1-\cos(\Phi))\bar{\boldsymbol{u}}\bar{\boldsymbol{u}}^T - \sin(\Phi)\underline{\mathbf{U}} \tag{2.49}$$

Where Φ is the rotation about the vector $\bar{\boldsymbol{u}}$ then:

$$\underline{\mathbf{U}} = \begin{bmatrix} 0 & -u_3 & u_2 \\ u_3 & 0 & -u_1 \\ -u_2 & u_1 & 0 \end{bmatrix} \tag{2.50}$$

By using the same small angle approximations as in (2.43) it becomes:

$$\underline{\mathbf{R}}(t+\Delta t) = \left(\underline{\mathbf{1}}_{3\times3} - \omega\Delta t\underline{\mathbf{U}}\right)\underline{\mathbf{R}}(t) \tag{2.51}$$

which reveals that:

$$\dot{\underline{\mathbf{R}}}(t) = -\underline{\boldsymbol{\Omega}}_{3\times3}\underline{\mathbf{R}}(t) \tag{2.52}$$

where:

$$\underline{\boldsymbol{\Omega}}_{3\times3} = \begin{bmatrix} 0 & -\omega_3 & \omega_2 \\ \omega_3 & 0 & -\omega_1 \\ -\omega_2 & \omega_1 & 0 \end{bmatrix}, \bar{\boldsymbol{\omega}} = \omega\bar{\boldsymbol{u}} \tag{2.53}$$

2.5.2 Dynamic equation

As shown on Figure 2.1 the satellite body converts the torques from the magnetorquers and the disturbances into an angular acceleration. This can be modelled as the dynamic equation of the satellite. Euler's second law states that change in angular momentum ${}^{\mathrm{i}}\dot{\bar{\boldsymbol{L}}}(t)$ around a fixed reference frame is equal to the external forces (${}^{\mathrm{i}}\bar{\boldsymbol{\tau}}_{\mathrm{ext}}(t)$) working on a rigid body.

$${}^{\mathrm{i}}\dot{\bar{\boldsymbol{L}}}(t) = {}^{\mathrm{i}}\bar{\boldsymbol{\tau}}_{\mathrm{ext}}(t) \tag{2.54}$$

The change from the inertial reference frame to the control reference frame is given by the multiplication by the rotation matrix ${}^{\mathrm{c}}_{\mathrm{i}}\underline{\mathbf{R}}$.

$${}^{\mathrm{c}}\bar{\boldsymbol{L}}(t) = {}^{\mathrm{c}}_{\mathrm{i}}\underline{\mathbf{R}} \cdot {}^{\mathrm{i}}\bar{\boldsymbol{L}}(t) \;\Rightarrow\; {}^{\mathrm{c}}\dot{\bar{\boldsymbol{L}}}(t) = {}^{\mathrm{c}}_{\mathrm{i}}\dot{\underline{\mathbf{R}}}(t) \cdot {}^{\mathrm{i}}\bar{\boldsymbol{L}}(t) + {}^{\mathrm{c}}_{\mathrm{i}}\underline{\mathbf{R}}(t) \cdot {}^{\mathrm{i}}\dot{\bar{\boldsymbol{L}}}(t) \tag{2.55}$$

The derivative of the rotation matrix from inertial reference frame to control reference frame (see section 2.1)is defined by 2.53:

$${}^{\mathrm{c}}_{\mathrm{i}}\dot{\underline{\mathbf{R}}}(t) = -{}^{\mathrm{c}}\underline{\boldsymbol{\Omega}}(t)_{3\times3} \cdot {}^{\mathrm{c}}_{\mathrm{i}}\underline{\mathbf{R}}(t) \tag{2.56}$$

Where:

$$ {}^{\mathrm{c}}\underline{\boldsymbol{\Omega}}(t)_{3\times3} = \begin{bmatrix} 0 & -\omega_3(t) & \omega_2(t) \\ \omega_3(t) & 0 & -\omega_1(t) \\ -\omega_2(t) & \omega_1(t) & 0 \end{bmatrix} \tag{2.57} $$

By inserting this in (2.55), this is obtained:

$$ {}^{\mathrm{c}}\dot{\bar{\boldsymbol{L}}}(t) = -{}^{\mathrm{c}}\underline{\boldsymbol{\Omega}}(t)_{3\times3} \cdot {}^{\mathrm{c}}_{\mathrm{i}}\underline{\mathbf{R}}(t) \cdot {}^{\mathrm{i}}\bar{\boldsymbol{L}}(t) + {}^{\mathrm{c}}_{\mathrm{i}}\underline{\mathbf{R}}(t) \cdot {}^{\mathrm{i}}\dot{\bar{\boldsymbol{L}}}(t) \tag{2.58} $$

By using ${}^{\mathrm{c}}_{\mathrm{i}}\underline{\mathbf{R}}(t)$ the way it is described in section 2.3 it is moved to the control reference frame as:

$$ {}^{\mathrm{c}}\dot{\bar{\boldsymbol{L}}}(t) = -{}^{\mathrm{c}}\underline{\boldsymbol{\Omega}}(t)_{3\times3} \cdot {}^{\mathrm{c}}\bar{\boldsymbol{L}}(t) + {}^{\mathrm{c}}\bar{\boldsymbol{\tau}}_{\mathrm{ext}}(t) \tag{2.59} $$

The angular momentum of a rigid body is given as following can be inserted where $\underline{\mathbf{I}}$ is the inertia matrix of the satellite which will be described later in section 2.8.

$$ {}^{\mathrm{c}}\bar{\boldsymbol{L}}(t) = \underline{\mathbf{I}} \cdot {}^{\mathrm{c}}\bar{\boldsymbol{\omega}}(t) \;\Rightarrow\; {}^{\mathrm{c}}\dot{\bar{\boldsymbol{\omega}}}(t) = \underline{\mathbf{I}}^{-1}[-{}^{\mathrm{c}}\underline{\boldsymbol{\Omega}}(t)_{3\times3}(\underline{\mathbf{I}} \cdot {}^{\mathrm{c}}\bar{\boldsymbol{\omega}}(t)) + {}^{\mathrm{c}}\bar{\boldsymbol{\tau}}_{\mathrm{ext}}(t)] \tag{2.60} $$

${}^{\mathrm{c}}\bar{\boldsymbol{\tau}}_{\mathrm{ext}}(t)$ is split up into the control torque ${}^{\mathrm{c}}\bar{\boldsymbol{\tau}}_{\mathrm{ctr}}(t)$ and the disturbance torque ${}^{\mathrm{c}}\bar{\boldsymbol{\tau}}_{\mathrm{dist}}(t)$ giving:

$$ {}^{\mathrm{c}}\dot{\bar{\boldsymbol{\omega}}}(t) = \underline{\mathbf{I}}^{-1}[-{}^{\mathrm{c}}\underline{\boldsymbol{\Omega}}(t)_{3\times3} \cdot (\underline{\mathbf{I}} \cdot {}^{\mathrm{c}}\bar{\boldsymbol{\omega}}(t)) + {}^{\mathrm{c}}\bar{\boldsymbol{\tau}}_{\mathrm{ctr}}(t) + {}^{\mathrm{c}}\bar{\boldsymbol{\tau}}_{\mathrm{dist}}(t)] \tag{2.61} $$

The inertia of the satellite is constant and the angular velocity can be measured. With this the angular acceleration is found as a function of the torques working on the satellite.

2.6 Attitude determination system

As previously mentioned an ADS has already been designet. In order to use that it needs to be defined what output that delivers.

As described in [Hemme et al., 2013] there is an error in the results due to noise from the sensors. The best results using simulation parameters equal to the disturbances observed on AAUSAT3 was by using an extended Kalman filter. Based on a simulation on 5830 seconds (approximately 1 orbit) there exists an average error on 2.1° and a maximum error on 3.9°. Since section 1.3 states that the attitude control system has a precision margin of 10° the ADS reduces that margin to 6.1° for the rest of the system.

2.7 Magnetorquer

A magnetorquer is a coil of conductive wire, with a current passing through it. It interacts with magnetic fields to generate force. When a electric current is passed through a magnetic field, like the one emitted by the Earth, it generates a force orthogonal to the magnetic field vector and the current [Nave, 2012]. In a coil there are always an equal and opposite force on each side of the coil. This means that the resulting force will be a torque around the centre of the coil, as seen on Figure 2.13.

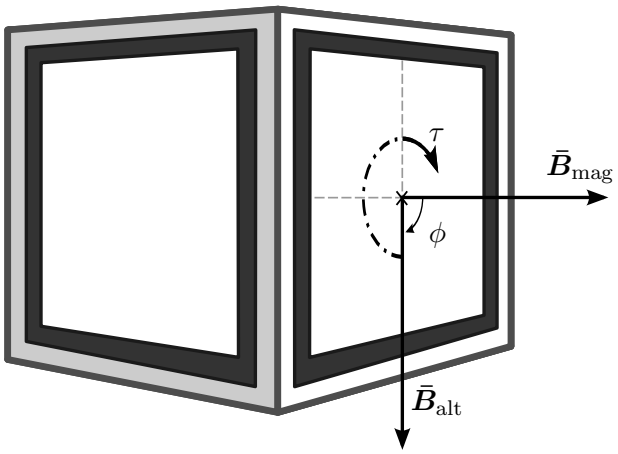

Figure 2.13: The torque will try to align the two magnetic fields (note that $\bar{\boldsymbol{B}}_{\text{mag}}$ and $\bar{\boldsymbol{B}}_{\text{alt}}$ are vectors.)

In order to control the magnitude of the force, the current must be controlled. This can be derived from a diagram of the coil, which can be seen on Figure 2.14.

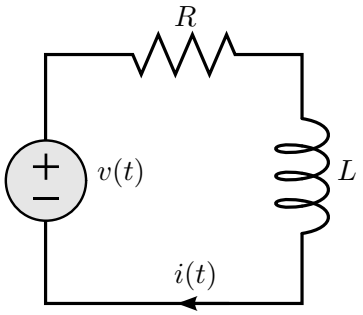

Figure 2.14: Electric diagram of the coil

With these two figures, the relation between the voltage and the force executed on the coil can be extracted. The relation between voltage and current can be seen as.

$$u(t) = L \cdot \frac{di(t)}{dt} + i(t) \cdot R \tag{2.62}$$

To isolate the current, the formula is Laplace transformed, and then the current can be isolated.

$$\begin{aligned} U(s) &= s \cdot L \cdot I(s) + I(s) \cdot R \\ I(s) &= \frac{U(s)}{s \cdot L + R} \end{aligned} \tag{2.63}$$

The interaction between the current in the wire and Earth's magnetic field is then given as [Wertz, 1995]:

$$\bar{\boldsymbol{\tau}}_{\text{ctr}}(s) = \frac{U(s)}{s \cdot L + R} \cdot n \cdot a \cdot \bar{\boldsymbol{B}}_{\text{alt}} \cdot \sin(\phi) \tag{2.64}$$

The transfer function can then be deducted as:

$$H(s) = \frac{\bar{\boldsymbol{\tau}}_{\text{ctr}}(s)}{U(s)} = \frac{1}{s + \frac{R}{L}} \cdot \frac{n \cdot a \cdot \bar{\boldsymbol{B}}_{\text{alt}} \cdot \sin(\phi)}{L} \tag{2.65}$$

Where

$\bar{\boldsymbol{B}}_{\text{alt}}$	Earth's magnetic field at a specific altitude	[T]
$\bar{\boldsymbol{\tau}}_{\text{ctr}}(s)$	Torque the coil is producing	[Nm]
U	Voltage over the coil	[V]
L	The coil inductance	[H]
R	Electrical resistance in the coil	[Ω]
I	Electrical current in the coil	[A]
a	Size of coil	[m^2]
n	Number of windings in the coil	[·]
ϕ	Angle between the coils and the Earth's magnetic field	[deg]

When the coils values are inserted the transfer function becomes:

$$H(s)\frac{128.906}{s+6166} \cdot \bar{\boldsymbol{B}}_{\text{alt}} \cdot \sin(\phi) \tag{2.66}$$

The pole placement was verified in Measurement journal C.1. Here it was seen that the pole for the magnetic fields transfer function was at R/L, and since the magnetic field is directly dependent on the current, it must have the same pole.

It turns out that the equation is a first order system, and it varies with respect to voltage and angle between the coil and the magnetic field. The Earth's magnetic field varies during an orbit. At polar orbit it can be approximated as [Wertz and Larson, 1999]:

$$\bar{\boldsymbol{B}}_{\text{alt}} = \frac{2 \cdot 7.96 \cdot 10^{15}\,\text{T} \cdot \text{m}^3}{D^3} \tag{2.67}$$

Where D is the distance from the centre of Earth to the satellite. The strength drops to half at the equator [Wertz and Larson, 1999], because the distances to the poles are longer. With the satellite being about 600 km above the Earth's surface, this result in the following minimum and maximum graphs.

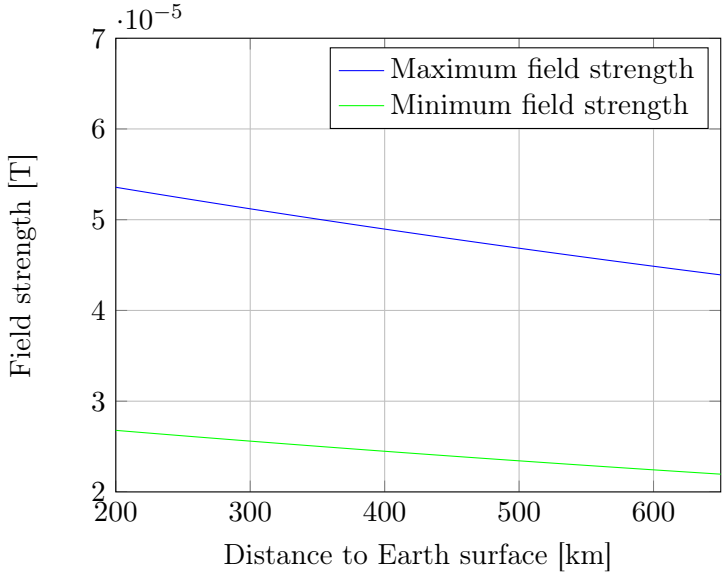

Figure 2.15: Shows the minimum and maximum field strength at different altitudes.

The torque can now be found as a function of the altitude and the angle. In order to find the maximum torque at any altitude, at both maximum and minimum field strength, the angle is set to 90 degrees. A graph of the torque can be seen on Figure 2.16

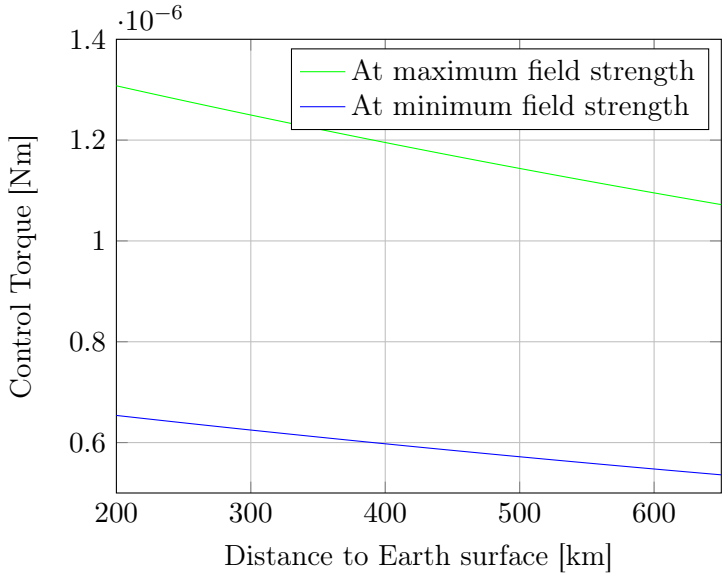

Figure 2.16: Shows the maximum and minimum torque the magnetorquers can generate.

The torque exerted by the magnetorquer, is exerted at the center of the magnetorquer. The magnetorquer is not centred in the satellite, which means that the torque is not in the centre of mass of the satellite. The further the distance a torque is from the axis of rotation, the less does it affect the rotation. Furthermore, if the torque is big enough in relation to the mass of the body, the body could move it's axis of rotation towards the torque. But in the AAUSAT4, the strength and distance are negligible in this regard, so the torque can be seen as affecting the centre of mass.

2.7.1 Yaw, pitch and roll control

The magnetorques can only act on magnetic fields perpendicular to them. This result in a system that, at any time only can control two rotation axes at a time. This can be shown, if the satellite is assumed to travel parallel to the Earth's magnetic field. This is shown on Figure 2.17.

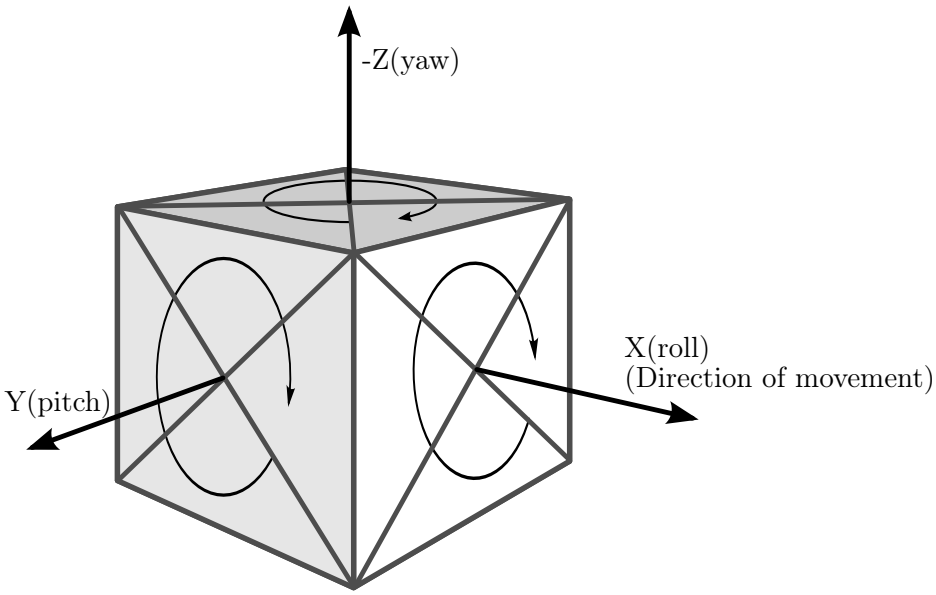

Figure 2.17: Pitch, yaw and roll in relation to the direction of movement

The magnetorquer in the yaw plane can only affect the pitch axis. The magnetorquer in the pitch plane is only able to affect the yaw axis and likewise the roll plane can affect the yaw and pitch axis. If the roll is to be adjusted, the satellite must first be rotated about another axis, so the roll becomes yaw or pitch.

2.8 Satellite body

Satellites in orbit are affected by a number of different forces acting as disturbances on the satellites forward momentum and angular momentum. This section elaborates on these disturbances by deriving models which describes the relationship between torques on the satellite and angular velocity.

2.8.1 Forward momentum

The forward momentum is the result of a mass moving at a velocity. The initial momentum of the satellite is generated by the launch rocket that sends the satellite into orbit. If the satellite has its own propulsion system more momentum can be added. The drag from particles in the atmosphere will slowly lower the momentum. The AAUSAT4 do not have a propulsion system, which means the only source of momentum is from the launch.

2.8.2 Angular momentum

The angular momentum is the result of a mass rotating about itself. The angular momentum comes from disturbances, the launch or from the satellites control actuators. The angular momentum can be expressed by the moment of inertia and the angular velocity, where the moment of inertia is constant and describes the mass distribution of the satellite in the different axis. The moment of inertia can be calculated on simple symmetrical objects or found through tests. Since the satellite in this project is designed

in Autodesk® Inventor® the moment of inertia matrix can be found through the design tool.

$$ {}^{s}\underline{\mathbf{I}} = \begin{bmatrix} i_{s,xx} & i_{s,xy} & i_{s,xz} \\ i_{s,yx} & i_{s,yy} & i_{s,yz} \\ i_{s,zx} & i_{s,zy} & i_{s,zz} \end{bmatrix} = \begin{bmatrix} 1.205 & 0.008 & -0.019 \\ 0.008 & 1.187 & -0.036 \\ -0.019 & -0.036 & 1.161 \end{bmatrix} \cdot 10^{-3} \qquad [\mathrm{kg} \cdot \mathrm{m}^2] \tag{2.68} $$

This corresponds to the following eigenvalues(λ) and eigenvectors(ε):

$$ \bar{\boldsymbol{\lambda}} = \begin{bmatrix} 1.1339 \\ 1.920 \\ 1.227 \end{bmatrix} \cdot 10^{-3} \quad , \quad \underline{\varepsilon} = \begin{bmatrix} 0.1608 & -0.7488 & -0.6430 \\ 0.5374 & 0.6129 & -0.5793 \\ 0.8278 & -0.2524 & 0.5010 \end{bmatrix} \cdot 10^{-3} \tag{2.69} $$

The moment of inertia is calculated in SBRF. The resulting Inertia matrix is:

$$ \begin{aligned} {}^{c}\underline{\mathbf{I}} &= \underline{\epsilon} \cdot {}^{s}\underline{\mathbf{I}} \cdot \underline{\epsilon}^{-1} \\ {}^{c}\underline{\mathbf{I}} &= \begin{bmatrix} 1.1339 & 0 & 0 \\ 0 & 1.920 & 0 \\ 0 & 0 & 1.227 \end{bmatrix} \cdot 10^{-3} \qquad [\mathrm{kg} \cdot \mathrm{m}^2] \end{aligned} \tag{2.70} $$

That is the inertia used in (2.61).

2.9 Disturbances

As previously mentioned the satellite experiences disturbances when in orbit. These can be divided into internal and environmental disturbances. The internal disturbances comes from thrusters, moving parts liquid sloshing etc. AAUSAT4 brings no moving parts no thrusters or liquids or anything, except for the antennas that unfolds when launched. Since that is one time only there are no internal disturbances relevant to this project.

There are four environmental disturbances. These includes the gravity gradient from Earth, solar radiation, aerodynamics and magnetic fields. But since there are no coils worth mentioning except for those used in controlling the attitude the magnetic field torque will not be modeled as a disturbance.

2.9.1 Gravity gradient

Newton's gravitational law states that two given elements influence each other with a force given by [Wertz and Larson, 1999]:

$$ \bar{\boldsymbol{F}} = \frac{G \cdot M_1 \cdot M_2}{r^2} \cdot \bar{\boldsymbol{r}} \tag{2.71} $$

Where

$\bar{\boldsymbol{F}}$	Force	[N]
G	Gravitational constant	$[\mathrm{m}^3\mathrm{s}^{-2}\mathrm{kg}^{-1}]$
M_1	Mass of the object 1	[kg]
M_2	Mass of the object 2	[kg]
r	Orbit radius	[m]
$\bar{\boldsymbol{r}}$	The unit vector from geometric centre to CoM	$[\cdot]$

In this case the force influencing the satellite can be considered as an integral over the satellite consisting of infinitesimal small masses each influenced by the gravitation from

the Earth. Since the mass of the satellite is not evenly distributed this will create a torque. That torque is a function of the Earth's gravity constant and the radius squared based on newtons gravity law. Then instead of using the masses the moment of inertia divided by the radius is used. This can be described as [Wertz, 1995], [Wertz and Larson, 1999] and [Bak, 1999]:

$$^{\mathrm{s}}\bar{\boldsymbol{\tau}}_{\mathrm{gg}} = \frac{3\mu}{R^3}\left[\bar{\boldsymbol{r}} \times (\underline{\mathbf{I}} \cdot \bar{\boldsymbol{r}})\right] \tag{2.72}$$

Where:

$^{\mathrm{s}}\bar{\boldsymbol{\tau}}_{\mathrm{gg}}$	Gravity gradient torque	[Nm]
μ	Earth gravity constant ($3986 \cdot 10^{14}$ $\mathrm{m^3 s^{-2} kg^{-1}}$)	$[\mathrm{m^3 s^{-2} kg^{-1}}]$
R	Orbit radius	[m]
$\underline{\mathbf{I}}$	Moment of inertia given in (2.68)	$[\mathrm{kg{\cdot}m^2}]$
$\bar{\boldsymbol{r}}$	Unit vector pointing at zenit	[·]

With the values for $\underline{\mathbf{I}}$ calculated in equation 2.69 that gives a maximum gravity gradient torque of 5.30 nNm at an altitude of 600 km.

2.9.2 Solar radiation

Radiation from the sun may cause a disturbance on the satellite. This is caused by the momentum flux that acts upon surfaces normal to the Sun's radiation [Wertz, 1995]. Since only some of the energy is reflected not all acts upon the satellite. This section is only concerning the torque which will only be present if the centre of solar pressure and the centre of gravity is not at the same place. For each side the solar radiation torque is proportional to the surface area since that is the space that will be hit by the solar radiation. The angle to the sun is included since that influences the relative area visible from the sun. Since surfaces can both absorb, reflect and diffuse the radiation a reflectance factor is included. This means that the torque is given by the following equation [Wertz and Larson, 1999]:

$$^{\mathrm{s}}\bar{\boldsymbol{\tau}}_{\mathrm{sr}} = \frac{F_{\mathrm{s}}}{c} A_{\mathrm{s}}(1+q)(\bar{\boldsymbol{c}}_{\mathrm{ps}} - \bar{\boldsymbol{c}}_{\mathrm{g}}) \tag{2.73}$$

Where

$^{\mathrm{s}}\bar{\boldsymbol{\tau}}_{\mathrm{sr}}$	Solar radiation torque	[Nm]
F_{s}	Solar constant (1367 $\mathrm{W/m^2}$)	$[\mathrm{W/m^2}]$
c	Speed of light ($3 \cdot 10^8$ m/s)	[m/s]
A_{s}	Surface Area	$[\mathrm{m^2}]$
q	Reflectance factor (between 0 and 1 [Wertz and Larson, 1999])	[·]
$\bar{\boldsymbol{c}}_{\mathrm{ps}}$	Centre of solar pressure	[m]
$\bar{\boldsymbol{c}}_{\mathrm{g}}$	Centre of gravity	[m]

With a reflectance factor of 1 and the largest distance between centre of solar pressure and centre of gravity allowed in SSD [Mølgaard et al., 2014] (such that $\|\bar{\boldsymbol{c}}_{\mathrm{ps}} - \bar{\boldsymbol{c}}_{\mathrm{g}}\| = 0.02$ m) the maximum solar radiation torque will only be 1.82 nNm.

2.9.3 Aerodynamics

Even though the atmospheric density is low there may still be an aerodynamic torque on the satellite. This will only be present if the centre of aerodynamic pressure is not at the same place as the centre of gravity. The aerodynamic drag is a function of the atmospheric density and the surface, becuse they decides the amount of mass that needs to be pushed aside. A drag coefficient based on the shape of the object and the velocity squared since the amount of air that needs to be moved is increased by the velocity and the speed at which it needs to be moved increases. According to [Wertz and Larson, 1999] the aerodynamic torque is given by:

$$^{\mathrm{s}}\bar{\boldsymbol{\tau}}_{\mathrm{a}} = \frac{1}{2}\rho\, C_{\mathrm{d}} A_{\mathrm{s}} v^2 (\bar{\boldsymbol{c}}_{\mathrm{pa}} - \bar{\boldsymbol{c}}_{\mathrm{g}}) \tag{2.74}$$

Where

$^{\mathrm{s}}\bar{\boldsymbol{\tau}}_a$	Aerodynamic torque	[Nm]
ρ	Atmospheric density	[kg/m^3]
C_{d}	Drag coefficient (usually 2 - 2.5 [Wertz and Larson, 1999])	[·]
A_{s}	Surface Area	[m^2]
v	Velocity	[m/s]
$\bar{\boldsymbol{c}}_{\mathrm{pa}}$	Centre of aerodynamic pressure	[·]
$\bar{\boldsymbol{c}}_{\mathrm{g}}$	Centre of gravity	[·]

At an altitude of 600 km the mean atmospheric density is $1.04 \cdot 10^{13}$kg/m^3 and the velocity is 7558 m/s. With a drag coefficient of 2.5 and $\|\bar{\boldsymbol{c}}_{\mathrm{ps}} - \bar{\boldsymbol{c}}_{\mathrm{g}}\| = 0.02$ m the maximum aerodynamic torque is 1.49 nNm [Wertz and Larson, 1999].

The relation between the toques and the altitude are as shown in Figure 2.18:

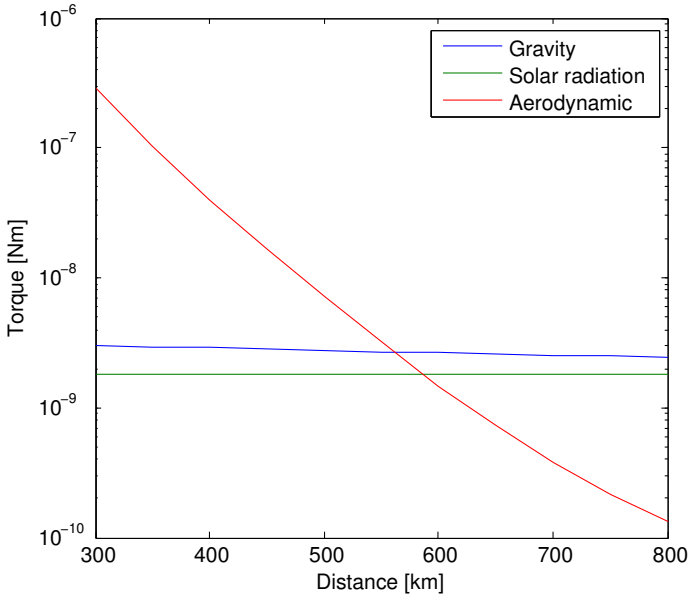

Figure 2.18: The relation between the disturbance torques and altitude.

As the figure shows, the altitude has a great influence on the resulting torque. The altitude of AAUSAT4 has not yet been decided, this leads to three cases to be considered. The case where the aerodynamic drag is much bigger than the other two disturbances at

below 500 km. A case where all three distances has to be taken into account at between 500 and 650 km and a case where only the gravity gradient and the solar radiation needs to be taken into account at altitudes above 650 km.

2.10 Overall satellite model

Recall Figure 2.1. This chapter has been about creating models for each of these blocks in the Figure 4.1. Now with these found they need to be put together in order to design a controller. With the reference frames defined these will have to be added to the model.

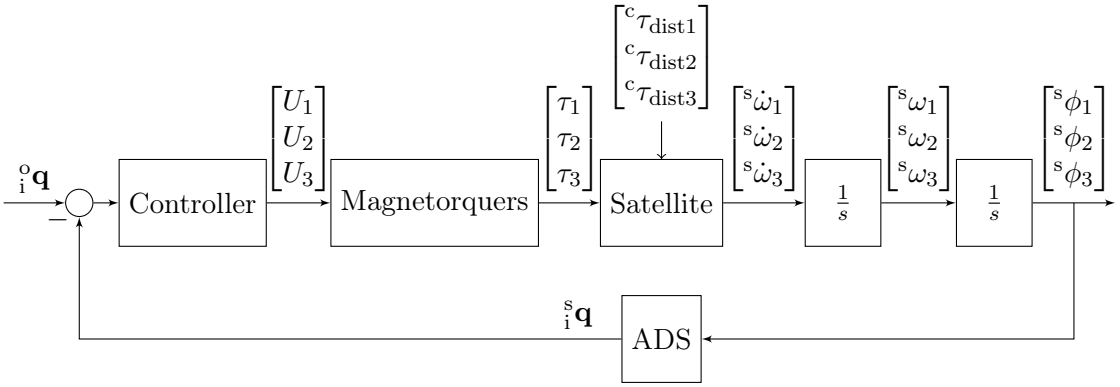

Figure 2.19: Shows the block diagram of the ADCS control loop following the signal through the blocks.

Recall that the model for the satellite is stated in (2.61) as:

$$ {}^{\mathrm{c}}\dot{\bar{\boldsymbol{\omega}}}(t) = {}^{\mathrm{c}}\underline{\mathbf{I}}^{-1}[-{}^{\mathrm{c}}\underline{\boldsymbol{\Omega}}(t)_{3\times 3} \cdot {}^{\mathrm{c}}\underline{\mathbf{I}} \cdot {}^{\mathrm{c}}\bar{\boldsymbol{\omega}}(t) + {}^{\mathrm{c}}\bar{\boldsymbol{\tau}}_{\mathrm{ctr}}(t) + {}^{\mathrm{c}}\bar{\boldsymbol{\tau}}_{\mathrm{dist}}(t)] \tag{2.75} $$

Where the torque from the magnetorquers are given in (2.64), but with the transformation it becomes:

$$ {}^{\mathrm{c}}\bar{\boldsymbol{\tau}}_{\mathrm{ctr}}(t) = {}^{\mathrm{c}}\bar{\boldsymbol{B}}_{\mathrm{mag}}(t) \times \left({}^{\mathrm{c}}_{\mathrm{f}}\underline{\mathbf{R}}(t) \cdot {}^{\mathrm{f}}\bar{\boldsymbol{B}}_{\mathrm{alt}}(t)\right) \tag{2.76} $$

The disturbance torques are given as a sum of the three disturbances described in section 2.9. In order to change it to the control reference frame ${}^{\mathrm{c}}_{\mathrm{s}}\underline{\mathbf{R}}$ is multiplied onto it:

$$ {}^{\mathrm{c}}\bar{\boldsymbol{\tau}}_{\mathrm{dist}} = {}^{\mathrm{c}}_{\mathrm{s}}\underline{\mathbf{R}}\,({}^{\mathrm{s}}\bar{\boldsymbol{\tau}}_{\mathrm{gg}} + {}^{\mathrm{s}}\bar{\boldsymbol{\tau}}_{\mathrm{sr}} + {}^{\mathrm{s}}\bar{\boldsymbol{\tau}}_{\mathrm{a}}) \tag{2.77} $$

The derivative of the rotation quaternion in (2.78) from control reference frame to orbit reference frame describes the orientation of the satellite, hence:

$$ {}^{\mathrm{o}}_{\mathrm{c}}\dot{\bar{\boldsymbol{\theta}}}(t) = \frac{1}{2}\underline{\boldsymbol{\Omega}}(t)_{4\times 4} \cdot {}^{\mathrm{o}}_{\mathrm{c}}\bar{\boldsymbol{\theta}}(t) \tag{2.78} $$

In order to make a controller these has to be linearized.

2.10.1 Linearized overall satellite model

The purpose of the ADCS is to make the satellite's z axis point at nadir at an infinitesimal small angular velocity. The equations of motion are linearized with a first order Taylor

approximation in ${}^{\mathrm{c}}\bar{\boldsymbol{\omega}} = \bar{\mathbf{0}}$ and ${}^{\mathrm{o}}_{\mathrm{c}}\bar{\boldsymbol{\theta}} = \begin{bmatrix}1 & 0 & 0 & 0\end{bmatrix}^{\mathrm{T}}$. The general form of a first order Taylor approximation is

$$f(x) \approx f(\bar{x}) + \left.\frac{\partial f(x)}{\partial x}\right|_{x=\bar{x}} \cdot \hat{x} \tag{2.79}$$

The satellite is rotating about the Earth which results in a relative angular velocity equal to one rotation per orbit [Wiśniewski, 1996]. From this follows:

$${}^{\mathrm{c}}\bar{\boldsymbol{\omega}} \approx {}^{\mathrm{c}}_{\mathrm{o}}\underline{\mathbf{R}} \begin{bmatrix}0 & {}^{\mathrm{o}}\omega_0 & 0\end{bmatrix}^{\mathrm{T}} + \delta{}^{\mathrm{c}}\bar{\boldsymbol{\omega}} \tag{2.80}$$

Where $\delta\bar{\boldsymbol{\omega}}$ is small perturbations in the angular velocity and ${}^{\mathrm{o}}\omega_0$ is the rotation due to the relative change in placement compared to the Earth. Notice that since ${}^{\mathrm{o}}_{\mathrm{c}}\bar{\boldsymbol{\theta}} \approx \begin{bmatrix}1 & 0 & 0 & 0\end{bmatrix}^{\mathrm{T}}$ the rotation operator ${}^{\mathrm{c}}_{\mathrm{o}}\underline{\mathbf{R}} \approx \underline{\mathbf{1}}_{3\times3}$. Likewise is the orientation equal to the operating point times a small perturbation and since the operating point is the trivial $\begin{bmatrix}1 & 0 & 0 & 0\end{bmatrix}^{\mathrm{T}}$ then

$${}^{\mathrm{o}}_{\mathrm{c}}\bar{\boldsymbol{\theta}} = \delta^{\mathrm{o}}_{\mathrm{c}}\bar{\boldsymbol{\theta}}. \tag{2.81}$$

2.10.2 Linearized dynamic model

Based on (2.80) the ${}^{\mathrm{c}}\underline{\mathbf{I}} \cdot {}^{\mathrm{c}}\bar{\boldsymbol{\omega}}$ part becomes (for convenience the inertia ${}^{\mathrm{c}}I_{\mathrm{xx}}$ is written as I_{x} and likewise with the other dimensions.)

$${}^{\mathrm{c}}\underline{\mathbf{I}} \cdot {}^{\mathrm{c}}\bar{\boldsymbol{\omega}} = \begin{bmatrix} I_{\mathrm{x}}\delta\omega_1 \\ I_{\mathrm{y}}\left(\delta\omega_2 + {}^{\mathrm{o}}\omega_0\right) \\ I_{\mathrm{z}}\delta\omega_3 \end{bmatrix} \tag{2.82}$$

so

$${}^{\mathrm{c}}\underline{\mathbf{I}}^{-1}\left(-{}^{\mathrm{c}}\underline{\boldsymbol{\Omega}}_{3\times3}\right){}^{\mathrm{c}}\underline{\mathbf{I}} \cdot {}^{\mathrm{c}}\bar{\boldsymbol{\omega}} = \begin{bmatrix} \sigma_{\mathrm{x}}\delta\omega_3\left(\delta\omega_2 + {}^{\mathrm{o}}\omega_0\right) \\ \sigma_{\mathrm{y}}\delta\omega_1\delta\omega_3 \\ \sigma_{\mathrm{z}}\delta\omega_1\left(\delta\omega_2 + {}^{\mathrm{o}}\omega_0\right) \end{bmatrix} \tag{2.83}$$

where

$$\sigma_{\mathrm{x}} = \frac{I_{\mathrm{y}} - I_{\mathrm{z}}}{I_{\mathrm{x}}}\ ,\ \sigma_{\mathrm{y}} = \frac{I_{\mathrm{z}} - I_{\mathrm{x}}}{I_{\mathrm{y}}} \text{ and } \sigma_{\mathrm{z}} = \frac{I_{\mathrm{x}} - I_{\mathrm{y}}}{I_{\mathrm{z}}} \tag{2.84}$$

Which with the first order Taylor approximation becomes:

$${}^{\mathrm{c}}\underline{\mathbf{I}}^{-1}\left(-{}^{\mathrm{c}}\underline{\boldsymbol{\Omega}}_{3\times3}\right){}^{\mathrm{c}}\underline{\mathbf{I}} \cdot {}^{\mathrm{c}}\bar{\boldsymbol{\omega}} \approx \begin{bmatrix} \sigma_{\mathrm{x}}\delta\omega_3{}^{\mathrm{o}}\omega_0 \\ 0 \\ \sigma_{\mathrm{z}}\delta\omega_1{}^{\mathrm{o}}\omega_0 \end{bmatrix} \tag{2.85}$$

2.10.3 Linearized kinematic model

(2.81) results in the kinematic equation being reduced to:

$$\dot{\delta^{\mathrm{o}}_{\mathrm{c}}\bar{\boldsymbol{\theta}}} = \frac{1}{2}{}^{\mathrm{c}}\underline{\boldsymbol{\Omega}}_{4\times4} \cdot \delta^{\mathrm{o}}_{\mathrm{c}}\bar{\boldsymbol{\theta}} \tag{2.86}$$

Recall from (2.42) and (2.43); small changes in orientation can be written as:

$$\delta^{\mathrm{o}}_{\mathrm{c}}\bar{\boldsymbol{\theta}} = \begin{bmatrix} 1 \\ \delta\theta_1 \\ \delta\theta_2 \\ \delta\theta_3 \end{bmatrix} \tag{2.87}$$

Since $\delta\bar{\boldsymbol{\omega}} \gg \delta\bar{\boldsymbol{\omega}} \cdot \delta\bar{\boldsymbol{\theta}}$

$$\dot{\delta^{\mathrm{o}}_{\mathrm{c}}\bar{\boldsymbol{\theta}}} = \frac{1}{2}\left(\underline{\boldsymbol{\Omega}}_{4\times4}\begin{pmatrix}0 & {}^{\mathrm{o}}\omega_0 & 0\end{pmatrix} \cdot \delta^{\mathrm{o}}_{\mathrm{c}}\bar{\boldsymbol{\theta}} + \delta{}^{\mathrm{c}}\bar{\boldsymbol{\omega}}\right) \tag{2.88}$$

where $\underline{\boldsymbol{\Omega}}_{4\times4}\left(0, {}^{\mathrm{o}}\omega_0, 0\right)$ is $\underline{\boldsymbol{\Omega}}_{4\times4}$ with the rotation speeds 0, ${}^{\mathrm{o}}\omega_0$ and 0. In the point of lineraization the aerodynamic drag and the solar radiation are considered constant, since

the only variables are respectively $\bar{\boldsymbol{c}}_{\mathrm{pa}} - \bar{\boldsymbol{c}}_{\mathrm{g}}$ for aerodynamic pressure (2.74) and $\bar{\boldsymbol{c}}_{\mathrm{ps}} - \bar{\boldsymbol{c}}_{\mathrm{g}}$ for solar radiation (2.73). Since the two integrations in the system as shown in Figure 4.1 makes it a type two system it will be able to compensate for it without a stationary error.

As for the gravity gradient the alignment of ORF and SCRF results in the pressure to be evenly distributed over the satellite. Because of that the satellite does not experience a torque from the gravity gradient.

2.10.4 State variable form

That allows the equations of motion to be rewritten on standard state variable form with the input $\bar{\boldsymbol{\tau}}_{\mathrm{ctr}}(t)$ and the output $\delta_{\mathrm{c}}^{\mathrm{o}}\bar{\boldsymbol{\theta}}(t)$[Franklin et al., 1989].

$$\begin{bmatrix} \delta_{\mathrm{c}}^{\mathrm{o}}\dot{\bar{\boldsymbol{\theta}}}(t) \\ \delta^{\mathrm{c}}\dot{\bar{\boldsymbol{\omega}}}(t) \end{bmatrix} = \underline{\mathbf{A}} \begin{bmatrix} \delta_{\mathrm{c}}^{\mathrm{o}}\bar{\boldsymbol{\theta}}(t) \\ \delta^{\mathrm{c}}\bar{\boldsymbol{\omega}}(t) \end{bmatrix} + \underline{\mathbf{B}}(t) \cdot \bar{\boldsymbol{\tau}}_{\mathrm{ctr}}(t) \tag{2.89}$$

Recall that the control torque is given as:

$$\bar{\boldsymbol{\tau}}_{\mathrm{ctr}}(t) = \left(\frac{\bar{\boldsymbol{U}}(t)}{\frac{\partial i(t)}{\partial t} L + R} \cdot n \cdot a \right) \times \bar{\boldsymbol{B}}_{\mathrm{alt}}(t) \tag{2.90}$$

The output is given as:

$$\delta_{\mathrm{c}}^{\mathrm{o}}\bar{\boldsymbol{\theta}}(t) = \underline{\mathbf{C}} \begin{bmatrix} \delta_{\mathrm{c}}^{\mathrm{o}}\bar{\boldsymbol{\theta}}(t) \\ \delta^{\mathrm{c}}\bar{\boldsymbol{\omega}}(t) \end{bmatrix} \tag{2.91}$$

where

$$\underline{\mathbf{A}} = \begin{bmatrix} 0 & 0 & \frac{1}{2}\omega_0 & \frac{1}{2} & 0 & 0 \\ 0 & 0 & 0 & 0 & \frac{1}{2} & 0 \\ -\frac{1}{2}\omega_0 & 0 & 0 & 0 & 0 & \frac{1}{2} \\ 0 & 0 & 0 & 0 & 0 & \sigma_x\omega_0 \\ 0 & 0 & 0 & 0 & 0 & 0 \\ 0 & 0 & 0 & \sigma_z\omega_0 & 0 & 0 \end{bmatrix} \tag{2.92}$$

,

$$\underline{\mathbf{B}} = \begin{bmatrix} \underline{\mathbf{0}}_{3\times3} \\ {}^{\mathrm{c}}\underline{\mathbf{I}}^{-1} \end{bmatrix} \tag{2.93}$$

and finally

$$\underline{\mathbf{C}} = \begin{bmatrix} \underline{\mathbf{1}}_{3\times3} & \underline{\mathbf{0}}_{3\times3} \end{bmatrix} \tag{2.94}$$

Based on that 9 transfer function can be calculated. One for each output based on each input.

2.10.5 Conversion from state space to transfer function

In order to make the transfer functions (2.89) and (2.91) needs to be converted to the s domain. Recall that the operating point makes the initial conditions equal to zero. So

$$s \begin{bmatrix} \delta_{\mathrm{c}}^{\mathrm{o}}\bar{\boldsymbol{\theta}}(s) \\ \delta^{\mathrm{c}}\bar{\boldsymbol{\omega}}(s) \end{bmatrix} = \underline{\mathbf{A}} \cdot \begin{bmatrix} \delta_{\mathrm{c}}^{\mathrm{o}}\bar{\boldsymbol{\theta}}(s) \\ \delta^{\mathrm{c}}\bar{\boldsymbol{\omega}}(s) \end{bmatrix} + \underline{\mathbf{B}} \cdot \bar{\boldsymbol{\tau}}(s) \tag{2.95}$$

and

$$\delta_{\mathrm{c}}^{\mathrm{o}}\bar{\boldsymbol{\theta}}(s) = \underline{\mathbf{C}} \cdot \begin{bmatrix} \delta_{\mathrm{c}}^{\mathrm{o}}\bar{\boldsymbol{\theta}}(s) \\ \delta^{\mathrm{c}}\bar{\boldsymbol{\omega}}(s) \end{bmatrix} + \underline{\mathbf{D}} \cdot \bar{\boldsymbol{\tau}}(s) \tag{2.96}$$

(2.95) can be written as (where $\underline{\mathbf{1}}_{6\times6}$ denotes a 6 by 6 identity matrix.):

$$(s \cdot \underline{\mathbf{1}}_{6\times6} - \underline{\mathbf{A}}) \begin{bmatrix} \delta_{\mathrm{c}}^{\mathrm{o}} \bar{\boldsymbol{\theta}}(s) \\ \delta^{\mathrm{c}} \bar{\boldsymbol{\omega}}(s) \end{bmatrix} = \underline{\mathbf{B}} \cdot \bar{\boldsymbol{\tau}}(s) \tag{2.97}$$

When isolating

$$\begin{bmatrix} \delta_{\mathrm{c}}^{\mathrm{o}} \bar{\boldsymbol{\theta}}(s) \\ \delta^{\mathrm{c}} \bar{\boldsymbol{\omega}}(s) \end{bmatrix} \tag{2.98}$$

such that

$$\begin{bmatrix} \delta_{\mathrm{c}}^{\mathrm{o}} \bar{\boldsymbol{\theta}}(s) \\ \delta^{\mathrm{c}} \bar{\boldsymbol{\omega}}(s) \end{bmatrix} = (s\underline{\mathbf{1}}_{6\times6} - \underline{\mathbf{A}})^{-1} \underline{\mathbf{B}} \cdot \bar{\boldsymbol{\tau}}(s) \tag{2.99}$$

it can be inserted in (2.96)

$$\delta_{\mathrm{c}}^{\mathrm{o}} \bar{\boldsymbol{\theta}}(s) = \underline{\mathbf{C}} \cdot (s\underline{\mathbf{1}}_{6\times6} - \underline{\mathbf{A}})^{-1} \underline{\mathbf{B}} \cdot \bar{\boldsymbol{\tau}}(s) + \underline{\mathbf{D}} \cdot \bar{\boldsymbol{\tau}}(s) \tag{2.100}$$

That gives the transfer function matrix.

$$\underline{\mathbf{H}}(s) = \underline{\mathbf{C}} \cdot (s\underline{\mathbf{1}}_{6\times6} - \underline{\mathbf{A}})^{-1} \underline{\mathbf{B}} + \underline{\mathbf{D}} \tag{2.101}$$

With this the transfer functions can be calculated as needed in chapter 4.

2.11 System identification

The models for the magnetorquers made in section 2.7 and the satellite made in section 2.10 will be verified in this section. That is done based on the test in appendix C.2. As described in the test the satellite dummy is mounted in a magnetic joint. In order to verify the model that is based on the satellite in space this has to be taken into account since that disturbance is not present in space. The model is based on the equation of motion stating that

$$\sum \tau = 0 \tag{2.102}$$

Which in this case becomes:

$$H_{\mathrm{Mag}}(s) \cdot \theta + B \cdot \omega + I \cdot \alpha = 0 \tag{2.103}$$

Then the system acts as shown in Figure 2.20

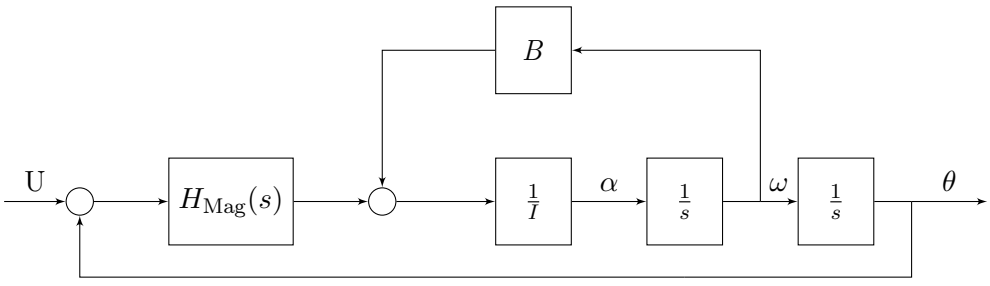

Figure 2.20: Block diagram for testing the transfer function.

Where B is a proportional gain and the magnetorquer ($H_{\mathrm{Mag}}(s)$) is a gain and a pole.

2.11.1 Disturbances

To find this disturbance a test that isolates the disturbance as much as possible is made. That is done by simply applying an angular velocity to the the satellite dummy and measure the settling time. The expected outcome of the test is non linear since the friction in a joint consists of a linear viscose friction a nonlinear coulomb friction and a nonlinear stiction. That means that the expected outcome of the test is the rotation stops more abruptly than it would have done if it was only stopped by the viscose friction. The model however will not take the nonlinear frictions into account. Since the satellite rotates at relatively low speeds the viscose friction will be modeled in an way so the best fits are at low velocities. The models are fitted to the data from the tests using the system identification toolbox in MATLAB which is based on least squared method.

$$\begin{aligned} &\text{minimize: } \sum \left(\bar{\boldsymbol{\theta}}_{\text{meas}} - \bar{\boldsymbol{\theta}}\right)^2 \\ &\text{subject to:} \\ &\ddot{\bar{\boldsymbol{\theta}}}(t) = -B\frac{1}{I}\left(\dot{\bar{\boldsymbol{\theta}}}(t) + \dot{\theta}(0)\right) \end{aligned} \tag{2.104}$$

Based on that a model is made for the friction (B). The step is compared to the measured data in Figure 2.21:

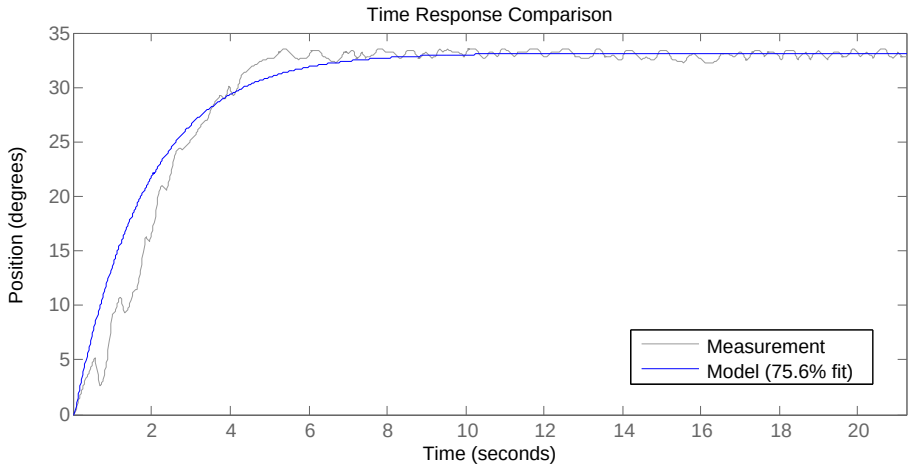

Figure 2.21: The measured position and the model. The fit is at 75.6%. Notice that the VICON-system, used to make the measurements, adds some noise to the results.

As seen on the figure there is quite excessive noise on the output. The satellite dummy has a positive velocity the first 4 or 5 seconds and does not move afterwards. That makes the fit worse than it would have been without the noise and difficult to tell how the actual dynamic behaves. The model is with at B value on $6.1708 \cdot 10^{-4} \frac{\text{Nm·s}}{\text{degree}}$ and the inertia as in 2.68. As seen on the figure the measurements seems to stop more abruptly than the model. This could be because of a nonlinear friction but it could just as well be random noise making it appear that way. Important however is that there is no steady state error.

2.11.2 Magnetorquers

This test is mainly to test the pole placement of the magnetorquer. It is done with a magnetometer which does not allow for a good test of the gain since that should have been

from voltage to torque. The input signal is a step and the model is made by the same principles as in (2.104). The transfer function for the test is:

$$H(s) = \frac{G}{s+P} \tag{2.105}$$

The best fit is then plotted along with the data from the test.

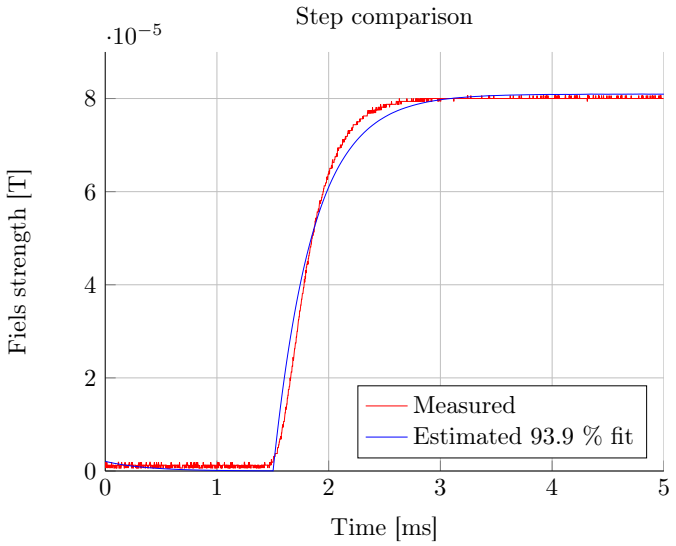

Figure 2.22: Comparison between measured data and estimated function

The model has a pole in 2772 which is lower compared to the calculated pole placement at 6166 but the exact location does not have much influence on the system. The found pole placement will be used in the next test of inertia and gain.

2.11.3 Inertia and gain

With this result a test of the remaining system can be made. That is done by applying an input signal to the magnetorquers which is shown in appendix C.2. Based on that the model is fit to the results as shown in Figure 2.23. That is done based on the same principles as in (2.104). The transfer function for this test is:

$$H(s) = \frac{G}{s+P} \cdot \frac{s}{sI+B} \tag{2.106}$$

The fit is then plotted along with the data.

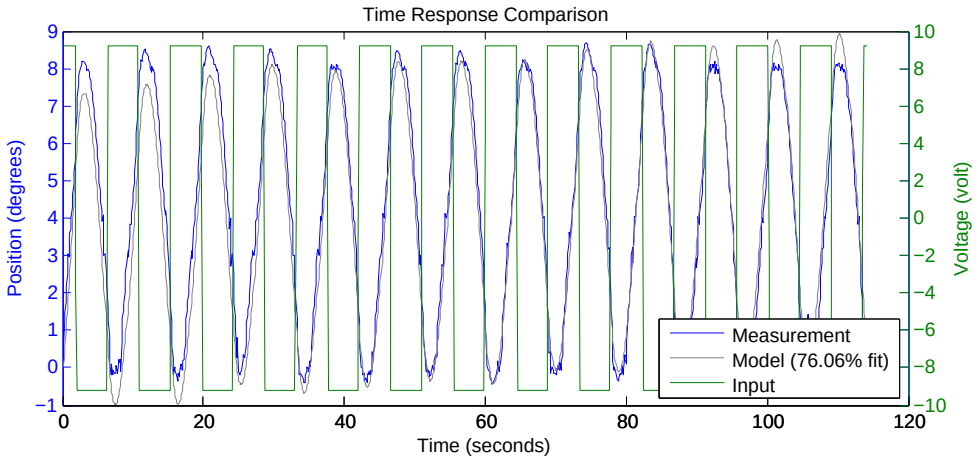

Figure 2.23: The measured position and the model. The fit is at 76.1%.

In order to test the inertia and the gain, a long rotation is preferred. The satellite however has to be close to the working point in order for the test to make sense. A smaller step size was considered but it would have made the friction larger compared to torque produced by the magnetorquers which would have made the test more inaccurate. The results from the model based on the results from the disturbance test and the magnetorquer test are that the inertia is a little smaller than expected ($0.962 \cdot 10^{-3}$ kg·m^2 compared to $1.134 \cdot 10^{-3}$ kg·m^2). This is rather unexpected since the a mass dummy was used with additional batteries and control circuit so it was expected to be a little higher but that might be explained from the inaccurate modeling of the friction. The DC gain in the magnetorquer is modeled as $0.232 \cdot 10^{-3}$ which is very high compared to the values it would have in space but with the stronger magnetic field the expected gain of the magnetorquer is $0.670 \cdot 10^{-3}$ which is off by a factor 3.

These tests are only in one axis and does not test the entire system but it shows, that the models made throughout the problem analysis are a good basis for the controller design in chapter 4.

The tests also confirms that the model can not be interpreted as an exact model and therefore it has to be more than marginal stable. Then the system will not be unstable if it turns out that the system acts different than the model suggests. A rule of thumb is 45 degrees phase margin and 10 dB gain margin.

2.12 Summary

In this chapter models has been made for the magnetorquers and the satellite. The model for the satellite is then linearized in order to be able to design a linear controller for the system. The models are then verified and adjusted trough tests in order to make them as precise as possible. That is important since the controllers will only work if the model used when designing them is a good description of the actual system.

Chapter 3

Requirements

In this chapter the requirements for the system are listed. Some requirements are listed for parts of the satellite that are outside the focus point of this study, these are marked with an asterisk (*) and will not be taken into account in this study. Each requirement contains a parent with the reference to the origin of the requirement and children which states if any sub-requirements are based on it. The verification refers to the corresponding test design in Appentix B.

3.1 Function requirements

No.	Title	Description	Parent	Children
R1*	Detumbling	The system must be able to detumble the satellite based on previously described sensors and actuators	Section 1.3 (Attitude determination and control system)	R1.1-R1.3
R2	Attitude control	The system must be able to control the attitude based on previously described sensors and actuators	Section 1.3 (Attitude determination and control system)	R2.1-R2.3
R3*	Redundancy	If the system stops or enters an error loop it must switch to the backup system ADCS1	Section 1.5 (Robustness)	R3.1-R3.3
R4	Hardware	The system must be able to function using only the hardware described in section 1.4	Section 1.4 (Accessible Hardware)	R4.1-R4.2
R5*	Power	The system must be able to run using no more than 80 mW in average	Subsection 1.4.7 (Solar cells)	
R6	Stability	The system must be stable even when exposed to small environmental changes.	Section 2.11 (System identification)	R6.1-R6.2

3.2 Detumbling requirements

There will not be worked further on detumbling in this project

No.	Title	Description	Parent	Children
R1.1*	Detumble	The system must be able to detumble the satellite to two revolutions per orbit	Req. R1 and section 1.3 (Attitude determination and control system)	
R1.2*	Detumble performance	The system must be able to detumble from $10\,^\circ/s$ to $0.3\,^\circ/s$ within 3 orbits.	Req. R1 and section 1.3 (Attitude determination and control system)	
R1.3*	Extended detumble performance	The system must be able to detumble from $720\,^\circ/s$ to $0.3\,^\circ/s$ within 2 weeks.	Req. R1 and section 1.3 (Attitude determination and control system)	

3.3 Attitude control requirements

No.	Title	Description	Parent	Children
R2.1	Angular velocity	The system must be able to rotate the satellite with a minimum angular velocity of $0.068\,^\circ/s$.	Req. R2 and section 1.3.1 (Attitude determination and control system)	Equation 4.1
R2.2	Attitude control performance	The system must be able to get the satellite to a certain attitude within 2 orbits	Req. R2 and section 1.3 (Attitude determination and control system)	Equation 4.4
R2.3	Attitude control precision	The system must be able to maintain a certain attitude within a margin of 6.1° with a 95% confidence interval.	Req. R2 and section 1.3 (Attitude determination and control system)	Equation 4.3

3.4 Redundancy requirements

There will not be worked further on Redundancy in this project

No.	Title	Description	Parent	Children
R3.1*	Failure detection	The system must be able to recognize internal failure	Req. R3 and section 1.5 (Robustness)	
R3.2*	Fall back	The system must be able to fall back to the backup system (ADCS1) if failure is detected	Req. R3 and section 1.5 (Robustness)	
R3.3*	Reboot	The system must be able to retake control when bugs have been corrected and the system restarted.	Req. R3 and section 1.5 (Robustness)	

3.5 Hardware requirements

There will not be focus on implementing the controllers on the ARM7 processor.

No.	Title	Description	Parent	Children
R4.1*	Processor	The algorithm must be able to run on an ARM7 processor	Req. R4 and section 1.4 (Accessible Hardware)	
R4.2	Magnetorquers	The system must be able to fulfill the control requirements using only the build in magnetorquers actuators	Req. R4 and section 1.4 (Accessible Hardware)	

3.6 Stability requirements

No.	Title	Description	Parent	Children
R6.1	Gain margin	The system must have at least 10 dB gain margin	Req. R6	
R6.2	Phase Margin	The system must have at least 45° phase margin	Req. R6	Equation 4.2

3.7 Verification and test methods

In the previous sections, some of the requirements for the satellite system was listed with the attitude control in focus. The goal of this project is to fulfill these requirements in order to accept the designed attitude controller. In order to test if the system satisfies the requirements an acceptance test is made in chapter 7. It should be noted that due to the difficulties of testing a 3-axis controller in the environment of the Earth's surface and not in orbit, the test is based on a 1-axis controller in a scaled environment. This causes the requirements to be scaled. The scaled requirements are found in section 6.1

The procedure for testing the unscaled ACS requirements are as follows.

3.7.1 ACS Speed

Requirement R2.1 states a minimum actuation speed of $0.068\,^\circ/\mathrm{s}$. This is tested by the rise time of a step of 10 degrees. The satellite is therefore rotated by 10° and should then regulate its attitude back to the target within the desired rise time given by the speed of the system, for the requirement to be fulfilled.

3.7.2 ACS Performance

Requirement R2.2 demands a settling time of maximum 2 orbits. During an orbit, the Earth's magnetic field changes direction and strength. The optimal test would therefore include a corresponding varying direction and strength of the magnetic field. But this equipment is not available. Therefore the test will be done in a static field. The satellite is given an attitude of 10° off target. If the satellite settles on this target within the specified settle time the requirement is fulfilled.

3.7.3 ACS precision

Requirement R2.3 demands maximum of 6.1° deviation from the target. This is tested by giving it a attitude of 10° off target, the controller should settle on the target and the resulting position should be measured.

The test of the satellites ACS will be carried out in chapter 7 Acceptance test.

Chapter 4

Control Design

In this chapter the controller for the ACS is designed. The purpose of the ACS, in this project, is to align the SBRF with the ORF, and thereby doing nadir pointing. The feedback for the control system is obtained via the ADS, which generates a quaternion representation the SBRF rotation relative to ECI. The controller then takes the error between the reference quaternion and the feedback quaternion, calculates the needed control output to the magnetorquer.

A block diagram of the system can be seen on figure 4.1.

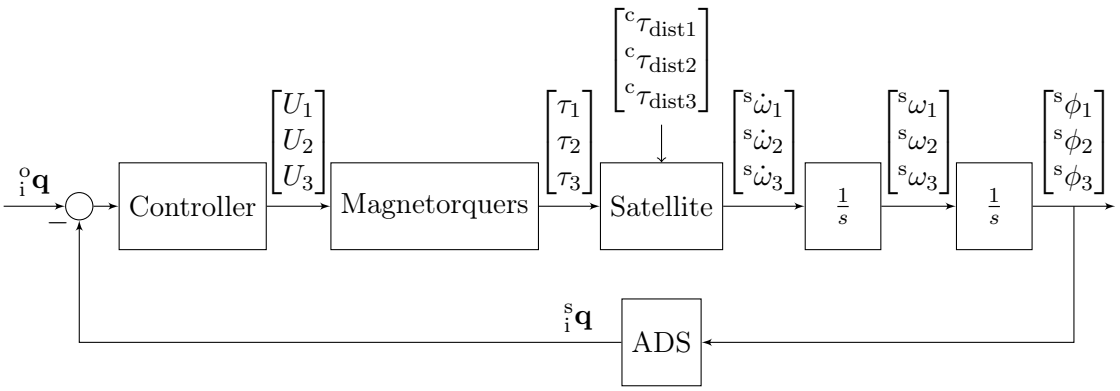

Figure 4.1: Block diagram for the ADCS.

The block diagram in Figure 4.1 is the basis for the controller design in this chapter.

4.1 Controller requirements

The controller is designed with respect to requirements specified in the previous chapter. These requirements demand a certain system response which can be described in the time domain as well as in the frequency domain. Due to the design methods used through the following sections its preferred to depict the system requirements by pole placement in the frequency domain. This section will elaborate on the system requirements and translate them into an allowable region of pole placement in the frequency domain.

The Requirements in chapter 3.3 states the following specifications for the system:

- Minimum angular actuation velocity $\omega_{\text{min}} = 1.2 \cdot 10^{-3}$ rad/s (From requirement R2.1).

- Settling time t_s of maximum two orbits (From requirement R2.2).
- Maximum deviation from target $\pm 3.05°$ (From requirement R2.3).

and from the stability requirements in section 3.6 the following specifications are stated:

- Minimum Gain Margin (GM) of 10 dB (From requirement R6.1)
- Minimum Phase Margin (PM) of 45° (From requirement R6.2).

Where the minimum angular actuator velocity is calculated in section 1.3.1 and is the satellites rotational speed when orbiting the earth. The settling time and the maximum deviation from target demands that the system response settles at the target at maximum two orbits within a margin of 6.1° according to the requirement found in section 1.3. The 3.05° deviation corresponds to $\pm 1.7\%$ of a maximum input step of 180°. This is used to define the settling time for the system. From these requirements it is possible to find the minimum undamped natural frequency ω_n and the closed loop damping ratio ζ. The two design parameters can then be plotted in the complex plane to image the desired pole placement of the system. As showed in section 2.11 the pole from the magnetorquer is placed relatively far out in the left half plane and will therefore have very little influence on the system response. The controller is therefore designed based on second order-system design rules.

4.1.1 Undamped natural frequency ω_n

The undamped natural frequency is related to the closed loop system bandwidth which is a measure of speed of response similar to the time domain responds rise time and peak time. The minimum angular actuation velocity of the satellite ω_{min}, corresponds to the minimum speed of the responds which sets the minimum requirement for the bandwidth of the system.

The bandwidth is defined to be the maximum frequency at which the output signal is attenuated -3 dB. The bandwidth can be said to be equal to the natural frequency ω_n of the closed-loop system, but this is only true for systems with a damping ratio $\zeta = 0.7$. For systems where $\zeta < 0.7$, the natural frequency ω_n is approximately equal to the bandwidth with an error less then a factor two [Franklin et al., 2010]. This is due to a larger resonant peak M_r of the closed-loop frequency response which causes the bandwidth to grow. This means that the systems minimum natural frequency depends on the damping ratio ζ, where

$$\omega_n = \begin{cases} BW & = 1.2 \cdot 10^{-3} \text{ rad/s} \quad \text{for } \zeta = 0.7 \\ \dfrac{BW}{2} & \approx 1.2 \cdot 10^{-3} \text{ rad/s} \quad \text{for } \zeta < 0.7 \end{cases}$$

thus creating a rise time $t_r \cong 1500$ seconds given as [Franklin et al., 2010]:

$$t_r \cong \frac{1.8}{\omega_n} \tag{4.1}$$

A small damping ratio will result in a large resonant peak M_r, which will cause the system to be more likely to resonate at frequencies of ω_n. The requirements for stability in 3.6 ensures that the system has sufficient damping. The required damping ratio is found in the next section.

4.1.2 Damping ratio ζ

The damping ratio is related to the PM of a control system, where the PM describes the amount of phase a system $G(j\omega)$ exceeds from $-180°$ when $|KG(j\omega)| = 1$ in relation the stability criteria, where

$$|KG(j\omega)| < 1 \;\text{ at }\; \angle G(j\omega) = -180°$$

But even if stability is ensured, the system response will still suffer from an unacceptable overshoots with PM $< 30°$. This is due to the resonant peak M_{r}, where; for a system with a PM of $30°$, the resonant peak will amplify the input signal approximately two times creating a overshoot of 50%. Hence the requirements for PM was chosen to be $45°$, which will allow an overshoot of maximum $\sim$20%.

The relation between PM and damping ratio ζ is given as

$$\mathrm{PM} = \tan^{-1}\left[\frac{2\zeta}{\sqrt{\sqrt{1+4\zeta^4} - 2\zeta^2}}\right]$$

where for a PM $< 70°$, the damping ratio can be approximated to a linear relationship where

$$\zeta \cong \frac{\mathrm{PM}}{100}$$

It should be noted that this approximation is only accurate for a second-order system. The minimum damping ratio ζ_{min} is then given as

$$\zeta \geq \frac{45°}{100} = 0.45 \tag{4.2}$$

The maximum settling time t_{s} is relative to the maximum settling variation of 1.7% for the step response. This relation can be seen as the product of an exponential decay $e^{-\sigma t}$ and the circular functions sine and cosine shown in Figure 4.2.

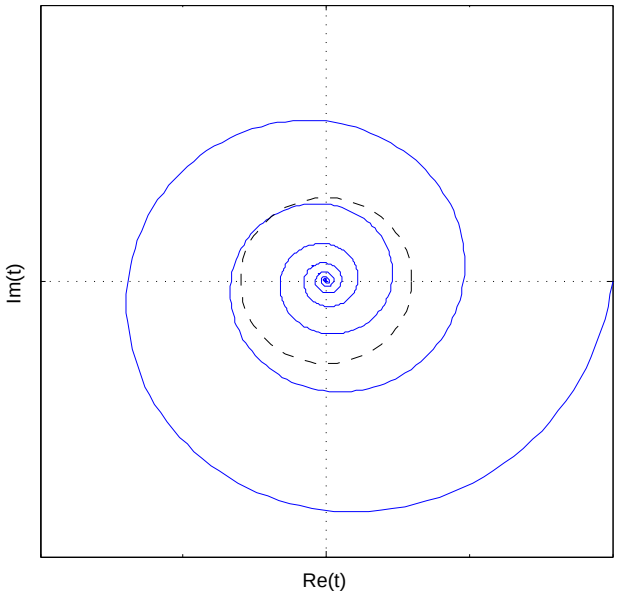

Figure 4.2: Shows the exponential decay of the circular function of sine and cosine, where the dashed circle represent the area defining the settling time t_{s}.

The settling time t_s is then defined as the value for when the exponential decay reaches 1.7%:

$$e^{-\sigma t_s} = 0.017 \tag{4.3}$$

where the value of σ is the negative real part of the system poles. The minimum σ value is then given as

$$\sigma \geq \frac{-\ln(0.017)}{t_s} = 0.34 \cdot 10^{-3} \ \frac{\text{rad}}{\text{s}} \tag{4.4}$$

To summarize the required specifications of the system, the boundaries from section 4.1.1, 4.2 and 4.4 are pictured in the pole-zero map in Figure 4.3 showing the allowable region for pole placement.

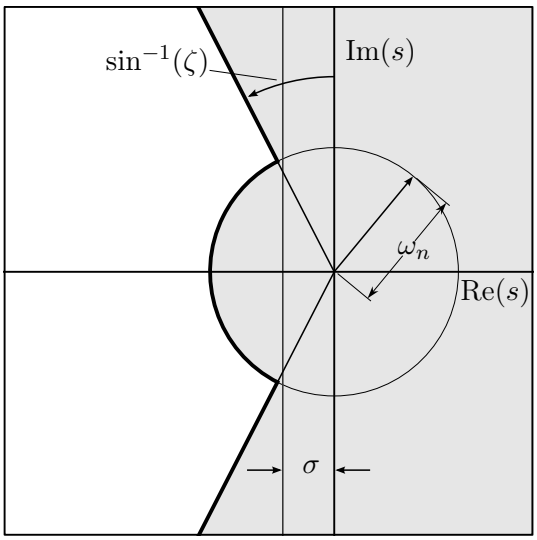

Figure 4.3: Shows the allowable region for pole-placement in the s-plane, where poles in the clear area are acceptable.

The minimum requirements are listed in the following table, relative to the time domain requirements and the frequency domain with respect to the open and closed loop system.

Time domain		**Frequency domain**			
Closed loop:	Req.	Closed loop:	Req.	Open loop:	Req.
Rise time t_r	1500 s	Bandwidth BW	$\sim 2\omega_n$ rad/s	Crossover frequency ω_c	$\sim$BW
Overshoot M_p	$\leq 20\%$	Resonant Peak M_r	≤ 1 (Gain)	Phase Margin PM	45°
				Gain Margin GM	10 dB
Settling time t_s	202 min.				

The specifications stated by the requirements in chapter 3 is now specified in the frequency domain and can be used in design of the controller to verify if the pole placement of the controller is in the acceptable region.

4.2 Multiple input, multiple output

As described in section 2.10 the system contains three inputs and three outputs. These are the three voltages over the magnetorquers and the rotation in the three axes. Depending on the rotation between the control reference frame and Earth's magnetic field all three inputs may effect all three outputs. In order to not just control the wanted output with a given input but also neglect effects on the other output 9 controllers may be designed

such that there is one controller from each input to each output as shown in Figure 4.4. By ignoring the relatively small ${}^{o}\omega_0$ in (2.92) 9 transfer functions are obtained. Note that

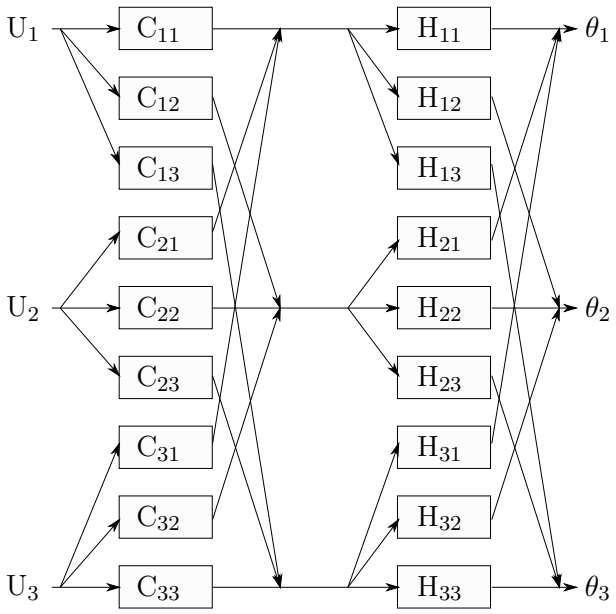

Figure 4.4: Shows the general design of a multiple input multiple output system with 3 inputs and 3 outputs. The arrows joining other arrows are interpreted as summations.

these include both the satellite and the magnetorquers from (2.65).

$$H_{11} = 0 \tag{4.5}$$

$$H_{12} = \frac{B_{\text{alt},3}}{|\bar{\boldsymbol{B}}_{\text{alt}}|} \cdot \frac{0.105}{(s+296)s^2} \tag{4.6}$$

$$H_{13} = \frac{B_{\text{alt},2}}{|\bar{\boldsymbol{B}}_{\text{alt}}|} \cdot \frac{-0.0589}{(s+296)s^2} \tag{4.7}$$

$$H_{21} = \frac{B_{\text{alt},3}}{|\bar{\boldsymbol{B}}_{\text{alt}}|} \cdot \frac{-0.111}{(s+296)s^2} \tag{4.8}$$

$$H_{22} = 0 \tag{4.9}$$

$$H_{23} = \frac{B_{\text{alt},1}}{|\bar{\boldsymbol{B}}_{\text{alt}}|} \cdot \frac{0.0589}{(s+296)s^2} \tag{4.10}$$

$$H_{31} = \frac{B_{\text{alt},2}}{|\bar{\boldsymbol{B}}_{\text{alt}}|} \cdot \frac{0.111}{(s+296)s^2} \tag{4.11}$$

$$H_{32} = \frac{B_{\text{alt},1}}{|\bar{\boldsymbol{B}}_{\text{alt}}|} \cdot \frac{-0.105}{(s+296)s^2} \tag{4.12}$$

$$H_{33} = 0 \tag{4.13}$$

As seen no magnetorquer can make a rotation around its own axis. That means that depending on the direction of the Earth's magnetic field a setup where either U_1 controls θ_2, U_2 controls θ_3 and U_3 controls θ_1 or where U_1 controls θ_3, U_2 controls θ_1 and U_3 controls θ_2 are preferable. The rest of the controllers needs to be designed in a way so they cancel out the unwanted effects on the other dimensions.

As described in section A.1 the path of the satellite is mostly in a north-south or south-north direction which means that it passes a magnetic pole twice per orbit but most of the

time the magnetic field will be in the x-direction in ORF. Based on that only H_{23} and H_{32} will differ significantly from zero in the operating point. To summarize, this means that only pitch and yaw are possible. Yaw with magnetorquer 2 and pitch with magnetorquer 3 as explained in section 2.7.1.

These two controllers have to be designed. That will be done based on the root lucus method.

4.3 Root locus method

Root locus is a graphical method to examine how a systems closed loop poles, and thereby the dynamic properties of the system, vary with change in some parameter. This parameter could be the control gain of the system. When plotting the root locus, one is essentially solving for the roots of the characteristic equation of the closed loop system, and repositioning them according to the new value of the parameter.

To design a controller by using the root locus design method some requirements are needed. These requirements can be both time domain and frequency domain specifications. With these requirements defined in section 4.1 it is possible to identify the valid regions of the complex plane. Plotting the root locus is then a way to find a valid parameter value and thereby placing the poles in the valid regions, ensuring the needed dynamic properties.

In a general feedback system:

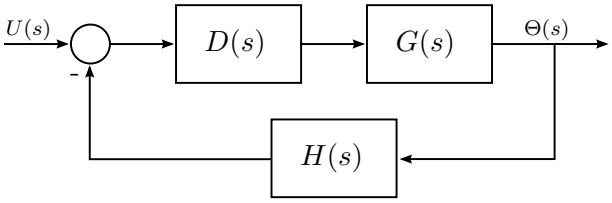

Figure 4.5: General feedback diagram.

With transfer function:

$$B(s) = \frac{\Theta(s)}{U(s)} = \frac{D(s)G(s)}{1 + D(s)G(s)H(s)} \tag{4.14}$$

The characteristic equation $1 + D(s)G(s)H(s)$ can be written in the form:

$$1 + KL(s) = 0 \tag{4.15}$$

Where K is the parameter to be examined, and $L(s) = \frac{b(s)}{a(s)}$ where $b(s)$ has order m and $a(s)$ has order n. The characteristic equation is important to examine due to the fact that the roots of this polynomial are the poles of the closed loop system.

A root locus can be sketched by complying to a set of 5 rules [Franklin et al., 2010]:

1. The n branches of the locus start at the poles of $L(s)$ and m branches end on the zeros of $L(s)$.

2. The loci are on the real axis to the left of an odd numbers of poles and zeros.

3. For large s and K, $n-m$ of the loci are asymptotic to lines at angles Φ_l radiating out from the center point $s=\alpha$ on the real axis, where:

$$\Phi_l = \frac{180^\circ + 360^\circ(l-1)}{n-m}, \quad l = 1, 2, \ldots, n-m$$
$$\alpha = \frac{\sum p_i - \sum z_i}{n-m}$$

4. The angles of departure of a branch of the locus from a pole of multiplicity q is given by:

$$q\Phi_{l,\text{dep}} = \sum \psi_i - \sum \Phi_i - 180^\circ - 360^\circ(l-1)$$

where ψ and Φ are respectively the angles between the real axis and the vector between the zeros and q, and the poles and q. The angle(s) of arrival of a branch at a zero of multiplicity q is given by:

$$q\psi_{l,\text{arr}} = \sum \phi_i - \sum \psi_i + 180^\circ + 360^\circ(l-1)$$

5. The locus can have multiple roots at points on the locus of multiplicity q. The branches will approach a point of q roots at angles separated by

$$\frac{180^\circ + 360^\circ(l-1)}{q}$$

and will depart at angles with the same separation, forming an array of $2q$ rays equally spaced. If the point is on the real axis, then orientation of this array is given by the real-axis rule. If the point is in the complex plane, then the angle of departure rule must be applied.

With this method defined it is possible to design controllers to be used for attitude control of the satellite.

4.4 Error quaternion

As stated earlier the aim of this project is to do nadir pointing with the satellite. The ADS returns a quaternion that represents the SBRF in ECI. The reference for the ACS is a quaternion that represents the ORF in ECI, when those two quaternions align; the satellite is nadir pointing.

From equation (2.12) and (2.18), it can be shown that; for two unit quaternions with angle Θ and Φ, the product between them is:

$$\begin{aligned} \mathbf{p} &= \cos\left(\frac{\Phi}{2}\right) + \bar{\boldsymbol{u}}\sin\left(\frac{\Phi}{2}\right) \\ \mathbf{q} &= \cos\left(\frac{\Theta}{2}\right) + \bar{\boldsymbol{u}}\sin\left(\frac{\Theta}{2}\right) \\ \mathbf{p}\otimes\mathbf{q} &= \cos\left(\frac{\Phi+\Theta}{2}\right) + \bar{\boldsymbol{u}}\sin\left(\frac{\Phi+\Theta}{2}\right) \end{aligned} \tag{4.16}$$

This means that $\mathbf{q}_{\text{ref}}$ will be the quaternion product:

$$\mathbf{q}_{\text{ref}} = \mathbf{q}_{\text{est}} \otimes \mathbf{q}_{\text{err}} \tag{4.17}$$

The error quaternion is then calculated as (4.18), recall equation (2.17); for a unit quaternion the inverse and the complex conjugated are equal.

$$\mathbf{q}_{\text{err}} = \mathbf{q}^*_{\text{est}} \otimes \mathbf{q}_{\text{ref}} \tag{4.18}$$

$\mathbf{q}_{\text{err}}$	The error quaternion.	$[\cdot]$
$\mathbf{q}_{\text{est}}$	The attitude estimation from ADS.	$[\cdot]$
$\mathbf{q}_{\text{ref}}$	The reference quaternion.	$[\cdot]$

Note that when ORF and SBRF align, thereby making $\mathbf{q}_{\text{est}}$ and $\mathbf{q}_{\text{ref}}$ equal. The error quaternion $\mathbf{q}_{\text{err}}$ will be only real valued; $\mathbf{q}_{\text{err}} = 1 + 0\bar{\boldsymbol{i}} + 0\bar{\boldsymbol{j}} + 0\bar{\boldsymbol{k}}$ and the rotation matrix constructed from $\mathbf{q}_{\text{err}}$ will be a 3×3 identity matrix, recall equation (2.27).

Equation (4.18) may be implemented as:

$$\mathbf{q}_{\text{err}} = \mathbf{q}^*_{\text{est}} \otimes \mathbf{q}_{\text{ref}} = \begin{bmatrix} q_{0,\text{ref}} & -q_{1,\text{ref}} & -q_{2,\text{ref}} & -q_{3,\text{ref}} \\ q_{1,\text{ref}} & q_{0,\text{ref}} & -q_{3,\text{ref}} & q_{2,\text{ref}} \\ q_{2,\text{ref}} & q_{3,\text{ref}} & q_{0,\text{ref}} & -q_{1,\text{ref}} \\ q_{3,\text{ref}} & -q_{2,\text{ref}} & q_{1,\text{ref}} & q_{0,\text{ref}} \end{bmatrix} \begin{bmatrix} q_{0,\text{est}} \\ -q_{1,\text{est}} \\ -q_{2,\text{est}} \\ -q_{3,\text{est}} \end{bmatrix} \tag{4.19}$$

In this project the $\mathbf{q}_{\text{ref}}$ is the quaternion representing the rotation from ECI to ORF (${}^{\text{o}}_{\text{i}}\mathbf{q}$) and the $\mathbf{q}_{\text{est}}$ is the attitude estimation from the ADS, being ${}^{\text{s}}_{\text{i}}\mathbf{q}$.

The three imaginary values of $\mathbf{q}_{\text{err}}$ represents the angular error in the three axes. A rotation can be represented as both about $\mathbf{q}$ or about $-\mathbf{q}$. Hence the error in each axis are:

$$\begin{aligned} {}^{\text{s}}\mathbf{q}_{\text{err}} &= q_0 + \bar{\boldsymbol{i}}q_1 + \bar{\boldsymbol{j}}q_2 + \bar{\boldsymbol{k}}q_3 \\ &\Downarrow \\ e_1 &= q_1 \cdot \text{sign}(\text{q}_0) \\ e_2 &= q_2 \cdot \text{sign}(\text{q}_0) \\ e_3 &= q_3 \cdot \text{sign}(\text{q}_0) \end{aligned} \tag{4.20}$$

Which is the input for the controllers designed in the next section.

4.5 Controller design

According to section 2 and section 4.2, there are two transfer functions relevant to design controller for. The two can be seen in (4.21).

$$\begin{aligned} H_{23}(s) &= \frac{B_{\text{alt},1}}{|\bar{\boldsymbol{B}}_{\text{alt}}|} \cdot \frac{0.0589}{(s+296)s^2} \\ H_{32}(s) &= \frac{B_{\text{alt},1}}{|\bar{\boldsymbol{B}}_{\text{alt}}|} \cdot \frac{-0.105}{(s+296)s^2} \end{aligned} \tag{4.21}$$

Where $H_{23}(s)$ is for yaw control and $H_{32}(s)$ is for pitch control. They are the only two relevant transfer functions due to the fact that the satellite is in a near polar orbit and thereby making the Earth's magnetic field near parallel to the satellites x-axis in SCRF. This property is true for when the satellite is in the linearisation point.

4.5.1 System and controller type

The system type is found by examining a pole-zero plot of each transfer function. These can be seen on Figure 4.6 and 4.7.

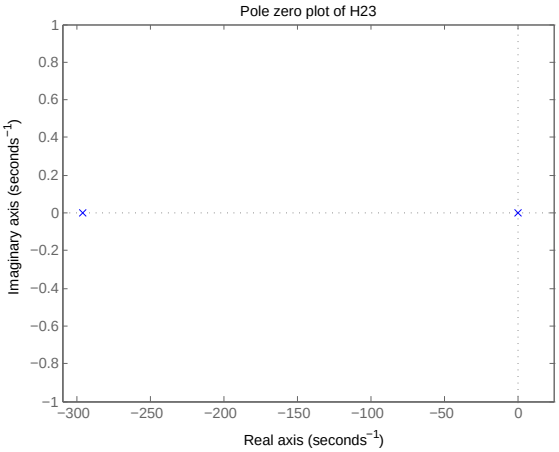

Figure 4.6: Pole-zero plot of H_{23}. H_{23} have two poles in origin and a pole near -300

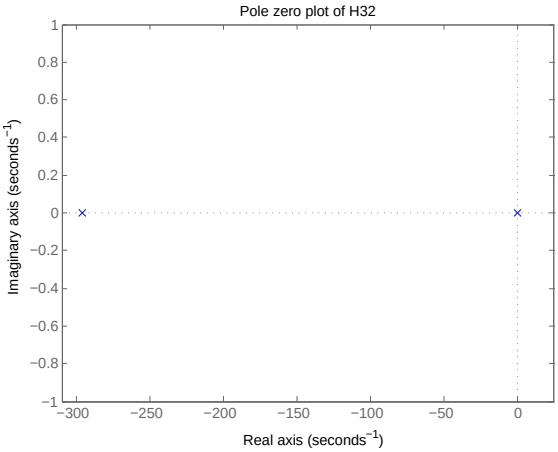

Figure 4.7: Pole-zero plot of H_{32}. H_{32} have two poles in origin and a pole near -300

From these two plots it can be seen that both transfer functions have two poles in origin and a real pole near -300 rad/s. This makes them both type two systems.

A type two system is capable of tracking step responses and ramp responses with a steady state error of zero [Franklin et al., 2010]. Both $H_{32}(s)$ and $H_{23}(s)$ are stable and thereby making it possible to calculate a steady state error for a parabolic reference using the final value theorem [Franklin et al., 2010].

$$\begin{aligned} e_{\text{ss}} &= \frac{1}{K_{\text{a}}} \\ K_{\text{a}} &= \lim_{s \to 0} s^2 \cdot H(s) \end{aligned} \tag{4.22}$$

Where:

e_{ss}	Steady state error.	$[\cdot]$
$H(s)$	$H_{23}(s)$ or $H_{32}(s)$	$[\cdot]$

Due to the satellites orbit about the Earth the actual reference will behave as a sine/cosine wave with a relatively low frequency. This can be modeled as ramp reference input and the parabolic steady state error is irrelevant.

With the third pole of the transfer functions only active for high frequencies compared with the two poles in origin, it is possible to neglect those poles in the design of the controllers. This is particular convenient because for 2nd order systems there exists a number of design rules that can be applied. Furthermore it will be shown in section 4.6, that when the controller is discretized that pole will have almost no impact on the output.

With the knowledge that both systems are type two systems, it can be concluded that the controller does not need an integral part. To decide a controller type, two root locus plots can be seen on Figure 4.8 and 4.9.

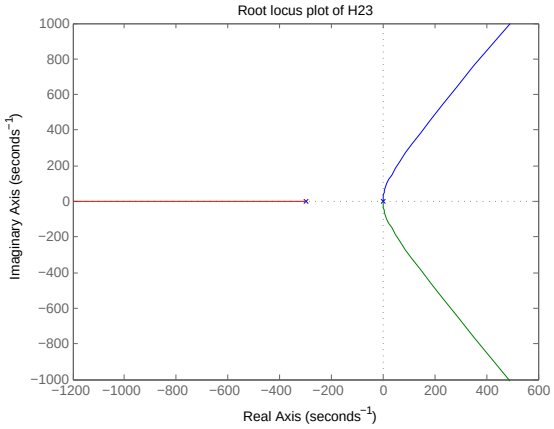

Figure 4.8: Root locus plot of H_{23}.

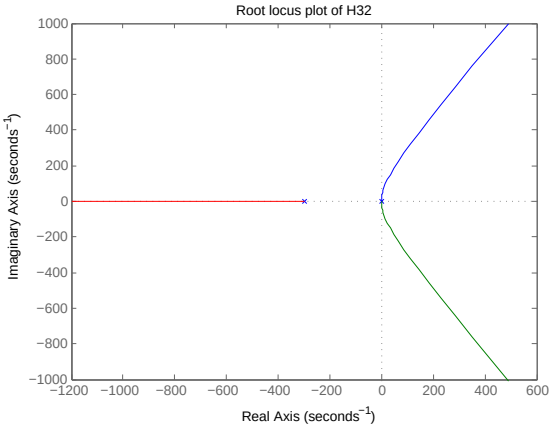

Figure 4.9: Root locus plot of H_{32}. Note that because of the negative gain in H_{32}; a negative gain is used in the controller.

As described in section 4.3 the root locus plot is done by adjusting a gain of the system, here the gain of a proportional controller. On both locus plots it can be seen that as the gain goes up, one or more pole wanders in the right half plane and thereby making the system unstable. A zero in the left plane is therefore needed to achieve stability.

A PD type controller is chosen. A PD controller consists of a proportional and a derivative part. The proportional gain actuates based on the orientation and the derivative actuates based on the angular velocity. This way it is possible to not just get it to the right orientation but also the right angular velocity:

$$u(t) = k_{\mathrm{p}} e(t) + k_{\mathrm{d}} \frac{d\, e(t)}{dt} \tag{4.23}$$

Where:

$e(t)$	Control loop error (controller input).	$[\cdot]$
k_{p}	Proportional gain	$[\cdot]$
k_{d}	Derivative gain	$[\cdot]$

This is Laplace transformed and rearranged to a transfer function:

$$\begin{aligned} D(s) &= k_{\mathrm{p}} + k_{\mathrm{d}} s \\ &= k_{\mathrm{d}} \left(s + \frac{k_{\mathrm{p}}}{k_{\mathrm{d}}} \right) \end{aligned} \tag{4.24}$$

However a pure PD controller is not practically feasible, due to the high gain, such controller would present for high frequencies. This will result in a system highly sensitive to high frequency noise. To counter this effect a pole is added to the PD controller hence making it a lead compensator of this form instead:

$$D(s) = k_{\mathrm{d}} \cdot \frac{s + \frac{k_{\mathrm{p}}}{k_{\mathrm{d}}}}{s + p_{\mathrm{l}}} \tag{4.25}$$

The pole (p_{l}) will be placed at a much higher frequency than the zero and thereby minimizing the poles effect on the systems dynamics. The pole is placed after the PD parameters are designed.

With the controller type defined; next step is to design controller parameter (k_{p}, k_{d}) so the system complies with requirements in section 4.1 and chapter 3.

4.5.2 Parameters

The controller parameters k_p and k_d will now be tuned so the system complies with requirements. This is done by using the Root locus design method described in section 4.3.

Before designing the parameters a nonlinear effect caused by actuator saturation must attended to. The Pulse Width Modulation (PWM) driver for the magnetorquers can, at most output ±1.25 V [Mølgaard et al., 2013]. This output saturation level implies that there will be a limit on how much gain the controller can have. To calculate a maximum controller gain the error at a given deviation of the system output is considered.

If the gain is too large the controller could meet saturation for even small errors and thereby corrupting the system dynamics. Also due to the fact that the transfer functions are linearized in a operating point, the system should maintain its dynamic properties in the vicinity of this point. Outside this point it will be accepted that the controller go in saturation and thereby actuate at maximum power.

As stated in section 4.1 the system can at most deviate from its reference ±3.05°. This leads to an error for each controller of; see section 4.4:

$$\left|e_\mathrm{max}\right| = \sin\left(\frac{3.05^\circ}{2}\right) = 0.027 \tag{4.26}$$

With a saturation level of 1.25 V, this leads to a maximum controller gain of:

$$k_\mathrm{max} = \frac{1.25}{0.027} = 47.0 \tag{4.27}$$

With the maximum allowed gain defined the controller parameters can now be designed.

Yaw controller

The yaw controller is designed by choosing closed loop pole locations for the two dominating poles and the controller is designed such that these pole locations are met. The pole locations are chosen such that the requirements are met.

The zero in the PD controller is placed so the root locus of the system pass through the chosen locations, and the system is solved for the needed gain.

If a ζ of 0.7 and a ω_n of 0.0012 is chosen then the pole locations will be:

$$\begin{aligned}
&\mathrm{Re}(p) = \omega_\mathrm{n} \cdot \zeta = 0.0012 \cdot 0.7 = 0.00084 \\
&\mathrm{Im}(p) = \omega_\mathrm{n} \cdot \sin\left(90 - \arcsin\left(\zeta\right)\right) = 0.0012 \cdot \sin\left(90 - \arcsin\left(0.7\right)\right) = 0.000857 \\
&\qquad \Downarrow \\
&\quad p = 0.00084 \pm 0.000857j
\end{aligned} \tag{4.28}$$

The zero in the controller is placed by using rule four in the root locus method described in section 4.3. An illustration of this can be seen on 4.10.

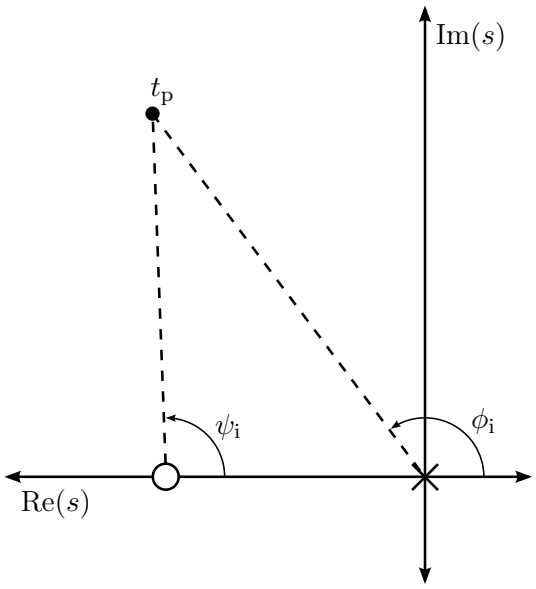

Figure 4.10: Visualizing how the zero placement is designed. ψ is the angle from the zero to a test point and ϕ is the angle from a pole to the test point.

A test point t_p is chosen to be the place of the desired closed loop pole placement. Only one test point is needed because complex poles always occur as a complex conjugated pair. From rule four it is derived that:

$$180^\circ = \sum \phi_i - \sum \psi_i \tag{4.29}$$

This means that the angle from the controller zero to the desired pole location can be calculated as:

$$\psi = \phi - 180^\circ \Rightarrow \psi = 2 \cdot (90 + \arcsin(0.7)) - 180^\circ = 88.85^\circ \tag{4.30}$$

Recall that there are two poles located in origin. Hence the zero location is found using the law of sines:

$$\begin{aligned} \mathrm{Re}(z) &= \frac{\omega_n \cdot \sin(180^\circ - (90^\circ - \arcsin(\zeta)) - \psi)}{\sin(\psi)} \\ &\Downarrow \\ &= \frac{0.0012 \cdot \sin(180^\circ - (90^\circ - \arcsin(0.7)) - 88.85^\circ)}{\sin(88.85^\circ)} = 0.000862 \end{aligned} \tag{4.31}$$

The root locus resulting from placing this zero can be seen on 4.11.

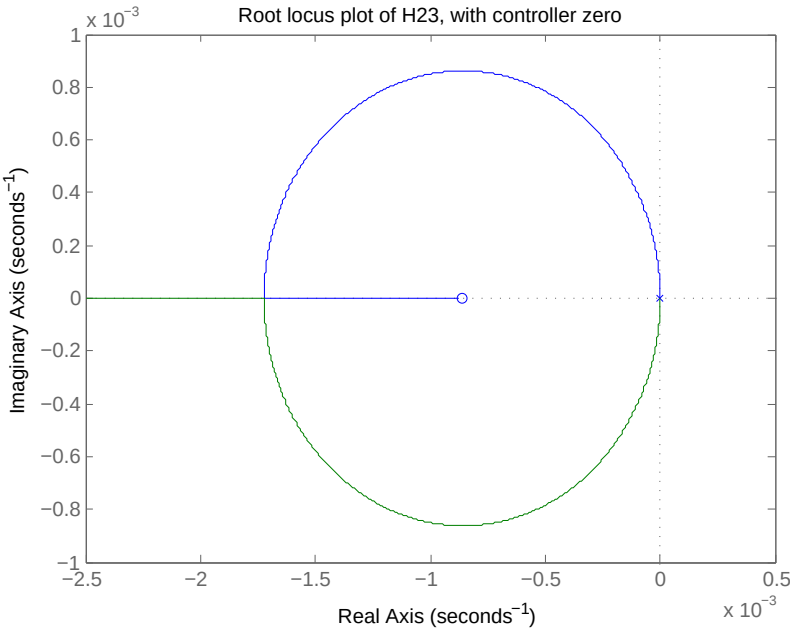

Figure 4.11: Root locus plot of H_{23} with zero.

The zero ensure that the root locus pass through the intended closed loop pole location. The next step is to calculate the necessary gain to obtain that location. Recall the characteristic equation (4.15):

$$1 + KL(s) = 0 \Rightarrow K = -\frac{1}{L(s)} \tag{4.32}$$

Where $L(s)$ is the open loop transfer function $D(s)H_{23}$.

The gain is calculated by inserting the desired pole location in $L(s)$ and calculate the size of $L(t_\mathrm{p})$.

$$K = \left| \frac{1}{L(t_\mathrm{p})} \right| \tag{4.33}$$

The yaw transfer function is rewritten to its standard form, without the pole from the magnetorquer resulting in a second order transfer function, assuming that the Earth's magnetic field is perpendicular to the magnetorquer:

$$H_{23}(s) = 0.000199 \cdot \frac{1}{s^2} \tag{4.34}$$

K is then calculated as:

$$K = \left| \frac{1}{L(t_\mathrm{p})} \right| = \left(\frac{0.000199 \cdot 0.000857}{0.0012 \cdot 0.0012} \right)^{-1} = 8.44 \tag{4.35}$$

These calculations amounts to the following PD controller:

$$D_{23}(s) = 8.44 \cdot (s + 0.000862) \tag{4.36}$$

Where $k_\mathrm{p} = 0.00727$ and $k_\mathrm{d} = 8.44$.

A pole is placed in $(s + 1)$ and the resulting lead compensator:

$$D_{23}(s) = 8.44 \cdot \frac{s + 0.000862}{s + 1} \tag{4.37}$$

The pole is located more than a factor 1000 from the zero, hence not disturbing the dynamics of the system.

Pitch controller

For the Pitch controller the same closed loop pole locations as the yaw controller are chosen. This amounts to the same calculations for both the zero and the lead compensator pole locations. The only thing left to decide then is the gain of the characteristic equation.

The pitch transfer function is written on its standard form, again assuming that the Earth's magnetic field is perpendicular to the magnetorquer:

$$H_{32}(s) = -0.000354 \cdot \frac{1}{s^2} \tag{4.38}$$

K for this controller is then calculated as:

$$K = \left| \frac{1}{L(t_\mathrm{p})} \right| = \left(\frac{0.000354 \cdot 0.000857}{0.0012 \cdot 0.0012} \right)^{-1} = 4.75 \tag{4.39}$$

Since the DC gain of H_{32} is negative the gain of the controller gain needs to be so also. This amounts to the following lead compensator for $H_{32}(s)$:

$$D_{32}(s) = -4.75 \cdot \frac{s + 0.000862}{s + 1} \tag{4.40}$$

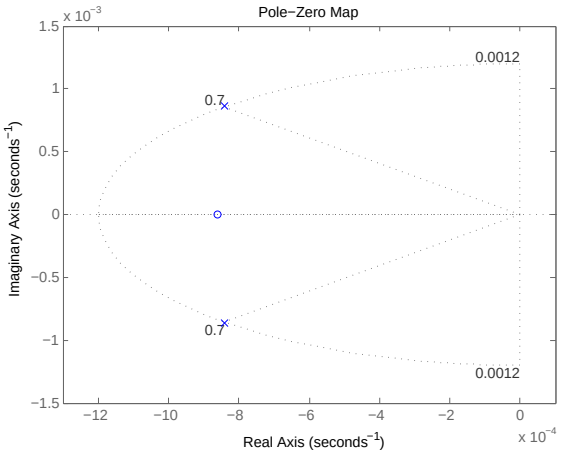

Figure 4.12: Resulting pole-zero plot of the closed loop poles of $H_{23}(s)$.

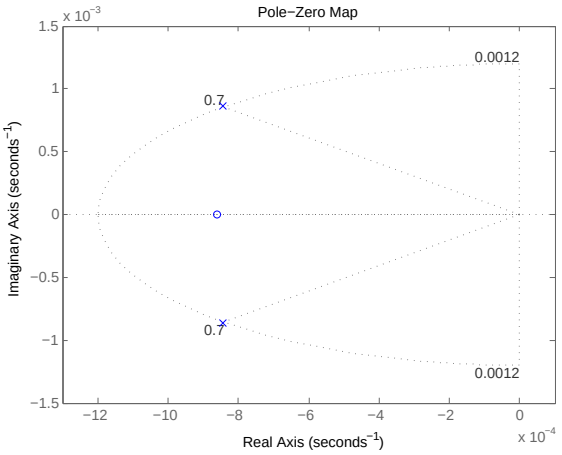

Figure 4.13: Resulting pole-zero plot of the closed loop poles of $H_{32}(s)$.

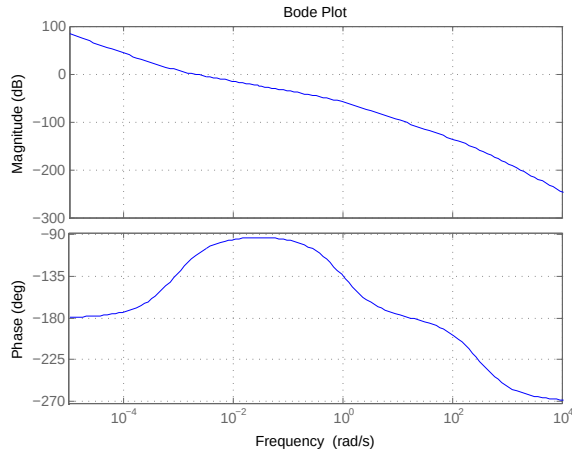

Figure 4.14: Resulting open loop bode plot of $H_{23}(s)$ with controller.

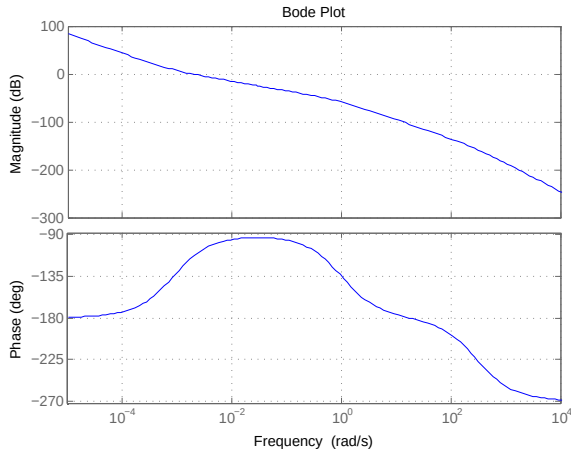

Figure 4.15: Resulting open loop bode plot of $H_{32}(s)$ with controller.

The results of both controller designs can be seen on Figures 4.12 to 4.15, the next step is to discretizise the controllers so they can be implemented in a digital system.

4.6 Digital control

Two controllers has been designed. These controllers are to be implemented on a microprocessor, and thereby making it necessary to convert the designed continuous time controllers, into discrete time controllers. In this section this will be done and the consequences of this discretization will be examined.

4.6.1 Bilinear approximation

A bilinear approximation, is a method of approximating a continuous time transfer function by a discrete time transfer function. In the bilinear approximation the continuous time transfer function is converted by replacing the s variable with an approximation of the z variable. This approximation is obtained by observing some characteristics of the two. A few equations concerning the Laplace and the z domain:

$$\begin{aligned} z &= e^{j\omega} \\ \omega &= T_\mathrm{d}\Omega \\ s &= j\Omega \end{aligned} \tag{4.41}$$

Where:

ω	The digital frequency	[rad/s]
Ω	The analog frequency	[rad/s]
T_d	Sampling period	[s]

It follows that:

$$z = e^{jT_\mathrm{d}\frac{s}{j}} \quad \Rightarrow \quad z = e^{T_\mathrm{d}s} \quad \Rightarrow \quad \ln(z) = T_\mathrm{d}s \quad \Rightarrow \quad s = \frac{1}{T_\mathrm{d}}\ln(z) \tag{4.42}$$

The natural logarithm function is a nonlinear function and therefore it is approximated by a first order taylor expansion, this means that (4.42) becomes:

$$s \approx \frac{2}{T_\mathrm{d}}\frac{1-z^{-1}}{1+z^{-1}} \tag{4.43}$$

A conversion is then done by substituting all s in the continuous time transfer function with (4.43).

4.6.2 Controller discretization

As previously described the controllers $D_{23}(s)$ and $D_{32}(s)$ are transformed to the discrete time transfer functions $D_{23}(z)$ and $D_{32}(z)$. As stated in section 1.3, an estimate of the attitude is calculated once every second, resulting in a sampling period of 1 second.

The two controllers can be seen in (4.44).

$$\begin{aligned} D_{23}(s) &= 8.44 \cdot \frac{s + 0.000862}{s + 1} \\ D_{32}(s) &= -4.75 \cdot \frac{s + 0.000862}{s + 1} \end{aligned} \tag{4.44}$$

First $D_{23}(s)$ is transformed. s in the transfer function is replaced with a z approximation.

$$\begin{aligned} D_{23}(z) &= 8.44 \cdot \frac{\frac{2}{T_\mathrm{d}} \frac{1-z^{-1}}{1+z^{-1}} + 0.000862}{\frac{2}{T_\mathrm{d}} \frac{1-z^{-1}}{1+z^{-1}} + 1} \\ &\Downarrow \\ &= 8.44 \cdot \frac{2(1-z^{-1}) + T_\mathrm{d}(1+z^{-1})0.000862}{2(1-z^{-1}) + T_\mathrm{d}(1+z^{-1})} \end{aligned} \tag{4.45}$$

With a T_d of 1 second this becomes:

$$D_{23}(z) = 8.44 \cdot \frac{0.667 + 0.666z^{-1}}{1 - \frac{1}{3}z^{-1}} \tag{4.46}$$

For this to be implemented it needs to be converted to a difference equation:

$$\begin{aligned} D_{23}(z) &= \frac{U_{23}(z)}{E_{23}(z)} = 8.44 \cdot \frac{0.667 + 0.666z^{-1}}{1 - \frac{1}{3}z^{-1}} \\ &\Downarrow \\ U_{23}(z)\left(1 - \frac{1}{3}z^{-1}\right) &= E_{23}(z)\left(5.629 - 5.621z^{-1}\right) \\ &\Downarrow \mathbb{Z}^{-1} \\ U_{23}[n] &= 5.629E_{23}[n] - 5.621E_{23}[n-1] + \frac{1}{3}U_{23}[n-1] \end{aligned} \tag{4.47}$$

It can be seen that this controller is dependent on both the current input, the former input and the former output.

In order to show the effects of the discretization a bode plot is made of the controller in discrete time.

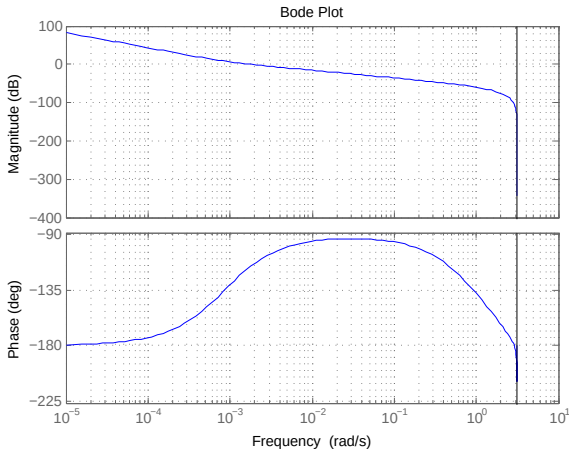

Figure 4.16: Resulting open loop bode plot $H_{23}(z)$ with controller.

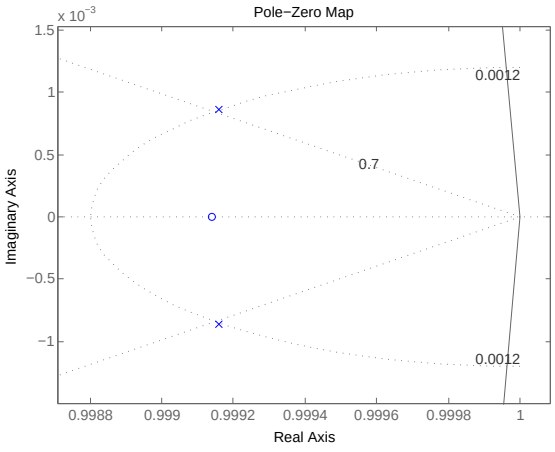

Figure 4.17: Plot of the closed loop poles and zeros of $H_{23}(z)$.

As seen on the bode plot on Figure 4.16 everything above 3.14 rad/s does not have any effect after the discretization. Based on that observation the pole from the magnetorquer has no effect on the system which was also the assumption in the design of the controller. The dominating closed loop poles on Figure 4.17 show that the designed pole locations still holds.

The 3.14 rad/s comes from the Nyquist frequency which with a sampling frequency of 1 Hz is 0.5 Hz or 3.14 rad/s.

$D_{32}(s)$ is transformed with the same method as $D_{23}(s)$. The two controllers has the same zero and pole location, so it is possible to substitute the gain in (4.46) with the gain needed in $D_{32}(s)$. This results in:

$$D_{32}(z) = -4.75 \cdot \frac{0.667 + 0.666z^{-1}}{1 - \frac{1}{3}z^{-1}} \tag{4.48}$$

Resulting in the difference equation:

$$\begin{aligned} D_{32}(z) &= \frac{U_{32}(z)}{E_{32}(z)} = -4.75 \cdot \frac{0.667 + 0.666z^{-1}}{1 - \frac{1}{3}z^{-1}} \\ &\Downarrow \\ U_{32}(z)\left(1 - \frac{1}{3}z^{-1}\right) &= E_{32}(z)\left(-3.168 + 3.164z^{-1}\right) \\ &\Downarrow \mathbb{Z}^{-1} \\ U_{32}[n] &= -3.168E_{32}[n] + 3.164E_{32}[n-1] + \frac{1}{3}U_{32}[n-1] \end{aligned} \tag{4.49}$$

Just like $U_{23}[n]$, $U_{32}[n]$ is dependent on both the current input, the former input and the former output.

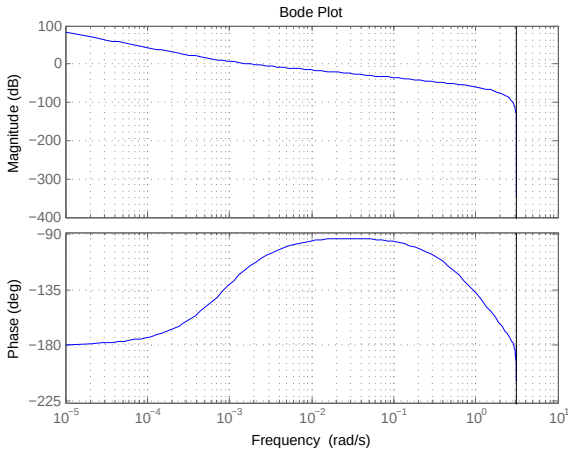

Figure 4.18: Resulting open loop bode plot of $H_{32}(z)$ with controller.

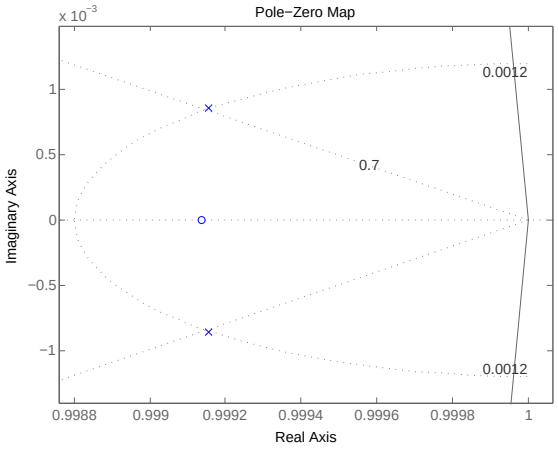

Figure 4.19: Plot of the closed loop poles and zeros of $H_{32}(z)$.

As seen on the bode plot on Figure 4.18 everything above 3.14 rad/s does not have any effect after the discretization. Based on that observation the pole from the magnetorquer has no effect on the system which was also the assumption in the design of the controller. The dominating closed loop poles on Figure 4.19 show that the designed pole locations still holds.

4.7 Summary

In this chapter, controllers for the satellite have been designed based on the root locus method. Then they are digitalized using bilinear transformation, so that they can be implemented in a digital system. In order to validate these controllers they will be simulated. In the next chapter the simulations will be described, both for the controllers designed for satellite in space, and for the controller designed for the test stand. When the controller for the test stand has been verified in a simulation, it will be implemented and tested.

Chapter 5

Simulation

Simulations can give a view into the behavior of a theoretical system. The simulations must be of the non linear system, not the linearized version. Two simulations will be made. A space flight simulation, including three dimensional attitude and two controllers, this simulation will be the only data on the real control system generated in this project. A simulation of the acceptance test is made as well to have data to compare the acceptance test with.

The simulations are made in Simulink, this is a tool that has been used to simulate the satellite in other projects. From previous AAUSAT projects a toolbox has been made. This toolbox is used in this simulation [Nielsen and Larsen, 2013]. In this toolbox the real part of the quaternions are placed as q_4 instead of q_0.

5.1 Space simulation

To verify the controllers the system is simulated as if it was in space. The simulation is done on the actual non-linear system.

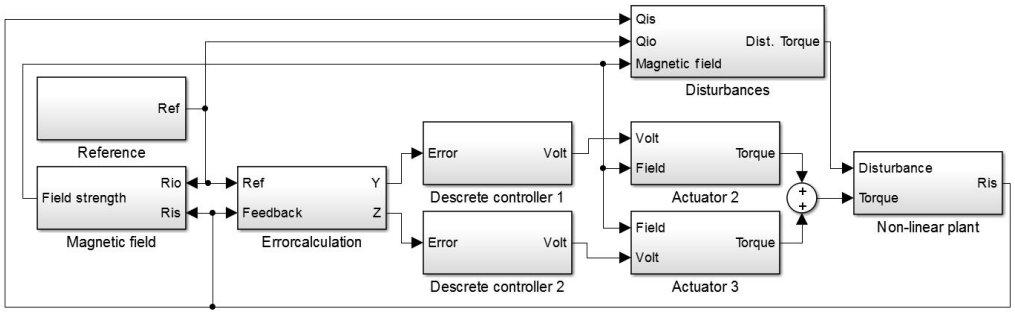

Figure 5.1: The space simulation environment

5.1.1 Input - orbit

The satellite is orbiting the Earth, and must during an orbit keep its ${}^{s}z$-axis pointed towards the center of Earth. The real orbit is close to being a circular polar orbit. The orbit will for simplicity be simulated as such. The satellite is set to start at the Equator. The reference quaternion can be made from the rotation matrix as described in section 2.4.1, then ${}^{o}_{i}q_4$ will always be positive and ${}^{o}_{i}q_2$ will go from -1 to 1 when ${}^{o}_{i}q_4$ should cross from positive to negative.

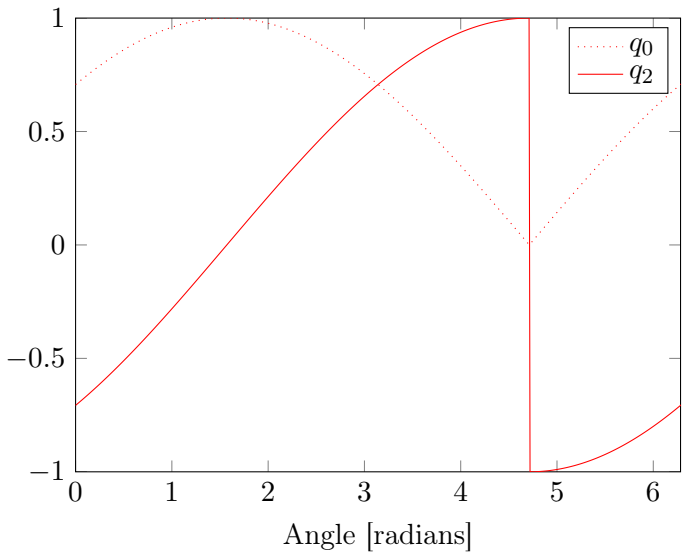

Figure 5.2: The reference quaternion derived from rotation matrix

This is a correct rotation quaternion from ECI to ORF, but as seen on the figure, it results in sudden shifts that can be misleading. The rotation quaternion is instead constructed directly as:

$$\begin{aligned} {}^{\mathrm{o}}_{\mathrm{i}}q_1 &= 0 \\ {}^{\mathrm{o}}_{\mathrm{i}}q_2 &= \sin\left(\frac{\pi}{t_{\mathrm{orb}}}\right) \\ {}^{\mathrm{o}}_{\mathrm{i}}q_3 &= 0 \\ {}^{\mathrm{o}}_{\mathrm{i}}q_4 &= \cos\left(\frac{\pi}{t_{\mathrm{orb}}}\right) \end{aligned} \tag{5.1}$$

Where t_{orb} denotes orbit time, for this simulation it runs from zero to 6000 seconds based on the orbit time being roughly 100 minutes. The resulting quaternion describes a rotation about the ${}^{\mathrm{s}}y$-axis, but it is twice as fast (therefore π not 2π), and it is phase shifted 90 degrees. This is controlled by lowering the slope in the ramp generator and offsetting its starting value by $\pi/4$.

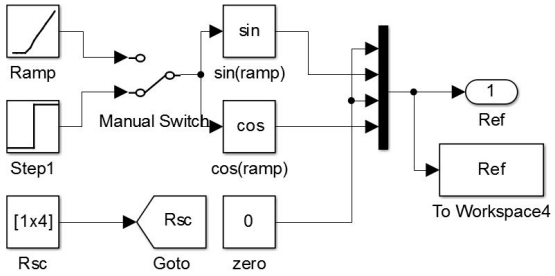

Figure 5.3: Both step and a ramp can be selected

5.1.2 Error

The error is found as described in section 4.4 as a quaternion multiplication of the inverted estimated position quaternion and the reference quaternion. It is then split into x, y and

z, which describes the errors around the different axis. These are then signed with the sign from $q_{4,\text{err}}$.

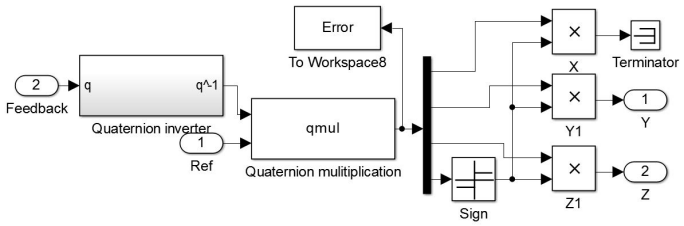

Figure 5.4: Error calculation

5.1.3 Controllers

The two controllers are implemented with a discrete controller, these sample with 1 Hz. These are set to give a maximum output of $\pm 1.25V$, to simulate saturation.

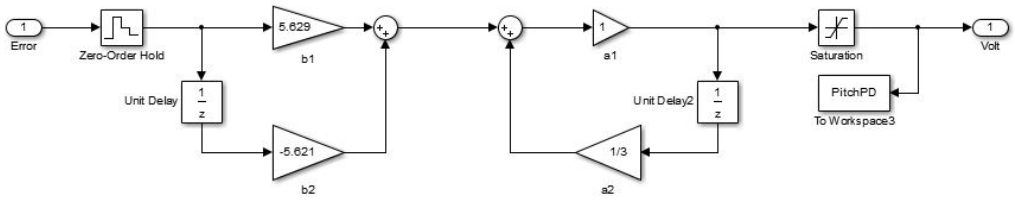

Figure 5.5: A controller on direct form 1

5.1.4 Magnetorquers

The torque around an axis is depending on the magnetic field strength orthogonal to both the torque axis and the magnetorquers axis. The magnetorquer is split into two parts, the coil and the magnetic field.

Magnetic field

The magnetic field changes along the orbit. Above the pole it is perpendicular (compared to Earth's surface) and above the equator it is parallel to the Earth's surface. The magnetic field is calculated as a unit vector indicating strength and and direction in ECI. A switch is implemented such that there can easily be switched from a static field (in ECI) and a changing field that follows the orbit.

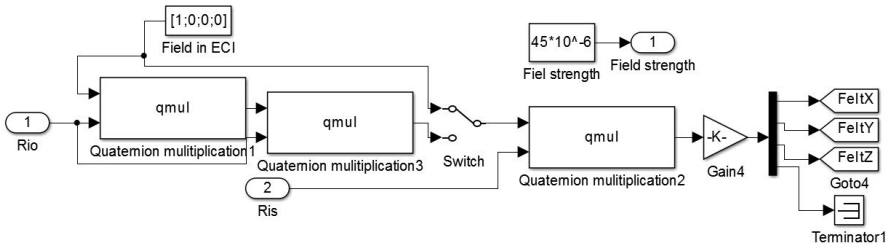

Figure 5.6: A simplified model of the varying magnetic field. Rio is ${}^{\text{o}}_{\text{i}}\mathbf{q}$ and Ris is ${}^{\text{s}}_{\text{i}}\mathbf{q}$

Coil

The coil block consist of the magnetorquers transfer function from equation 2.65, but without the Earth's magnetic field strength and the angle between the Earth's and the magnetorquer's magnetic field. The resulting transfer function for the coil is then:

$$C(s) = \frac{128.90625}{s + 6167} \tag{5.2}$$

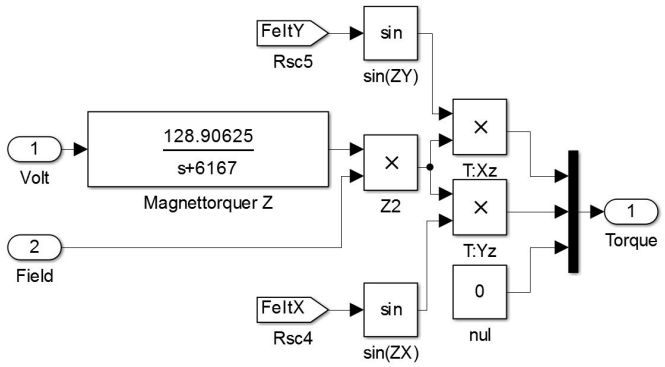

Figure 5.7: Each magnetorquer can generate torque on two axes

The strength is multiplied with the output of the coil. The magnetorquer only interacts with the fields components perpendicular to its magnetic field. The Earth's magnetic field is therefore rotated into SBRF, and the vector is divided into x, y and z components. The components are then multiplied with the coil and field strength, but only the two axes perpendicular to the magnetorquer. The final result from each magnetorquer is a 3D-vector where each component describes the torque around that axis. The vectors from each magnetorquer is added together.

5.1.5 Disturbances

As described in section 2.9, the satellite is exerted to a variety of disturbances. Only the atmospheric resistanceis implemented with the AAUSAT3 toolbox.

5.1.6 Non-linear plant

The controllers are designed to fit the linearized system. But to test if they work in reality, they must be simulated with the real non-linear system. The non-linear plant can be described by its dynamics and kinematics, these are found in section 2.5 to be:

$${}^{\mathrm{c}}\dot{\bar{\boldsymbol{\omega}}}(t) = {}^{\mathrm{c}}\underline{\mathbf{I}}^{-1}[-{}^{\mathrm{c}}\underline{\boldsymbol{\Omega}}(t)_{3\times 3} \cdot {}^{\mathrm{c}}\underline{\mathbf{I}} \cdot {}^{\mathrm{c}}\bar{\boldsymbol{\omega}}(t) + {}^{\mathrm{c}}\bar{\boldsymbol{\tau}}_{\mathrm{ctr}}(t) + {}^{\mathrm{c}}\bar{\boldsymbol{\tau}}_{\mathrm{dist}}(t)] \tag{5.3}$$

$${}^{\mathrm{o}}_{\mathrm{c}}\dot{\bar{\boldsymbol{\theta}}}(t) = \frac{1}{2}\underline{\boldsymbol{\Omega}}(t)_{4\times 4} \cdot {}^{\mathrm{o}}_{\mathrm{c}}\bar{\boldsymbol{\theta}}(t) \tag{5.4}$$

These are implemented with the AAUSAT3 toolbox. It summarizes the torques and applies them to the non-linear system with a given inertia and ${}^{\mathrm{c}}_{\mathrm{s}}\mathbf{q}$.

5.1.7 Feedback

The feedback is the rotation quaternion describing SBRF in ECI. The feedback is sampled once every second.

5.1.8 Simulation - step

A step is simulated. The step represents a change in the wanted attitude. The Earth's magnetic field is also set to be static, simulating the satellite staying in the same place. The start attitude of the system is set to be the same as the initial reference attitude. The result can be seen below:

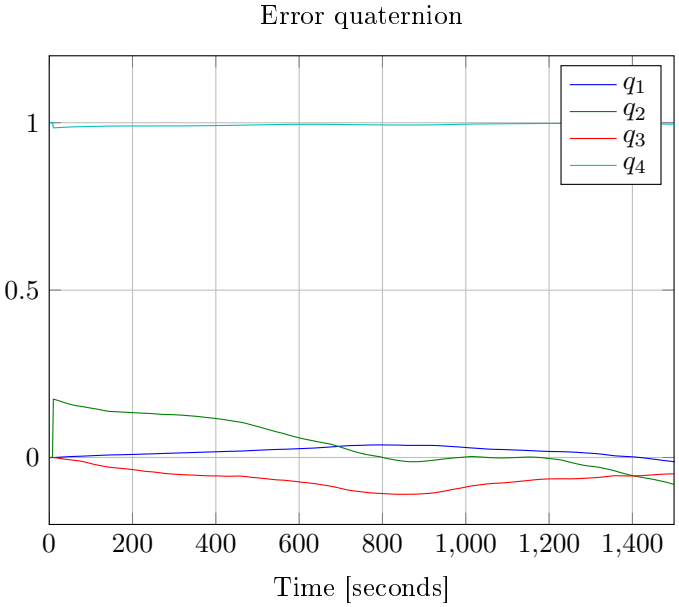

Figure 5.8: Error response

The system starts to correct q_3, but the actuation from this increases the error on q_1 and q_2 and this effect eventually makes the system unstable. It is estimated that the uncontrolled error on q_1 moves the system out of the operating area the controllers are designed for, and therefore makes the system unstable.

5.1.9 Simulation - orbit

In this simulation the generated orbit reference is used, it rotates once every 6000 seconds.

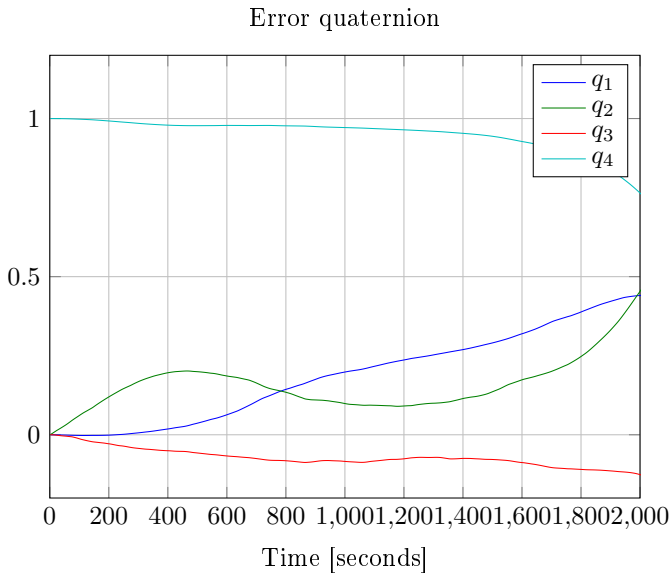

Figure 5.9: Error response, when the system is exerted to disturbances

Figure 5.9 is a plot of the errors from the simulation. It can be seen that the system tries to minimizes the first 1200 seconds. Hereafter the errors start to rise again. It is estimated that this is due to the shift in the magnetic field, and q_1 shifting the system out of the operating point.

5.2 Test simulation

The space simulation represents an approximation of the real system, but that is not the system that is tested in the acceptance test. Therefore another simulation is made that represents the test environment. In this section the main changes from the space simulation to the test simulation will be outlined.

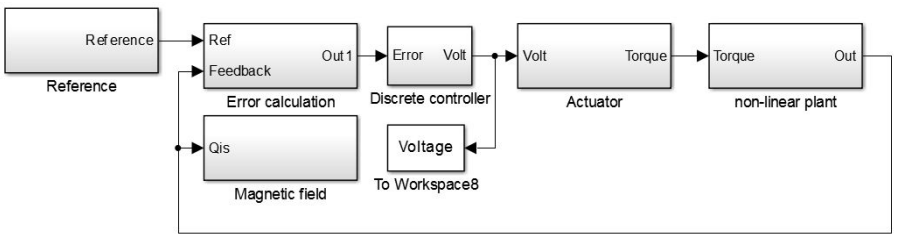

Figure 5.10: Complete acceptance test simulation environment

5.2.1 Input

The input in the acceptance test will be start position and a rotation as reference, but only about the ${}^{s}z$-axis. This is due to the fact that the test stand is only able to rotate about the ${}^{s}z$-axis. The input is generated as in the space simulation, as a direct function of sine and cosine.

5.2.2 Controller

Only one controller will be used in the acceptance test and therefore also in this simulation. The controller is discrete as the real system samples at 1 Hz. The acceptance test will

sample with 40 Hz. The controller designed for the test stand turned out not to perform well in the simulation. To solve that a zero is inserted to cancel out the pole created by the friction. The zero is moved further out and the gain is increased based on the same principles as in 4.5.2 to fulfill the scaled requirements which will be described further in section 6.2.1. In addition to that a filter is added corresponding to a pole in -250.

That results in the following transfer function in the s-domain.

$$H(s) = \frac{U(s)}{E(s)} = \frac{(s + 0.0212)(s + 0.15)}{s(s + 250)} \tag{5.5}$$

That is converted to discrete time as in section 4.6.

$$H(z) = \frac{145.8z^2 - 290.9z + 145.1}{z^2 - 0.4848z - 0.5152} \tag{5.6}$$

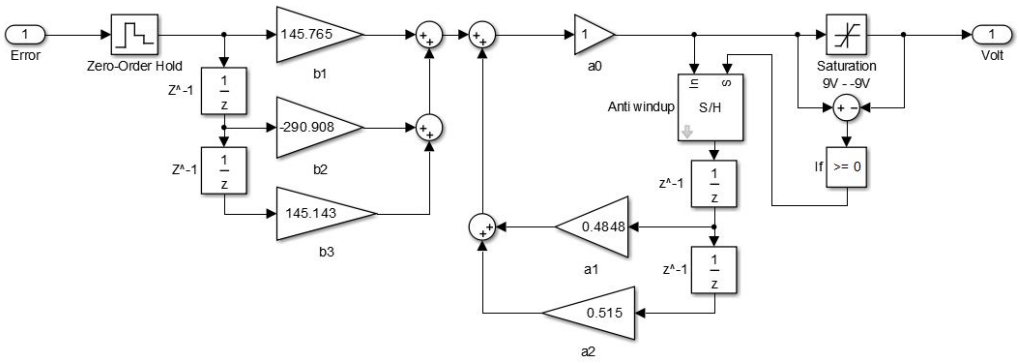

Figure 5.11: Discrete filter with anti wind-up

5.2.3 Magnetorquers

There will only be used one coil in the test, and likewise in the simulation. The magnetic field in the acceptance test is static in ECI, as it is generated by a single Helmholtz coil. The simulation will also be set-up such that, only torque about the z-axis is transferred on to the plant. The system is also scaled as it will be in the acceptance test, by increasing the magnetic field strength from $45 \cdot 10^{-6}$ T to $900 \cdot 10^{-6}$ T. To simplify this block, the magnetic field strength is multiplied into the actuator beforehand.

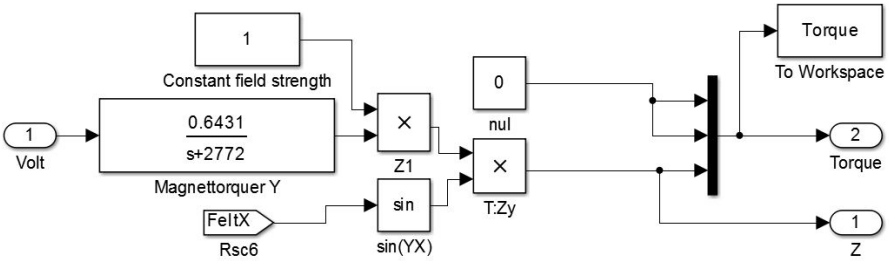

Figure 5.12: One magnetorquer that interacts with the field around the z-axis

5.2.4 Non-linear plant

The plant is implemented with a plant block from the AAUSAT3 toolbox. It contains the non-linear dynamics and kinematics. This block needs the rotation between SBRF

and SCRF. In this simulation these are set to be aligned, this is to prevent torques from affecting more than one axis.

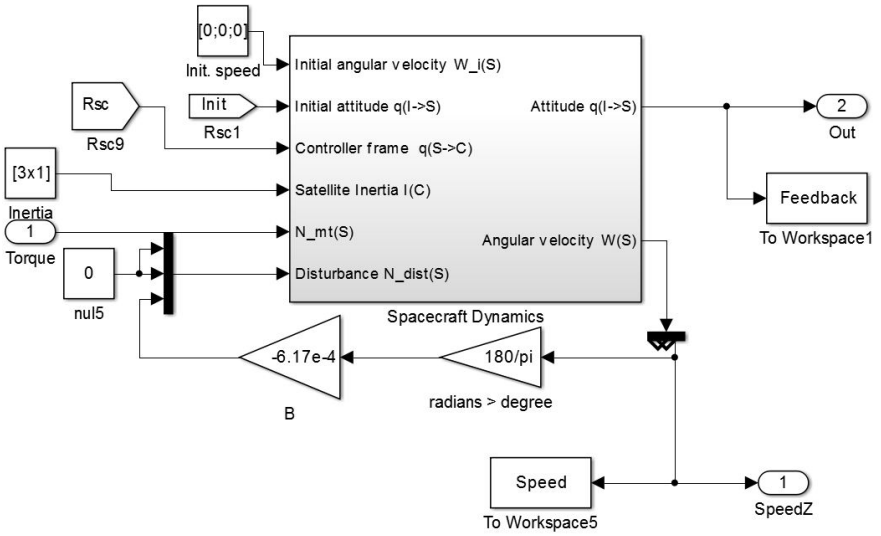

Figure 5.13: The non-linear plant, it also specifies start values

The B-value originates from the system identification in section 2.11.

5.2.5 Simulation - step

A step is simulated. The step represent a change in the wanted attitude. The start position of the system is set to be the same as the initial reference attitude.

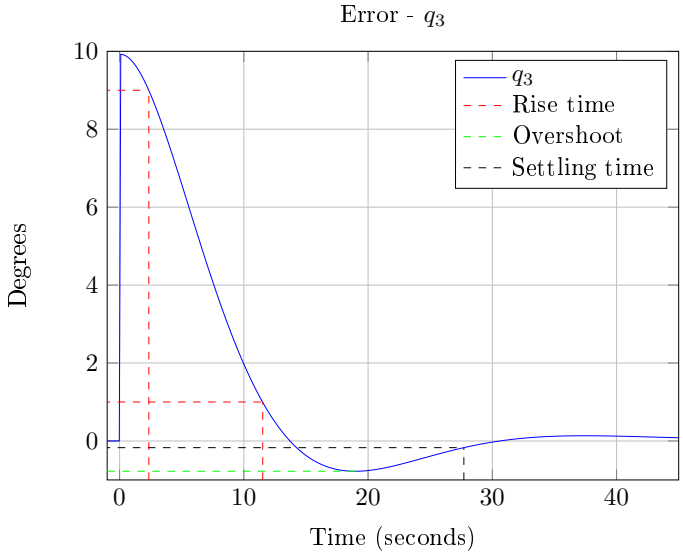

Figure 5.14: The error response from a 10 degree step

As it can been seen on the plot of the simulation on Figure 5.14, the system settles from a step of 10 degrees after 27 seconds, the scaled requirements demands a settle time of 31.58s. The scaled requirements also demands a rise time of 9.77s, it is seen to be 9.2s. The overshoot must be under 20% it is 7.7%.

5.3 Summary

Two test environments where designed and run. One with the theoretical non-linear plant for the satellite in space, and one for the system identified non-linear system in the test stand. The resulting simulations showed that the designed controllers for the real satellite in space worked for what they where designed for. But the assumptions they where based of only work in a small area, and the non-linear system takes it outside of that area, and the controllers therefore loose control. This could be properly be prevented if more controllers in the mimo system was implemented. The system also showed a vulnerability towards rotation of the magnetic field, a system that tracked this rotation and corrected the controllers output after it would be needed in the real satellite. The test simulation showed that the scaled requirements could be held, although the controller did need some modifications to get within the limits. The controller used in the test simulation can now be implemented in the test stand, and should make the acceptance test stay within the requirements.

Chapter 6

Implementation of Controller

The satellite attitude controller is not implemented to flight in space, due to the complications of verifying the controller properties in space. In order to test the controller in a digital system, a test setup is designed in Appendix B to verify a scaled version of the attitude controller.

Since the requirements mentioned in the Attitude control requirements in section 3.3 still is applied, they have to be scaled in order to verify the controller in the scaled test.

6.1 Scaling of test

Due to the torque in the suspension the magnetic field strength requires additional scaling of the input signals in order to measure usable response data. The scaling should be as small as possible since any non-linear effects will corrupt the results.

Naturally stiction and coulomb friction in the system has a non-linear contribute at small velocities which makes it more sensitive and could be canceled out by larger scaling. One solution is a compromise. It will not be possible to tell where eventual non-linearities comes from but it will be possible to tell whether they are there or not.

The magnetic field created by the Helmholtz coil is scaled 20 times compared to what would be available in orbit. The input signal to the magnetorquer is scaled according to the maximum voltage V_t delivered by the test setup in relation to the maximum actuation voltage V_r the real satellite can deliver. The total scaling factor is given by

$$G_\mathrm{scale} = \frac{V_\mathrm{t} \cdot G_\mathrm{H}}{V_\mathrm{r}} = \frac{9.6 \cdot 20}{1.25} = 153.6$$

where:

G_scale	scaling factor used through the test setup	$[\cdot]$
G_H	scaling factor of the Helmholtz coil	$[\cdot]$
V_t	maximum actuation voltage in the test setup	$[V]$
V_r	maximum actuation voltage used in the real satellite	$[V]$

thus scaling the natural frequency ω_n of the system to

$$\omega_\mathrm{n,scaled} = \omega_\mathrm{n} \cdot G_\mathrm{scale} = 184.32 \cdot 10^{-3} \text{ rad/s}$$

The sampling rate in the actual satellite is 1 Hz provided by the ADS. For the test to be realistic, the sampling rate of the test setup must be scaled too. The true controller

demands a sampling rate of 3.8 mHz where the actual sampling frequency is ∼262 times larger. This demands a scaled sampling frequency of ∼150 Hz of the test setup. However the test setup is not able to provide this sampling frequency, seen in the following sections, but this is not relevant considering that the purpose of the test is to verify the controller step response requirements and not all the satellites applications.

6.2 Overall setup

The relationship between the different subsystems in the test setup is shown in Figure 6.1 where the detailed description of the test design is described in Appendix B.

It is seen that the motion capture system has a different sampling rate than the rest of the setup. This is due to the previous mentioned limitations created by the transmission time to the on-board μController and because $T > T_{\mathrm{v}}$, the transmission time T is used as the common sampling time.

The on-board microcontroller is equipped with a H-bridge driver to deliver current to the magnetorquer. The output of the digital controller is then scaled and passed on through the wireless setup to the on-board microcontroller. The received control values are used to define a PWM signal to output on the microcontrollers D/A converter and then hold on to the input of the H-bridge driver. The driver feeds the magnetorquer with an effective voltage corresponding to the effective voltage input of the driver with a step interval of 38 mV. The output of the driver ranges with ±9.6 V.

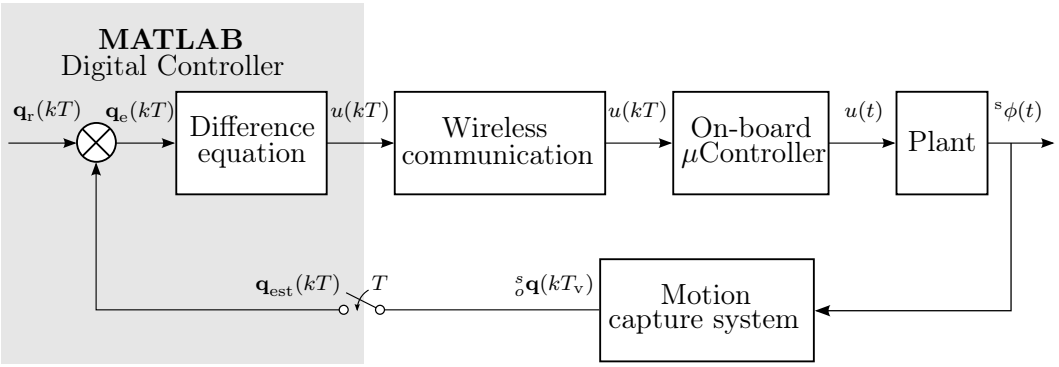

Figure 6.1: The overall test setup with a discrete controller implemented in a MATLAB environment and the wireless communication to the on-board microcontroller actuating on the satellite magnetorquer as the plant. The motion capture system functions as a feedback with its own sampling frequency of T_{v}.

The digital controller is implemented in the MATLAB environment with the VICON data as input and a controller actuation value as output. The input to the difference equation is an error quaternion describing the attitude error, which needs to be countered by the controller. The creation of this error quaternion was described in the previous section 4.4, by quaternion multiplication

$$\mathbf{q}_{\mathrm{err}} = \mathbf{q}^{*}_{\mathrm{est}} \otimes \mathbf{q}_{\mathrm{ref}}$$

elaborated in section 4.4. The error quaternion is then passed on to the the difference equation, acting on the potential error. It should be noted that since the test setup only allows rotation round one axis. Hence only one imaginary part of the quaternion is used as input to the controller.

6.2.1 Scaled system response

The scaling of the test setup found in the previous section 6.1, will have an effect on the step response of the system. The system should be 153 times faster than the unscaled system. Thus the test results should comply with a

$$t_{\mathrm{r,scaled}} \leq \frac{1.8}{\omega_{\mathrm{n,scaled}}} = 9.77\,s \tag{6.1}$$

$$t_{\mathrm{s,scaled}} \leq \frac{-\ln(0.017)}{\omega_{\mathrm{n,scaled}} \cdot \zeta} = 31.58\,s \tag{6.2}$$

to stay inside the requirements for the satellites ACS.

6.3 Controller design

As stated this test is done using scaled system requirements. This leads to a new controller design. This controller is designed by using the parameters found in section 2.11. A model of the test system is constructed first, then the controller for the acceptance test is designed.

6.3.1 Model

The model for the test is based on the system identification made in section 2.11. This leads to the following transfer function:

$$H(s) = \frac{0.643}{s(s+2772)(s+0.6417)} \tag{6.3}$$

That corresponds to a type 1 system but through tests it is found out that it made a steady state error on a step with a PD controller. Based on that observation it is concluded there is no integrator but 3 poles located in the left half plane. It is assumed that the third pole is located somewhere close to the other pole from the plant making the system:

$$H_{\mathrm{test}}(s) = \frac{0.643}{(s+2772)(s+0.6417)^2} \tag{6.4}$$

Based on that the controller is redesigned.

6.3.2 Controller

In order to make it a type 1 system an integrator is added to the controller in order to eliminate the steady state error on a step input. In addition to that another zero is inserted to keep the system stable. Since it is assumed that the two influential poles are located close to each other a new zero is placed in the same point as the first. Unfortunately since there is only one integrator the locus of that would go directly towards the zero. To keep the ω_{n} as high as needed the zeros has to be moved further to the left. The gain is adjusted through tests to give the best possible response. The new controller then becomes:

$$C_{\mathrm{test}}(s) = 58\frac{(s+0.288)^2}{s(s+1)} \tag{6.5}$$

It ends up with the root locus looking as shown in Figure 6.2.

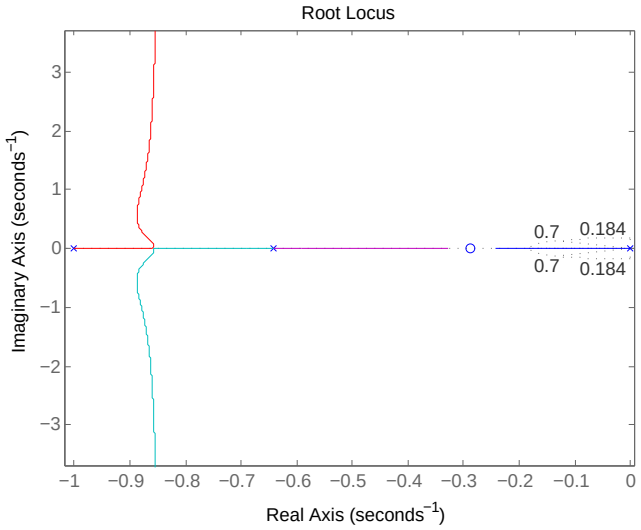

Figure 6.2: The root locus for the accept test with the redesigned controller.

This is when assuming that the two poles from the plant is in the exact same location. The controller is tested in the acceptance test in chapter 7.

6.3.3 Anti windup

When implementing an integrator it is essential to implement anti windup as well. Without it, the integrator might keep integrating up even when the system reaches saturation which may cause big overshoots. Therefore a the integrator is limited.

The limit should not be implemented directly on the integrator since a big output from the integrator might be needed. The limit should therefore be on the output of the controller. That however does not stop the integrator from integrating up. To solve that the difference between the output and the saturated output is subtracted from the input the the integrator, this essentially stops the integrator.

The block diagram of the anti windup looks like this:

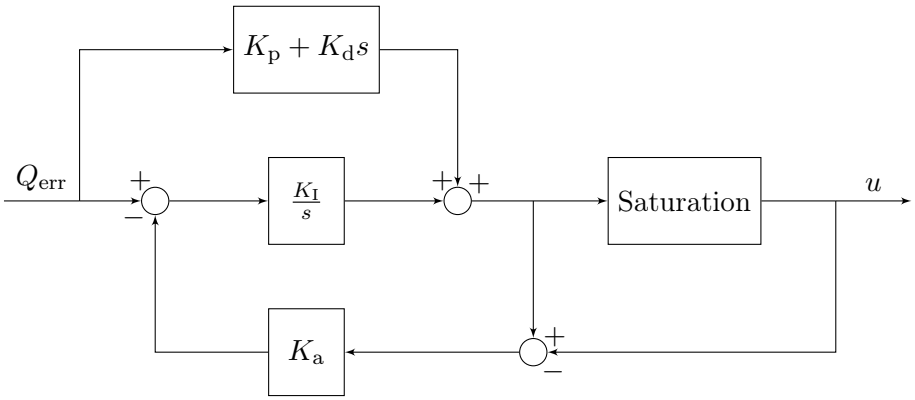

Figure 6.3: Block diagram for the anti windup function.

Discrete anti windup

Since the controller will be implemented in a digital system it must be discrete, including the anti windup. The anti windup must stop the integrator from increasing its output

value. In the discrete system this is done by holding the value that is to be delayed. The system uses the difference between the value before and after the saturation to determine if the anti windup should be triggered. The implementation of this in the system can be seen on Figure 5.11

Chapter 7

Acceptance Test

Through the previous chapters, a controller has been designed with the properties of actuating on a magnetic field and thereby controlling the satellites position relative to a reference position. The requirements from chapter 3 demands that the controller meets requirements related to control speed, stability and and accuracy. The acceptance test will test if the controller meets these requirements by following the test procedure stated in section 3.7.

7.1 Test results

The acceptance test is based on the redesigned controller found in section 6.3 equation 6.5 and compared to the scaled requirements found in section 6.1. Figure 7.1 and 7.2 show the step response of the ACS with a step of 10°.

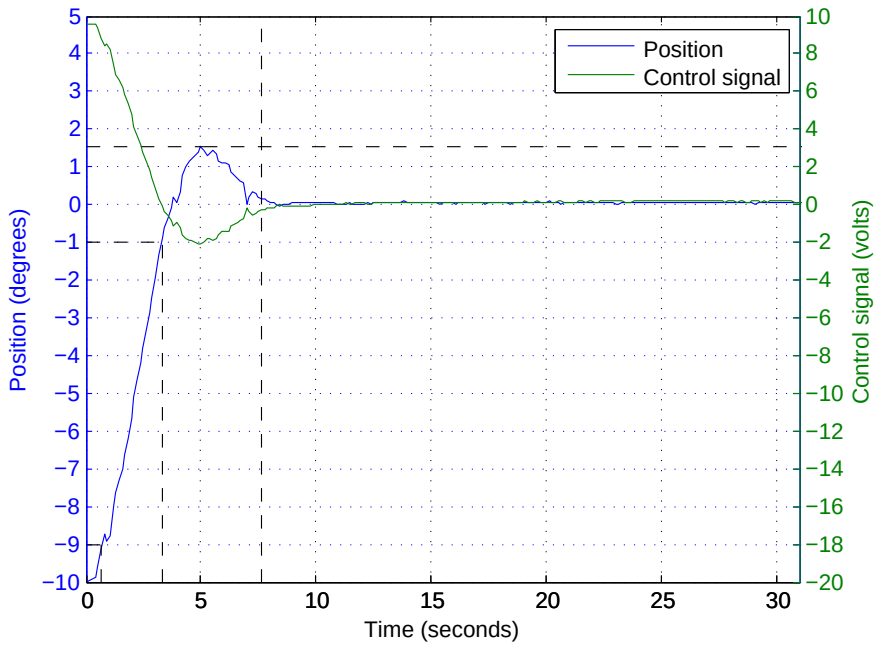

Figure 7.1: Shows the test results of a step of 10°where the rise time t_r, settle time t_s and overshoot M_p is marked by the dashed lines.

The rise time t_r, settling time t_s and overshoot M_p can be derived from Figure 7.1 and compared to the scaled requirements shown in the following tabular.

Time domain - Test 1		
	Req.	Test results
Rise time $t_{r,scaled}$	≤ 9.77 s	2.6 s
Settling time $t_{s,scaled}$	≤ 31.58 s	~7.6 s
Overshoot M_p	$\leq 20\%$	15.2%

The test was repeated with the same step size but in the opposite direction several times to insure consistent results. These test shows that the system does have steady state error as shown in Figurer 7.2.

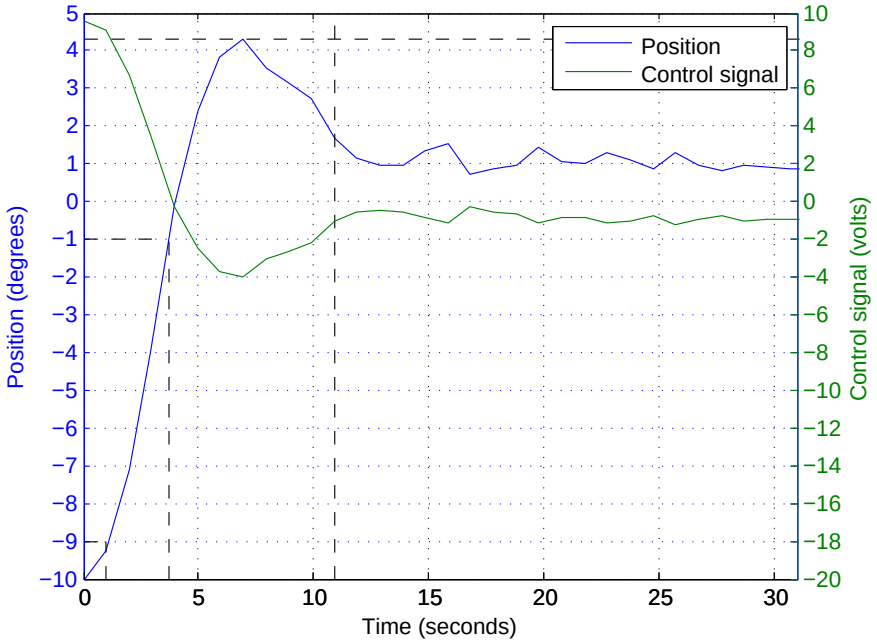

Figure 7.2: Shows the test results of the position error and the input signal with steady state error

The step response data is shown in the following tabular, where it can be seen that due to a potential operational point in the satellites suspension a significant overshoot appears which makes the test results unacceptable.

Time domain - Test 2		
	Req.	Test results
Rise time $t_{r,scaled}$	≤ 9.77 s	2.7 s
Settling time $t_{s,scaled}$	≤ 31.58 s	10.9 s
Overshoot M_p	$\leq 20\%$	43%

In the step response a steady state error of ~1° is also occurring. This is due to non linear friction in the suspension between the two magnetic spheres. If the torque generated by the magnetorquers are not sufficient enough to overcome this stiction at low velocities, the satellite will not move. This results in a continuously increasing integration of the steady state error until the controller output is great enough to correct the error.

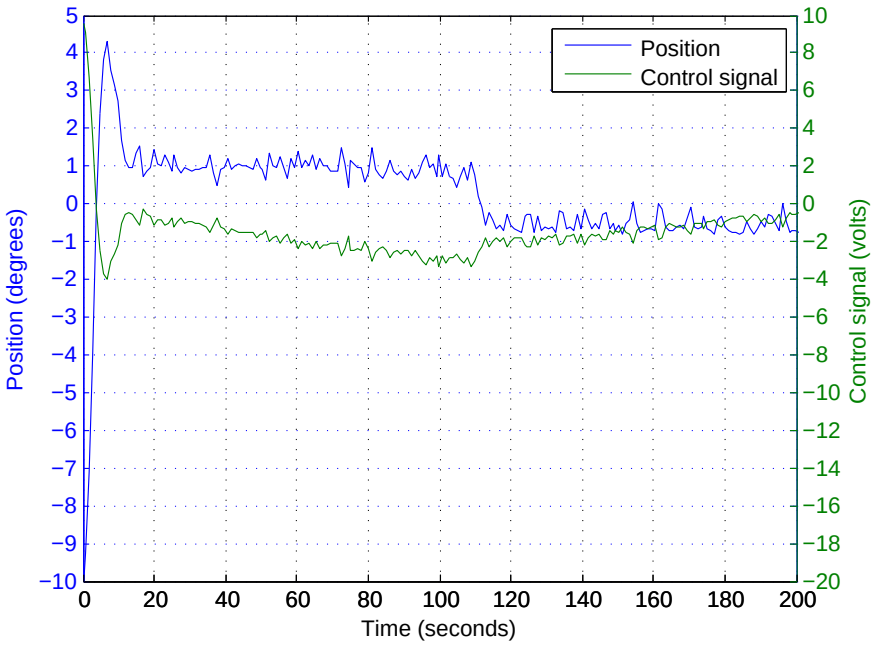

Figure 7.3: Shows the test results of the position error and the input signal with steady state error

Figure 7.3 shows the integrator part of the controller acting on the error as the control signal increases. Around 110 seconds into the test the stiction is overcome and the satellite rotates but overshoots. The satellite will keep this position until the integrator part takes action again.

7.1.1 Test conclusion

As seen from the test results the test stand adds some uncertainty to the tests. The rise time and settling time are well within the requirements in all cases. The overshoot varies a lot in the tests which presumably is due to misalignment in the magnetic joint which is placed inside the Helmholtz coil. On average the overshoot is too high but a lower gain would have resulted in bigger steady state errors. The steady state errors was rather unexpected based on the model but occurs because the friction torque is high compared to the torque the actuators are able to produce. These problems however will not occur on the satellite in space and the steady state error is smaller than the accepted error in requirement 3.3 of 3.05°.

Chapter 8

Closure

Different aspects of satellite attitude control has been researched and tested in this project. This chapter contains the conclusions drawn based on the study and ideas for further improvements.

8.1 Conclusion

Throughout the study the following conclusions has been drawn.

8.1.1 Need for attitude control

The need for an attitude control system is high when the satellite needs a specific attitude. This is relevant with payloads like cameras or other directional sensitive payloads. The satellite this project is based on has neither and its antennas are almost omni directional. An attitude control system is therefore not critical to the payload, although it does lower the noise levels and stabilizes the current flow from the sun panels.

For AAUSAT3 and AAUSAT4 detumbling is enough for the payloads to function, but attitude control is still wanted for optimization. Furthermore future AAUSAT's may carry a camera.

8.1.2 Use of magnetorquers

Magnetorquers does not allow control of rotation around the direction of the magnetic field. With the alignment used in this study that corresponds to roll control, which would be essential for payloads like cameras. Magnetorquers are therefore not the ideal choice to make 3 axes attitude control, but they are cheap and easy to make and implement and they work well in rotations round one axis.

8.1.3 Selection of orbit

When using magnetorquers the orbit has a lot to say in regards to control ability. A North-South orbit will give a small period of time with a strong field through the ^{o}z axis, allowing for some roll control. But the system will also have to constantly adjust for the varying field direction and field strength. An equatorial orbit will give a weaker field to actuate but it would be more stable in strength and direction, but would not allow for pitch control.

8.1.4 Attitude determination

The attitude determination is vital for the attitude control to function. In general the faster and more precise it is the better, since errors will ripple through the system. For this project a VICON system is used for testing which is reliable, but tends to generate a lot of noise. The VICON system however is not available in space where other sensors have to be used.

8.1.5 Attitude control

Based on the requirements for the AAUSAT4 and the linearization controllers are designed both for the satellite in space and the test stand. Based on simulations it is concluded that the satellite needs to switch controllers as the direction of the Earth's magnetic field changes. It will also need to switch between attitude control and detumbling since it is only able to actuate in two directions at a time.

The controller for the test stand however gave good results in the simulations after a slight adjustment. It has the advantage of only being able to rotate around one axis which makes it stay in the operating point as long as the controller works.

Based on that result it was tested on the test stand. It turned out that the friction applied from the test stand was different than first expected which led to more adjustments of the controller. The results turned out to have some variations but was generally within or close to the requirements which was scaled without taking the friction from the test stand into account.

The rise time got down to $\sim$2.7 s compared to the requirement of 9.77 s. The settling time got down to $\sim$10 s compared to the requirement of 31.58 s. The overshoot varied quite a bit with results of both 15.2 % and 43 % compared to the requirement of 20%. The variation is caused by the test stand where small misalignments in the magnetic joint will contribute with a disturbance.

In the test a steady state error occurred which is due to the high friction compared to the control torque. That however is within the limits of from the requirements of 3.05 ° and will not occur in space.

In space without the additional friction, attitude control around one axis would be possible assuming that the rotation around the other axes were kept zero.

8.2 Further improvements

There are many ways to improve the attitude control, some of them are described here.

8.2.1 Linearization

In this study the linearization has limited the controllers from roll control. If the linearization had been done in an other orientation it might have been possible to rotate around all axes relative to the satellite. This however would have made every actuation result in rotation around two axes which creates a need for compensation against unwanted rotations.

8.2.2 Roll control

Given the linearization used in this study actual roll control is not possible with magnetorquers. If a payload needs a specific attitude for more than a brief moment,

then roll control is needed. It can be done by rotating the satellite, such that the roll axis becomes pitch or yaw, it can then be set to a target speed and rotated back. The roll will then be adjusted, but disturbances and torque from the other two magnetorquer will over time change it away from the target speed.

8.2.3 Torque wheel

Torque wheels can be used to make fast changes in attitude, and they work about all three axis at any time in any orbit. Torque wheels function by accelerating a mass and exerting the same torque on the plant. Since they have a maximum speed they will eventually go into saturation. The wheel will then need to "dump" some energy, but it can not do that without affecting the plant. By combining torque wheels and magnetorquers, the magnetorquers can then counteract small torques from the torque wheels as they are slowing down. A combined system of magnetorquers and torque wheels are a good solution for attitude control, although it is difficult to implement on a hardware level, since it will need to be space graded and fall under the Cubesat standard [California Polytech State University, 2009], which does not allow for fluids or gas, making a smooth bearing difficult to make.

8.2.4 Aerodynamic flaps

A very different approach has been suggested for future editions of the AAUSAT project. A control system based on aerodynamic could potentially be implemented. In section 2.9 the aerodynamic disturbance is described as being up to $2 \cdot 10^{-7}$ Nm, a tenth of the torque the magnetorquers can exert. If the new satellite was designed with its centre of mass at the front, and yaw pitch flaps at the back. Then the satellite would get a shuttlecock effect, and stabilize yaw and pitch. Roll could also be controlled with two symmetrical flaps turning opposite of each other about either the z- or y-axis. The disadvantage to such a system would be, its dependency on almost non existent gas, higher chances of hitting debris, and limited yaw and pitch control.

Bibliography

Azurspace. 28% triple junction gaas solar cell/datasheet, April 2012.

Thomas Bak. *Spacecraft Attitude Determination - a Magnetometer Approach*. PhD thesis, Aalborg University Denmark, 1999.

celestrack.com. Two-line element set format. `http://celestrak.com/NORAD/documentation/tle-fmt.asp`, 2004.

Analog Devices. Adsp-bf537/datasheet.

Gene Franklin, J. David Powell, and Abbas Emami-Naeini. *Feedback Control of Dynamic Systems*. PEARSON, 1989.

Gene F. Franklin, J. David Powell, and Abbas Emami-Naemi. *Feedback Control of Dynamic Systems*. Pearson Prentice Hall, 2010.

Kasper Hemme, Britt Jacobsen, Kevin Lyn-Knudsen, Mathias Mølgaard, and Michael Nauheimer. Estimating spacecraft attitude based on in-orbit sensor measurements. Technical report, December 2013.

Felix R. Hoots and Ronald L. Roehrich. Spacetrack report no.3 - models for propagation of norad element sets. `http://www.amsat.org/amsat/ftp/docs/spacetrk.pdf`, 1980.

Jack B. Kuipers. *Quaternions and Rotation Sequences*. Princeton University Press, 2002.

Micronmeters. Awg36/datasheet.

Mathias Mølgaard, Britt Jacobsen, Kevin Lyn-Knudsen, Michael Nauheimer, Kasper Hemme, Jens Dalsgaard Nielsen, and Jesper A Larsen. Aausat4 cubesat design desciption. Technical report, Aalborg University Denmark, December 2013.

Mathias Mølgaard, Britt Jacobsen, Kevin Lyn-Knudsen, Michael Nauheimer, Kasper Hemme, Jens Dalsgaard Nielsen, and Jesper A Larsen. Aausat4 system specification document. Technical report, Aalborg University Denmark, Feburary 2014.

Carl Rod Nave. Hyperphysics. `http://hyperphysics.phy-astr.gsu.edu/hbase/magnetic/forwir2.html`, 2012.

Jens D. Nielsen and Jesper A. Larsen. space.aau.dk. `http://www.space.aau.dk/`l, 2013.

Marcel J. Sidi. *Spacecraft Dynamics & Control*. Cambridge University Press, 1997.

ST.com. Lpy403al/datasheet, October 2009.

James Joseph Sylvester. A demonstration of the theorem that every homogeneous quadratic polynomial is reducible by real orthogonal substitutions to the form of a sum of positive and negative squares. *Philosophical Magazine*, 4, 1852.

California Polytech State University. Cubesat design specification rev. 12. Master's thesis, California Polytech State University, January 2009.

Kasper Vinter and Kasper Fuglsang Jensen. Attitude determination and control system for aausat3. Master's thesis, Aalborg University Denmark, 2010.

James R. Wertz. *Spacecraft Attitude Determination and Control.* Kluwer Academic Publishers, 1995.

James R. Wertz and Wiley J. Larson. *Space Mission Analysis and Design.* Space Technology Library, 1999.

Rafał Wiśniewski. *Satellite Attitude Control Using Only Electromagnetic Actuation.* PhD thesis, Aalborg University Denmark, 1996.

Xtrinsic. Xtrinsic mag3110 magnetometer/datasheet.

Appendix A

Two Line Element and Simplified Perturbation Models

A.1 Two-line element (TLE)

The TLE is a data format for describing Keplerian orbits. The TLE is a data format developed by North American Aerospace Defense Command (NORAD) and is available online within a few weeks. TLE is a compact and structured format designed to convey as much information as possible in few characters, it consists of two lines with each 69 characters. These characters are divided into individual fields. A prototype of a TLE can be seen here:

```
1 NNNNNC NNNNNAAA NNNNN.NNNNNNNN +.NNNNNNNN +NNNNN-N +NNNNN-N N NNNNN
2 NNNNN NNN.NNNN NNN.NNNN NNNNNNN NNN.NNNN NNN.NNNN NN.NNNNNNNNNNNNN
```

Where:

Line 1	
Column	**Description**
01	Line Number of Element Data
03-07	Satellite Number
08	Classification (U=Unclassified)
10-11	International Designator (Last two digits of launch year)
12-14	International Designator (Launch number of the year)
15-17	International Designator (Piece of the launch)
19-20	Epoch Year (Last two digits of year)
21-32	Epoch (Day of the year and fractional portion of the day)
34-43	First Time Derivative of the Mean Motion
45-52	Second Time Derivative of Mean Motion (decimal point assumed)
54-61	BSTAR drag term (decimal point assumed)
63	Ephemeris type
65-68	Element number
69	Checksum (Modulo 10) (Letters, blanks, periods, plus signs = 0; minus signs = 1)

Table A.1: Line one of TLE [celestrack.com, 2004].

Line 2	
Column	**Description**
01	Line Number of Element Data
03-07	Satellite Number
09-16	Inclination [Degrees]
18-25	Right Ascension of the Ascending Node [Degrees]
27-33	Eccentricity (decimal point assumed)
35-42	Argument of Perigee [Degrees]
44-51	Mean Anomaly [Degrees]
53-63	Mean Motion [Revs per day]
64-68	Revolution number at epoch [Revs]
69	Checksum (Modulo 10)

Table A.2: Line two of TLE [celestrack.com, 2004].

An example of a TLE from AAUSAT3 can be seen below:

```
AAUSAT3
1 39087U 13009B   14099.00343562  .00001087  00000-0  40102-3 0  3389
2 39087  98.6229 293.5342 0013260 148.6403 211.5587 14.34480230 58394
```

From this TLE it can be seen that, AAUSAT3's orbit has an inclination of 98.6229°and a Right Ascension of the Ascending Node of 293.5342°. Its orbit has a eccentricity of 0.0013260 (the decimal point is assumed). Argument of perigee is 148.6403°. From these informations it can be derived that AAUSAT3 is in a near polar and an almost circular orbit. These orbit parameters are elaborated in section 2.2.

A.2 Simplified perturbations models

Simplified perturbations models are a set of orbital models consisting of SGP, SGP4, SDP4, SGP8 and SDP8. These models can be used to predict position and velocity using a TLE. The simplified general perturbations models (SGP, SGP4 and SGP8) are used for orbiting objects with an orbit revolution time less than 225 minutes and the simplified deep space perturbations models (SDP4 and SDP8) are used for objects with a orbit revolution time greater than 225 minutes. NORAD uses the SGP4 model to generate the TLE, the AAUSAT4 needs then the SGP4 model to calculate position and velocity [Hoots and Roehrich, 1980]. These are in turn used for calculating the ORF relative to ECI, see section 2.4.1.

Appendix B

Test Setup

The test setup is designed with the purpose of generating a static magnetic field, simulating the Earth's magnetic field and a friction free rotational suspension. The following topics will be elaborated in this chapter.

- Construction of magnetorquers
- Satellite and suspension
- Wireless communication to satellite
- Attitude feedback though motion capture laboratory (VICON system)
- MATLAB controller algorithm
- On-board microcontroller algorithm

B.1 Construction of magnetorquers

For the tests a magnetorquer is needed. A physical description is provided in [Mølgaard et al., 2013]. However no magnetorquers was made so it had to be constructed. That was done with a setup made by the AAUSAT group with a custom made mould. The procedure included winding up the wire, adding glue for every 25 rounds and making sure the the glue stayed evenly distributed while it dried.

B.2 Satellite suspension

The actual satellite is replaced by a mass-dummy, with the same dimensions and weight. In an ideal test setup, the satellite should be able to rotate friction free round one axis. This setup is acquired by use of a magnetic suspension, consisting of two magnetic spheres with brackets to mount to satellite on as shown in Figure B.1. The setup will achieve minimal torsional friction found by system identification in section 2.11. The suspension with the satellite is then placed in the centre of a Helmholtz coil which simulates the Earth's magnetic field, by creating a static field. The setup would not be able to change the angle of the magnetic field, for this a two dimensional Helmholtz coil should be used, but this is not the case.

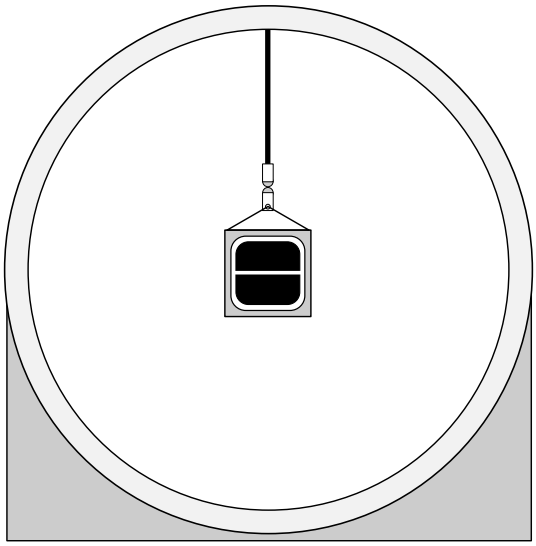

Figure B.1: Shows the satellite mounted in the Helmholtz coils

B.3 Motion capture system

The goal of the test is to measure the response of the attitude controller as the satellite rotates. This is done by use of a motion capture laboratory called VICON. The motion capture system is able to track the attitude of the satellite in real time with a sampling rate of 100 Hz which corresponds to a delay of 10 ms. This is sufficient related to the maximum actuation speed of the satellite.

As mentioned in the controller design in chapter 4, the Attitude controller is a part of a larger system where a reference attitude is given and an actual attitude is fed back through the ADS. In this project the use of an ADS is replaced with feedback through the motion capture system called VICON. The output of the VICON system is represented as an estimated quaternion describing the orientation of the satellite relative to the room. The link between the VICON system and the satellite will be described in the next section.

B.4 Wireless setup

The satellite attitude is fed back through the motion capture system to a computer equipped with a written MATLAB software. The computer handles all the data from the VICON system and phrases it to the digital attitude controller in the MATLAB environment.

The MATLAB computer is handling all the data by calculating an angular error between the reference quaternion and the estimated quaternion of the satellite measured by the VICON system. The quaternion error is then passed to the controller, which calculates an actuations voltage to counter the error. The output of the controller is then sent through a wireless setup to the satellite. The communication link between the computer and the satellite is limited by a delay of ∼25 ms which minimizes the samplings rate of the overall system to a maximum of ∼40 Hz. This is sufficient in relation to the maximum scaled actuation speed of the satellite, where an acceptable samplings rate would be 20 times $\omega_{\text{n,scaled}}$. Thus

$$\omega_{\text{s}} = 20 \cdot \omega_{\text{n,scaled}} = 3.69 \text{ rad/s}$$

where 3.69 rad/s corresponds to 0.59 Hz, which makes the systems samplings rate more than sufficient.

B.5 MATLAB to microcontroller

The test setup is as mentioned controlled by running software in a MATLAB environment in cooperation with software running on the microcontroller in the satellite setup. The algorithms used in the test are described in the following sections.

B.5.1 MATLAB algorithm

The algorithm is imaged in the simplified block diagram in Figure B.2 consisting of the following blocks.

Configure test

The configuration of the test include the definition or calculation of the:

- Sample time
- Step size
- Continuous controller
- $\mathbb{Z}$-transform of the controller

These informations are later used in the calculations of the digital controller, reference- and error-quaternion.

Calculate reference quaternion $\mathbf{q_{ref}}$

The first time the algorithm runes, an initial satellite position is received from the VICON system. The reference quaternion is then calculated from the initial position of the satellite rotated by the step size and is given as

$$\mathbf{q}_{\text{ref}} = \mathbf{q}_{\text{step}} \otimes \mathbf{q}_{\text{init}} \tag{B.1}$$

The reference quaternion is then used as the reference to the control loop.

Calculate error quaternion $\mathbf{q_{err}}$

The digital controller acts on an error between the reference and the estimated attitude given by the Vicon system. This error is given as

$$\mathbf{q}_{\text{err}} = \mathbf{q}^*_{\text{est}} \otimes \mathbf{q}_{\text{ref}}$$

The error is then phased on to the digital controller.

Digital controller

The digital controller consists of a difference equation, where its coefficients are defined in the configure test block. The block also includes an anti windup for the controller to insure performance for when the controller goes into saturation.

Depending on the order of the chosen continuous controller defined in the Configure test block in Figure B.2 the difference equation takes the following form

$$u[n] = -a_2 \cdot u[n-1] - a_3 \cdot u[n-2] + b_1 \cdot e[n] + b_2 \cdot e[n-1] + b_3 \cdot e[n-2]$$

where:

u	Controller output	$[V]$
e	Quaternion error	$[\cdot]$
b_i	The $\mathbb{Z}$-transform zeros coefficients	$[\cdot]$
a_i	The $\mathbb{Z}$-transform pole coefficients	$[\cdot]$

Anti-windup is implimented by logic. If the controller meets saturation, the integrator part of the controller should stop integrating hence leave the integrated value at saturation point stay locked at that value until the controller comes out of saturation.

Write to microcontroller

In order to convert the digital value of the controller output into a voltage, the output is converted into to a PWM value. The on-board microcontroller has an D/A converter with a resolution of 255 values and since it should be able to have both positive and negative values the values span from 0-510 values which corresponds to a voltage of ± 9.6 V for a fully charged battery. The converted controller output values is the written serial through a wireless setup to the on-board microcontroller.

After the values have been sent, the loop starts over.

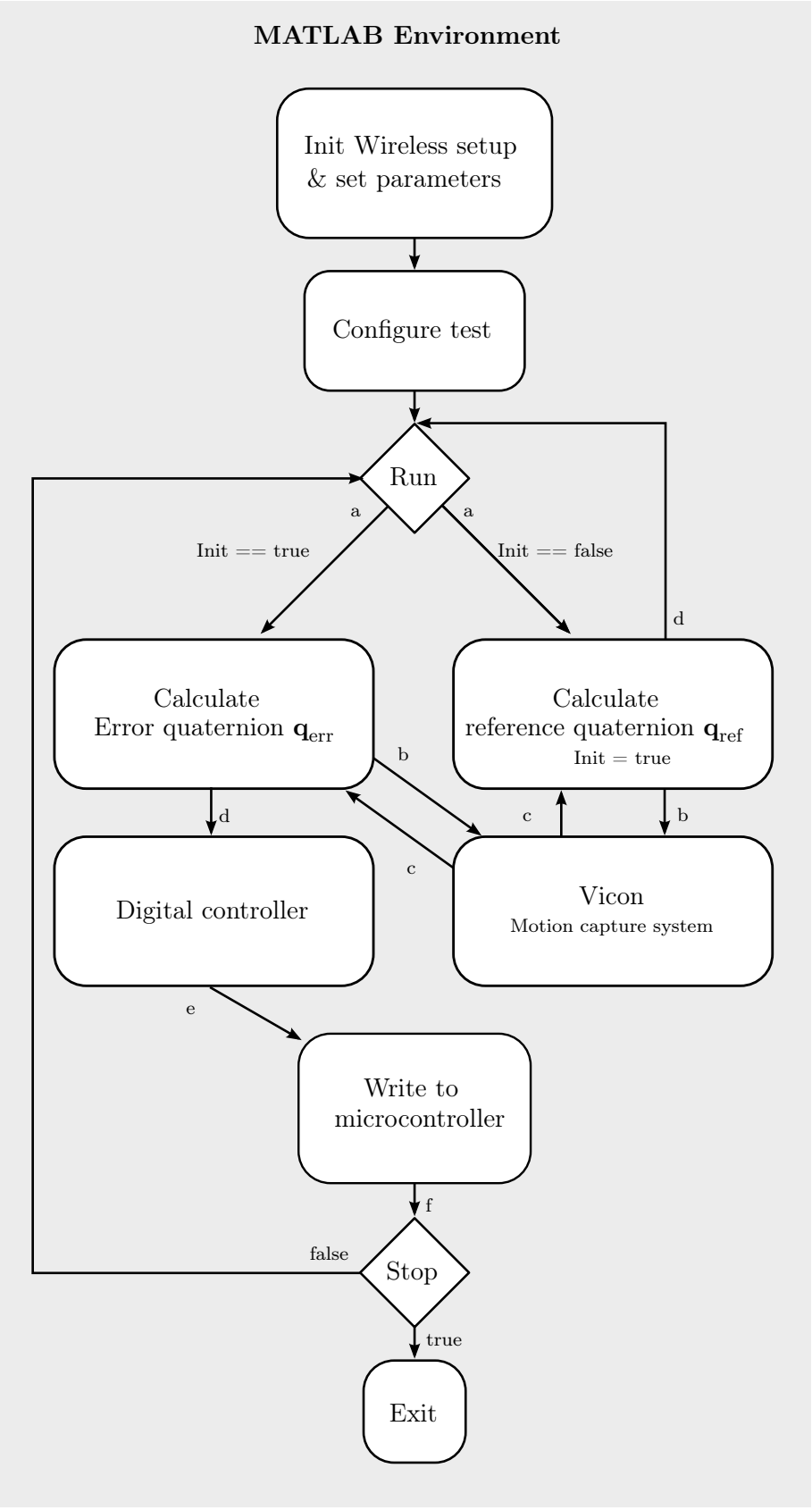

Figure B.2: Shows a simplified block diagram of the MATLAB algorithm written for the test of a satellite 1-Axis attitude controller.

B.5.2 Microcontroller algorithm

The on-board microcontroller is as mentioned equipped with a H-bridge and a magnetorquer to actuate on. The algorithm is designed to listen for serial communication from the wireless module. When Serial data is available the data is read until a new line character appears. The algorithm then uses the value to define a PWM signal on the microcontrollers D/A converter and outputs it to the H-Bridge. The duty cycle of the PWM signal then corresponds to a certain percentage of the supply voltage which is set over the magnetorquer. The algorithm then waits for new values to be set.

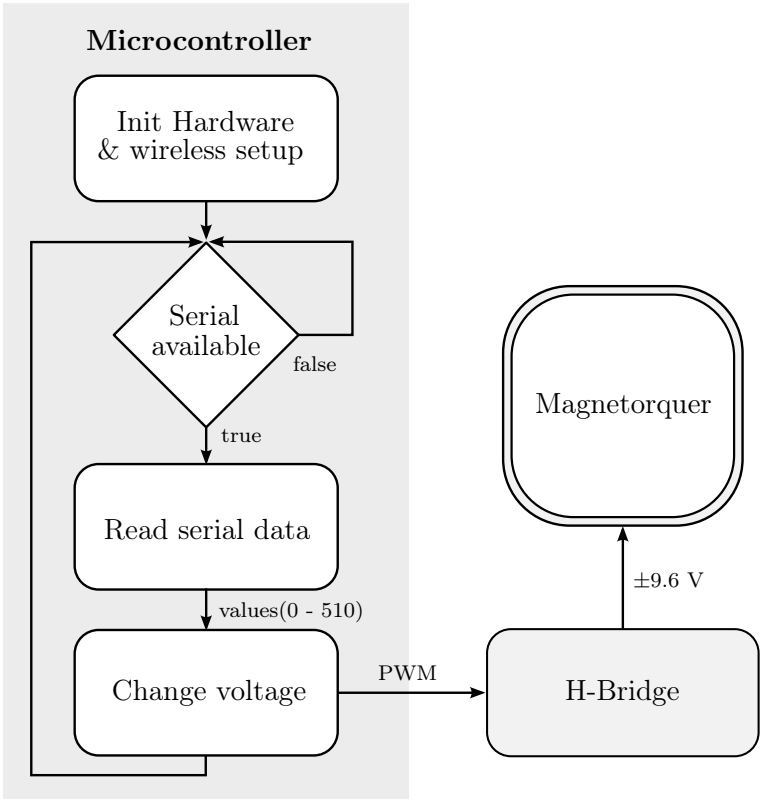

Figure B.3: Shows the algorithm running in the microcontroller in relation to the H-bridge and the magnetorquer.

Appendix C

Measurements Journal

C.1 Magnetorquer test

These measurements are made to verify the magnetic field that a magnetorquer makes.

C.1.1 Theory

A coil will generate a magnetic field when a current is passed through it. When the current in the coil is changed, the change in the magnetic field will make the coil act as a generator, and it will try and generate a current opposite to the change exerted on it. The current will therefore have a rise time dependent on the design of the coil. The current can be expressed as:

$$I(s) = \frac{U(s)}{s \cdot L + R} \tag{C.1}$$

Where

$I(s)$	Current in the coil	[A]
$U(s)$	Voltage over the coil	[V]
L	The coils inductance	[H]
R	The Coils electrical resistance	[Ω]

The magnetic field is directly dependent on the current. The formula for magnetic field strength is derived from Biot-Savarts law for a square multi turn coil as:

$$B(s) = \frac{\sqrt{2} \cdot \mu_0 \cdot N \cdot I(s)}{\pi \cdot r} \tag{C.2}$$

Where

$B(s)$	Magnetic field strength	[T]
$I(s)$	Current in the coil	[A]
μ_0	Vacuum permeability	[H/m]
N	Number of windings	[·]
r	Radius of the coil	[m]

(C.3)

The transfer function from voltage to field strength is then:

$$H(s) = \frac{B(s)}{U(s)} = \frac{\sqrt{2} \cdot \mu_0 \cdot N \cdot \frac{1}{s \cdot L + R}}{\pi \cdot r} = \frac{1}{s + \frac{R}{L}} \cdot \frac{\sqrt{2} \cdot \mu_0 \cdot N}{L \cdot \pi \cdot r} \tag{C.4}$$

It is expected that the gain will be lower, since the probe is not placed 100% due to the aluminum plate the coil is attached to.

C.1.2 Test stand

There are three parts to this test stand, the input generator, the coil being tested, and the measurement of the magnetic field.

The input is a step, for this a signal generator is used, since that gives the least noise when stepping. The signal generator will have its output connected to the coil and to an oscilloscope. This way the input to the coil can be recorded.

The coil is placed perpendicular and with its center to the magnetic field probe, this is important to ensure maximum field strength measured. The coil should be placed in an environment with as little magnetic fields as possible.

The magnetic field probe is placed in a holder, and angled both horizontally and vertically in a way so the probe does not measure the Earth's magnetic field with the probe axis in use. The probe is then setup with the coil, and the probe is connected to the oscilloscope.

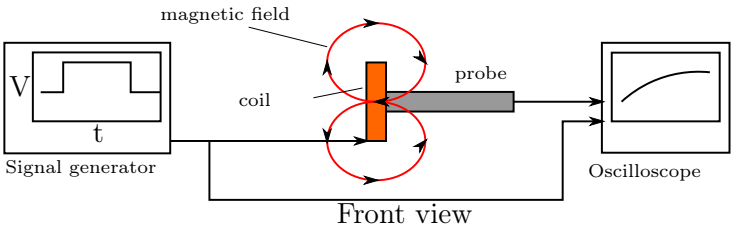

Figure C.1: Front view

C.1.3 Procedure

Setup The first thing that should be done is finding a place to do the test. It is important that there is no magnetic field that will disturb the test. This is done by using the probe.

When a suitable place have been found the probe is placed. It needs to be angled so it does not measure Earth's magnetic field. This is again done by watching the output while changing the angle. This is critical for the precession of the test.

The coil can the be placed in a holder so it is centered and perpendicular to the magnetic field probe.

The signal generator can then be connected to the coil and oscilloscope. The signal generator is set up to make steps from 0.0 V to 2.4 V. The step is verified on the oscilloscope.

Testing The oscilloscope is set to make a single measurement, triggering on a rising edge from the signal generator. The data from both the magnetic field probe and the signal generator is then saved and used as a result.

The test can also be done while triggering on a falling edge, which will give the dynamics of shutting the coil down.

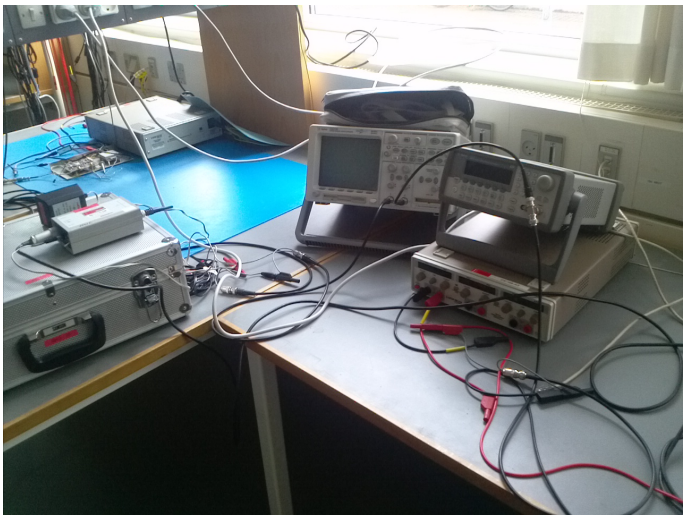

Figure C.2: Input and output equipment

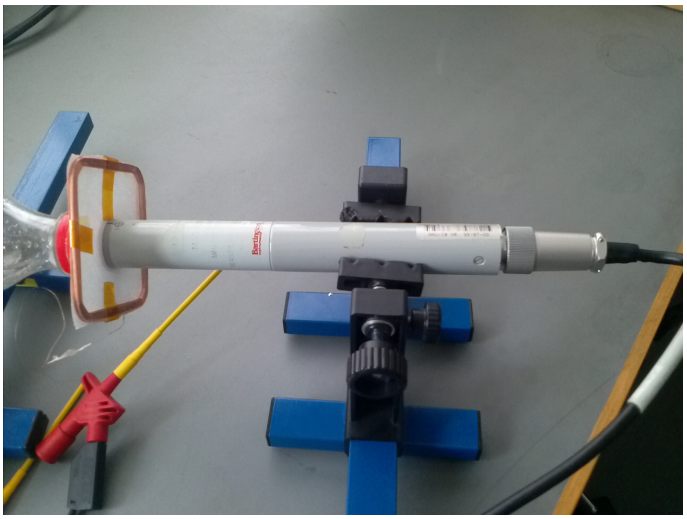

Figure C.3: Coil and magnetic field probe

C.1.4 Equipment list

Instrument	AAU number	Company and type	unit
A6-211-MAG-03	33137-00	Bartington 3-axis Magnetometer	10 $\frac{\mu T}{V}$
33220A	75485	Agilent	
TDS 2012B	64586	Tektronix oscilloscope	

C.1.5 Results

The data from the oscilloscope can be seen on Figure C.4

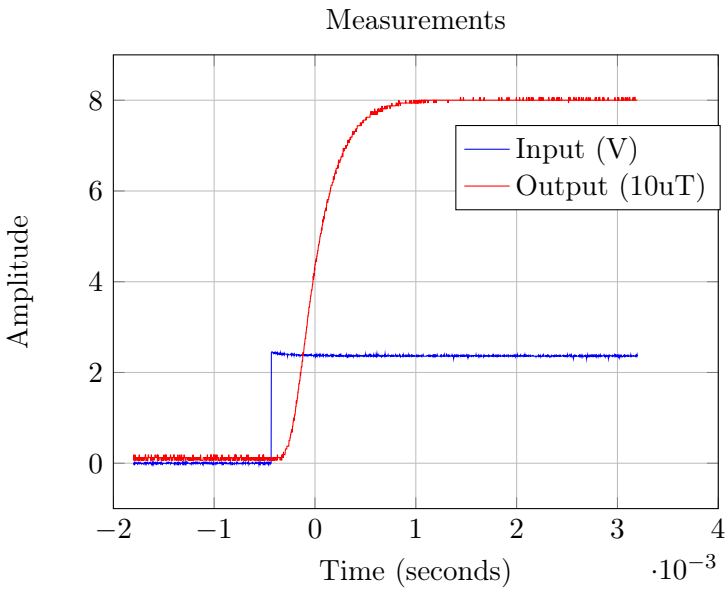

Figure C.4: Measurements from test

The system identification toolbox in MATLAB is used to estimate the function. It is know that the system has one pole, the toolbox then uses least square to find the best parameters. A comparison between the measured data and the estimated function can be seen on Figure C.5.

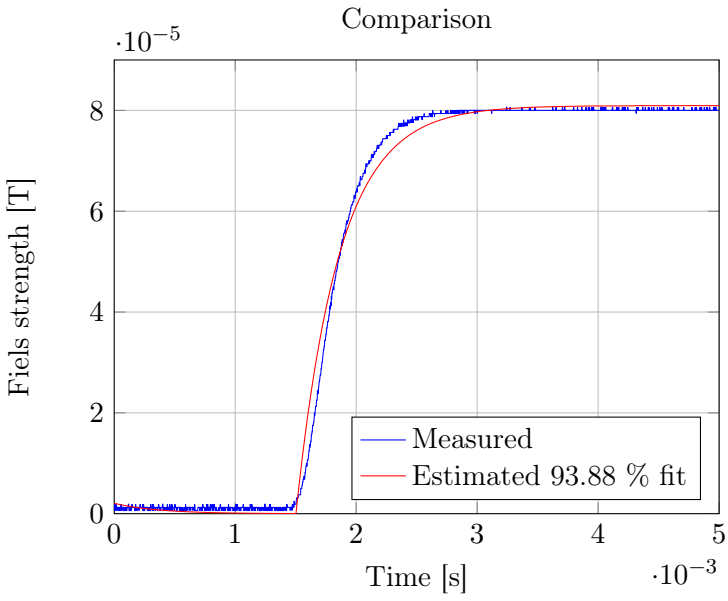

Figure C.5: Comparison between measured data and estimated function

The estimated function is:

$$H(s) = \frac{3.4237e - 05}{1 + 0.00036063s} \tag{C.5}$$

The coil in the test was stepped with 2.4V. The theoretical transfer function C.4 is stepped with 2.4V and plotted with the estimated and the measured data

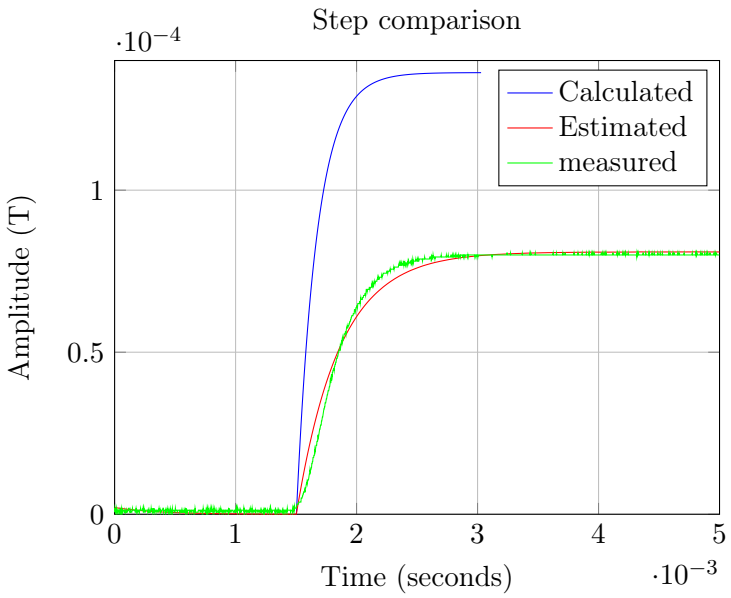

Figure C.6: Comparison between theoretical, measured data and estimated function

It is seen that the rise time is close to be the same for the theoretical and the data, but the amplitude is wrong. This is due to the magnetic field probes placement. It was later found that its sensor was not in the centre of the coil, when placed there under the same voltage, the probe measured about 136 μT. This error does not affect the time constant, and is therefore accepted.

C.1.6 Conclusion

With basis in Figure C.6 it is concluded that formula C.4 describes the relation ship between voltage and the magnetic field.

C.2 Model test

The measurements are for the model of the AAUSAT4. Although the test is made on a mass dummy, which has similar mass and mass distribution. The test is made to have data to compare an extrapolated model with.

This test can only do one axis at a time. And the mounting exerts some torque which will have to be overcome, so the test is made with stronger fields.

C.2.1 Theory

The satellite have three magnetorquers. These can interact with magnetic fields to realign the satellite, this realignment is also called attitude control. The satellites moment of inertia will slow any change in rotational speed, so a bigger moment of inertia will result in a slower system. The moment of inertia can either be found through test or by calculating it.

The magnetic field the satellite will interact with in flight, is the Earth's magnetic field, the magnetic field strength decreases with relation to the distance to the center of Earth. Therefore the field strength is too high on the surface, it also comes in at an angle, which is not wanted. This is counteracted by using a Helmholtz coil.

C.2.2 Test stand

The test is made in a special laboratory, equipped with a VICON system. This is a camera tracking system, which can be used to track movement in a three dimensional space. This will act as the output of the test.

Inside the laboratory a Helmholtz coil is placed. A magnetically sensitive probe(MAG-03) is used to set the angle and voltage on the Helmholtz coil. The magnetic field inside should optimally be horizontal and have a strength between 20 to 50 μ T. But since the torque from the mounting will be too strong, the field strength is increased to its maximum strength of 975μ T. Inside the Helmholtz coil the satellite is suspended in a magnetic joint. The satellite will hang horizontal. In order for the VICON system to track the satellite, small reflective balls must be attached to it, in such a pattern that at no point can the camera mistake on side for another. The test stand must be placed, so that no matter the rotation, each dot can be seen by at least four cameras.

Since wires to the satellite dummy will create a torque the magnetorquers is powered by batteries and the input signal is delivered wireless to an Arduino.

C.2.3 Procedure

1. Make sure the VICON system is calibrated to an acceptable level.
2. Clear the VICON room for any objects that could disturb the test, such as reflecting surfaces.
3. The Helmholtz coil is now placed in the VICON room, and is angled horizontally so its field is parallel with the Earth's magnetic field, use a magnetically sensitive probe(MAG-03) to measure this field.
4. The satellite is equipped with reflective balls as described in the test stand, and with wires connected to one magnetorquer.
5. The satellite is mounted in the magnetic joint in the center of the Helmholtz coil.
6. The satellite is loaded into the VICON system and it is checked if the system can track it during a 360°turn. This is done by turning the satellite by hand while watching the data on the computer. If not successful, the Helmholtz coil can be moved as long as the angles stay the same.
7. The batteries and the control system is connected to the magnetorquers.
8. The angle between the side of the satellite with the magnetorquer and magnetic field is noted, the side is also noted in the VICON system.

Calibration
The magnetically sensitive probe(MAG-03) is used to measure the magnetic fields at different voltages. This is done because the probe does not have a high enough range. By making several measurements an approximation of the field at higher voltages can be made. Thereby the voltages can be turned to higher values, while the field is still known. These measurements can be found in the attached Excel file.

Instrument	AAU number	Company and type	unit
A6-211-MAG-03	33137-00	Bartington 3-axis Magnetometer	10 $\frac{\mu T}{V}$
HM7042-3	60771	Hameg power supply	
TDS 2012B	64586	Tektronix oscilloscope	
	75459	VICON 10 camera tracking system	
		Helmholtz coil	32 $\frac{\mu T}{V}$

C.2.4 Equipment list

C.2.5 Results

In order to be able the make a test of the system disturbances needs to be taken into account. One major disturbance is the friction in the magnetic joint. To test that the input is kept turned off and the satellite dummy is given a start angular velocity.

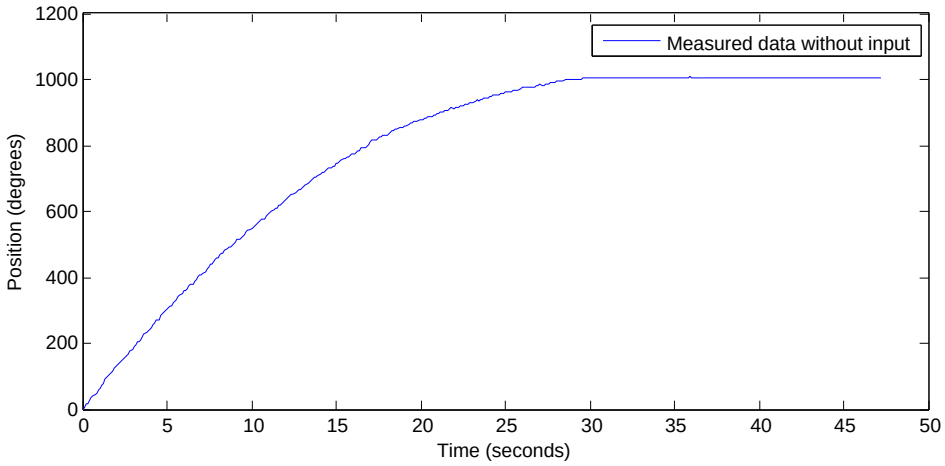

Figure C.7: The measured position without input but with a start angular velocity.

As seen on the plot the VICON system adds some noise to the position. A model for the friction can be made based on the test which is done in section 2.11. With this done an input can be put on the system and a model can be made for the entire system. That gives the following response.

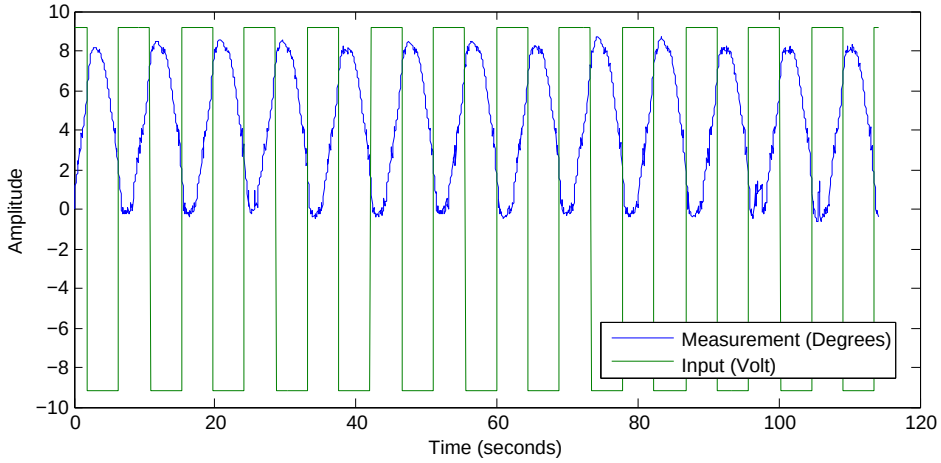

Figure C.8: The measured position with input and a start angular velocity.

Based on this measurement a model for the system can be made and values for the inertia the gain in the magnetorquer and the pole placement can be estimated. That is done in section 2.11.

Appendix D

CD

```
DVD
|
|_ space_simulator_AAUSAT3
|    The toolbox used for the simulations
|
|_ MATLAB_scripts
|    Various scripts used for e.g. accetance test
|
|_ report.pdf
|    PDF version of the thesis
|
|_ AAUSAT4_doc
|    Various documents pertaining to AAUSAT4
|
|_ Simulations
|  |_ Acceptance_test
|  |    Simulation of the acceptance test
|  |_ Space
|  |    Simulation of the space controllers
|
|_ Data
|  |_ Magnetic_field
|  |    Data from measurements of the magnetorquers
|  |    and Helmholtz coils
|  |_ Simulations_data
|  |  Data from the simulation
|
|_ Media
|    Video and photos of the acceptance test
```